Development of microfluidics-based neutrophil migration analysis systems for research and clinical applications

by

Jiandong Wu

A thesis submitted to the Faculty of Graduate Studies of

The University of Manitoba

in partial fulfilment of the requirements of the degree of

Doctor of Philosophy

Department of Biosystems Engineering

The University of Manitoba

Winnipeg, Manitoba, Canada

Publication list

A significant part of this thesis (i.e. Chapter 1.3; 1.4; Chapter 2-4; Appendix) is based on the following peer-reviewed journal and conference publications, and patent applications.

Journal Articles

1. **J.D. Wu**, C. Hillier, P. Komenda, R. Lobato de Faria, S. Santos, D. Levin, M. Zhang, F. Lin, “An all-on-chip method for testing neutrophil chemotaxis induced by fMLP and COPD patient’s sputum”, **Technology**, 2016, accepted.
2. **J.D. Wu,** C. Hillier, P. Komenda, R. Lobato de Faria, D. Levin, M. Zhang and F. Lin, “A microfluidic platform for evaluating neutrophil chemotaxis induced by sputum from COPD patients”, **PLoS ONE**, 2015 May 11;10(5):e0126523.
3. **J.D. Wu**, L.P. Ouyang, N. Wadhawana, J. Li, M. Zhang, S. Liao, D. Levin and F. Lin, "A compact microfluidic system for cell migration studies", **Biomedical Microdevices**, 2014, 16(4): 521-528.
4. **J.D. Wu** and F. Lin, “Recent developments in electrotaxis assays". **Advances in Wound Care**, 2014, 3(2):149-155.
5. **J.D. Wu,** X. Wu and F. Lin, “Recent developments in microfluidics-based chemotaxis studies". **Lab on Chip**. 2013, 13(13):2484-99.

Conference Proceeding

6. **J.D. Wu**, L.P. Ouyang, M. Zhang, S. Liao, C. Hillier, P. Komenda, R.L. de Faria and F. Lin, “Assessing neutrophil chemotaxis in COPD using a compact microfluidic system”, The 36th Annual International Conference of the IEEE Engineering in Medicine and Biology Society **(EMBC’14)**, Chicago, U.S.A., August 26-30, 2014.

Patent Applications

1. F. Lin and **J.D. Wu**, “Low-cost portable microfluidic system for cell migration studies”, PCT/CA2013/050697, Canada
2. F. Lin and **J.D. Wu,** “An easy-to-use microfluidic device for cell migration studies integrated with on-chip cell isolation, cell docking, and gradient generation”, Provisional filed.

Abstract

Immune cell migration and chemotaxis plays a key role in immune response. Further research to study the mechanisms of immune cell migration and to develop clinical applications requires advanced experimental tools. Microfluidic devices can precisely apply chemical gradient signals to cells, which is advantageous in quantifying cell migratory response. However, most existing microfluidic systems are impractical to use without specialized facilities and research skills, which hinders their broad use in biological and medical research communities. In this thesis, we integrated several new developments in microfluidic gradient generating devices, compact imaging systems, on-chip cell isolation, cell patterning, and rapid data analysis, to provide an easy-to-use and practical solution for immune cell migration and chemotaxis experiments. Using these systems, we quantitatively studied neutrophil migration for both research and clinical applications.

First, we developed a compact USB microscope-based Microfluidic Chemotaxis Analysis System (UMCAS), which integrates microfluidic devices, live cell imaging, environmental control, and data analysis to provide an inexpensive and compact solution for rapid microfluidic cell migration and chemotaxis experiments with real-time result reporting. To eliminate the lengthy cell preparation from large amounts of blood, we developed a simple all-on-chip method for magnetic isolation of untouched neutrophils directly from small volumes of blood, followed by chemotaxis testing on the same microfluidic device. Using these systems, we studied neutrophil migration in gradients of different chemoattractants, such as interleukin-8 (IL-8), N-formyl-methionyl-leucyl-

phenylalanine (fMLP), and clinical sputum samples from Chronic Obstructive Pulmonary Disease (COPD) patients.

Previous studies have shown that COPD is correlated with neutrophil infiltration into the airways through chemotactic migration. The thesis work is the first application of the microfluidic platform to quantitatively characterizing neutrophil chemotaxis to sputum samples from COPD patients. Our results show increased neutrophil chemotaxis to COPD sputum compared to control sputum from healthy individuals. The level of COPD sputum induced neutrophil chemotaxis was correlated with the patient's spirometry data.

Collectively, the research in this thesis provides novel microfluidic systems for neutrophil migration and chemotaxis analysis in both basic research and clinical applications. The developed microfluidic systems will find broad use in cell migration related applications.

Acknowledgements

First, I would like to sincerely thank my supervisor, Dr. Francis Lin, for the opportunity to work in his research group. I came to the lab without strong background in biology and microfluidics. He trusted me and provided excellent guidance, mentorship, and support throughout my Ph.D. program. As a supervisor, his door is always open to the students for discussion. Dr. Lin gives his students space to explore their ideas and manage their own problems. Under his supervision, I not only learned many great experimental and research skills, but also acquired the confidence to approach the unknown area independently.

To my co-supervisor, Dr. David Levin, thank you for the invaluable guidance and support during my Ph.D. program. Dr. Levin was always supportive in helping revising manuscripts and providing access to use the facilities in his laboratory.

Great thanks to my doctoral committee members, Dr. Jason Morrison and Dr. Andrew Goertzen, for your valuable suggestions and constructive advice during my research.

I am grateful to my external examiner, Dr. Carolyn Ren, University of Waterloo, for examining my thesis and providing valuable comments.

To the members in Immunotrafficking lab, your great assistance and guidance is invaluable. Specifically, to Dr. Saravanan Nandagopal and Jing Li, thank you for teaching me the knowledge of microfluidics and cell biology in the early days after I came to the lab. To Xun Wu, Kanmani Natarajan, and Dr. Dan Wu, thank you for the helpful discussions and assistance in my research. To Ning Hao, thank you for teaching me cell culture skills. To Jolly Hipolito, thank you for maintaining a great work

environment and support to the lab. I'd also like to thank the other lab members, Dr. Hagit Peretz-Soroka, Dr. Meili Dong, Dr. Zimin Ma, Ke Yang, Iris Halilovic, Jing Ma, Hayden Anning, for all their help and friendship.

I thank Mr. Dwayne Chrusch from Nano Systems Fabrication Laboratory (NSFL) for helping me with the device fabrication. Great thanks to the Victoria General Hospital (VGH) and Seven Oaks General Hospital (SOGH) for helping obtaining blood and sputum samples, to Manitoba Health Research Council (MHRC) for the Graduate Student Fellowships, to CMC Microsystems for the microfluidic device fabrication financial support, to the Department of Physics and Astronomy and Department of Biosystems Engineering for the excellent support to my graduate study.

Many thanks to Dr. Song Liu from Department of Biosystems Engineering at the University of Manitoba, Dr. Michael Zhang from SOGH, Dr. Yong Liu and Dr. Ling Zhu from the Chinese Academy of Science for their great support.

Finally, I would like to thank my family and friends who have given their unwavering support.

Table of content

List of figures

List of tables

List of abbreviations

1-D	one-dimensional
2-D	two-dimensional
3-D	three-dimensional
A1AD	Alpha-1 Antitrypsin Deficiency
C.I.	Chemotactic Index
C. elegans	*Caenorhabditis elegans*
COPD	Chronic Obstructive Pulmonary Disease
dcEF	direct current electric fields
DEP	dielectrophoresis
E. coli	*Escherichia coli*
ECM	extracellular matrix
EC	endothelial cell
EGF	epithelial growth factor
FITC	Fluoro-iso-thiocyanate
fMLP	N-formyl-methionyl-leucyl-phenylalanine
hiPS	human induced pluripotent stem
IL-8	interleukin-8
LTB4	Leukotriene B4
P. haloplanktis	*Pseudoalteromonas haloplanktis*
PCR	polymerase chain reaction
PDMS	Polydimethylsiloxane
S. marcescens	*Serratia marcescens*

S. typhi	*Salmonella typhimurium*
SEM	standard error of the mean
SLT	secondary lymphoid tissues

Permission of using published materials

- Figure 1.1A is reproduced from Integrative Biology, 2009, 1, 170-181 with permission from The Royal Society of Chemistry.
- Figure 1.1B is reproduced from Lab on Chip, 2008, 8, 34-57 with permission from The Royal Society of Chemistry.
- Figure 1.1C is reproduced from American Journal of Physiology - Cell Physiology, 2008 294(2), C526-C534. Permission is not required for use in thesis.
- Figure 1.2A is reproduced from Microfluidics and Nanofluidics 2012, 12(6), 887-895 with permission from Springer.
- Figure 1.2B is reproduced from Lab on Chip, 2008, 8, 227-237 with permission from The Royal Society of Chemistry.
- Figure 1.2C is reproduced from Lab on Chip, 2010, 10, 116-122 with permission from The Royal Society of Chemistry.
- Figure 1.2D is reproduced from Lab on Chip, 2007, 7, 763-769 with permission from The Royal Society of Chemistry.
- Figure 1.3A&B is reproduced from Lab on Chip, 2009, 9, 2707-2714 with permission from The Royal Society of Chemistry.
- Figure 1.3C&D is reproduced from Lab on Chip, 2012, 12, 3968-3975 with permission from The Royal Society of Chemistry.
- Figure 1.4A is reproduced from Langmuir, 2007, 23(22), 10910–10912 with permission from American Chemical Society.
- Figure 1.4B is reproduced from Biomedical Microdevices 2009, 11(4), 827-835 with permission from Sprinter.

- Figure 1.5A is reproduced from PloS one, 2011, 6(3), p. e18183. Open-Access License. Permission is not required.
- Figure 1.5B is reproduced from Integrative Biology, 2010, 2, 639-647 with permission from The Royal Society of Chemistry.
- Figure 1.5C is reproduced from PloS one, 2012. 7(1), p. e29211. Open-Access License. Permission is not required.
- Figure 1.5D is reproduced from Lab on Chip, 2012, 12, 3861-3865 with permission from The Royal Society of Chemistry.
- Figure 1.6A&B is reproduced from PloS one, 2010. 5(7), p. e11921. Open-Access License. Permission is not required.
- Figure 1.6C is reproduced from Integrative Biology, 2010, 2, 630-638 with permission from The Royal Society of Chemistry.
- Figure 1.7A is reproduced from Biomicrofluidics, 2012, 6, 034116 with permission from AIP Publishing LLC.
- Figure 1.7B is reproduced from Biomicrofluidics, 2012, 6, 014102 with permission from AIP Publishing LLC.
- Figure 1.7C is reproduced from Biomicrofluidics, 2012, 6, 024121 with permission from AIP Publishing LLC.
- Figure 1.7D is reproduced from Cellular and Molecular Life Sciences, 2012, 69(16), 2779-2789 with permission from Sprinter.
- Section 1.3 is reproduced from Lab on Chip, 2013, 13, 2484-99 with permission from The Royal Society of Chemistry.

- Section 1.4 is reproduced from Advances in Wound Care, 2014, 3(2), 149-155 with permission from Mary Ann Liebert, Inc..
- Chapter 2 and Appendix is reproduced from Biomedical Microdevices, 2014, 16(4), 521-528 with permission from Springer.
- Chapter 3 with the exception of 3.4.4 is reproduced from PLoS ONE, 2015, 10(5), e0126523. Open-Access License. Permission is not required.
- Chapter 4 is reproduced from "J.D. Wu, C. Hillier, P. Komenda, R. Lobato de Faria, S. Santos, D. Levin, M. Zhang and F. Lin, An all-on-chip method for testing neutrophil chemotaxis induced by fMLP and COPD patient's sputum, Technology, accepted 2016" with permission from World Scientific Publishing Company.

Chapter 1

Introduction

1.1 Overview of directed cell migration and chemotaxis

1.1.1 Directed cell migration and chemotaxis

Cell migration is an essential phenomenon in a vast variety of biological processes. For example, bacteria are able to find food by sensing and swimming towards the gradient of food molecules, or to flee from unfavorable chemicals [1]. At an injury site, a physiological direct current electric field (dcEF) is produced and can attract epithelia cells towards wound [2]. The fibroblasts respond to gradients of platelet-derived growth factor and migrate into the site of a wound [3]. These cells promote healing by reforming the extracellular matrix (ECM) to provide a scaffold for new cell growth and to contract the wound. Metastatic cancer cells have shown the ability to take advantage of the chemotactic signaling pathway used by other cells to respond to gradients of molecules such as epithelial growth factor (EGF) to migrate out of the tumor, into the blood stream and eventually into other tissues [4].

Another set of processes heavily dependent on directional cell migration is that of the immune system [5]. Cells of the innate immune system, such as neutrophils and macrophages, respond to a variety of chemoattractants, produced by invading pathogens, damaged tissues or other components of the immune system, in order to migrate to the site of an infection and to locate and phagocytose pathogens [6]. The trafficking of lymphocytes and dendritic cells of the adaptive immune system is highly dependent on directional cues [7]. Chemoattractic signals recruit these cells to secondary lymphoid

tissues (SLT) such as lymph nodes to enable communications between antigen-presenting cells and effector cells. Later, the effector cells respond to chemical guiding signals to exit SLT and circulate throughout the body for immune surveillance.

Cell migration can be regulated by many externals signals, such as the mechanical properties (mechanotaxis or durotaxis) [8], surface chemical gradient (haptotaxis) [9], soluble chemical gradient (chemotaxis) [10], thermal gradient (thermotaxis) [11], and electric field (electrotaxis or galvanotaxis) [12]. Among them, chemotaxis research shows a significantly high ratio due to its critical importance both in biology and medicine researches [13]. Two types of chemotaxis has been widely studied, the bacteria chemotaxis and eukaryotic cell chemotaxis.

The mechanism of chemotaxis between these two groups is quite different. The bacteria can't sense the spatial concentration gradient due to their small size. Instead, they used temporal sensing mechanism to decide whether the moving direction is correct towards the higher concentration [14]. In contrast, the eukaryotic cells can sense the minute concentration difference across their body and then trigger complex downstream signal cascades and cytoskeleton re-organization to drive directional migration toward the gradient [15]. For example, *Dictyostelium* cells and neutrophils need a concentration difference of 1-percent between front and tails along their length [16, 17].

Chemoattractants are the molecules capable of eliciting chemotactic responses. A number of chemoattractants have been identified. The formyl peptides, such as N-formyl-methionyl-leucyl-phenylalanine (fMLP), are bacterial by-products which have characteristic chemoattractant effects in neutrophils and monocytes [18]. The complement proteolytic fragment C5a and C3a are another type of chemoattractants for

neutrophil and monocytes [19]. Chemokines are a family of small cytokines involved in a variety of immune responses [20]. The chemokines can be classified into four subfamilies by the arrangement of the conserved cysteine residues: CXC, CC, CX3C and XC. Chemokines act as chemoattractants of specific types of leukocytes by activating G protein-coupled receptors. The homing and trafficking of T cells during an adaptive immune response is highly regulated by the chemokines CCL19 and CCL21 and their receptor CCR7 [21]. CXCL-8 (also called interleukin-8, IL-8) is a well-known inflammatory chemokine for guiding the neutrophils migrating into the damaged area during infection or injury [22]. Leukotrines are another type of chemoattractants in leukocyte chemotaxis, which are produced by the oxidation of arachidonic acid. A typical member of this group is Leukotrine B4 (LTB4), another extensively studied neutrophil chemoattractant [23].

Study of the cell chemotaxis has great clinical significance in many aspects. For example, modification of the chemotactic ability of pathogens can help decrease or inhibit the ratio of infections. The disorder of chemotaxis has high relevance in the development of many diseases. For example, impaired CCR7-dependent T-cell chemotaxis was reported in HIV-infected patients [24]. In Chediak-Higashi syndrome, the chemotaxis response of granulocytes are decreased by 60% compared with the normal cells [25]. Reduced neutrophil chemotaxis has also been described in burn victims [26] and in patients with bacterial sepsis or diabetes [27, 28]. Understanding the underlying mechanism of cell chemotaxis in diseases can provide new insights to better monitor and cure these diseases.

1.1.2 Neutrophils, neutrophil migration and chemotaxis

Neutrophils are the most abundant white blood cells. Neutrophils play an essential role in innate immune system as the primary cellular defenders against infection [6]. During infection, neutrophils are guided towards the site of infection following a sequence of tightly regulated steps, including rolling and adhesion in the inner wall of blood vessel, transmigration through gaps between endothelial cells, and chemotactic migration guided by tissue-derived chemoattractants such as IL-8 and LTB4, as well as the pathogen-derived chemoattractants such as fMLP. After recognition of pathogens by specific surface receptors, neutrophils then engulf the microorganisms and utilize oxygen-dependent and oxygen-independent microbicidal approaches to destroy infectious agents.

Neutrophils are widely used as model cell system for cell migration and chemotaxis studies because they are fast-migrating cells and show robust response to multiple chemoattractants. To name a few, researchers have studied neutrophil migration in overlapping gradients of different chemoattractants [29], in temporal switching gradient [30], in confined structures [31], and in two-dimensional (2-D) [32] and three-dimensional (3-D) microenvironments [33]. These studies help understand the underlying mechanism in neutrophil migration and provide useful implications for studying the migration of other cells types.

1.1.3 Conventional cell chemotaxis assay

Chemotaxis research requires assays that can configure controlled chemical concentration gradients. Several conventional experimental methods have been developed and widely used for testing a chemotactic response of cells **(Fig. 1.1)**. A pioneer chemotaxis chamber was constructed by Boyden in 1962 **(Fig. 1.1A)** [34]. A

membrane filter with small holes was placed to separate the chamber into an upper chamber and a lower chamber. Cells were loaded into the upper chamber, while the chemoattractants was filled into the lower one. A diffusion-based gradient through the filter was generated. If a significant number of cells moved through the filter, it confirmed the chemotaxis for that cell type. The Boyden chamber was limited by uncontrolled gradient generation and invisible cell migration process.

Subsequently, in order to enable real time monitoring of single cell migration, the Zigmond chamber was developed [17]. The Zigmond chamber was constructed by two horizontal wells and a shallow channel on the top to connect them. Cells were placed onto a glass coverslip that was placed over the device, bridging the two wells so that the cells contacted with the medium in the shallow channel. The wells were filled with different concentration of chemoattractant and a diffusion based concentration gradient was developed over the bridge. Then the migration of cells towards the higher concentration can be observed. The Dunn chamber is a variant of the Zigmond chamber where the two wells were concentrically placed **(Fig. 1.1B)** [35].

The micropipette-based method is another widely used chemotaxis technology because of its simplicity. A chemoattrantant is introduced near the cells via a micropipette tip and a concentration gradient is generated due to the diffusion (**Fig. 1.1C**) [36]. The steepness of the gradient can be controlled by varying the distance between the cells and the pipette, as well as the chemical injection rate.

Figure 1.1 Conventional chemotaxis assays.

(A) The Boyden chamber [34]; **(B)** The Dunn Chamber [35]; **(C)** The Pipette-based assay [36].

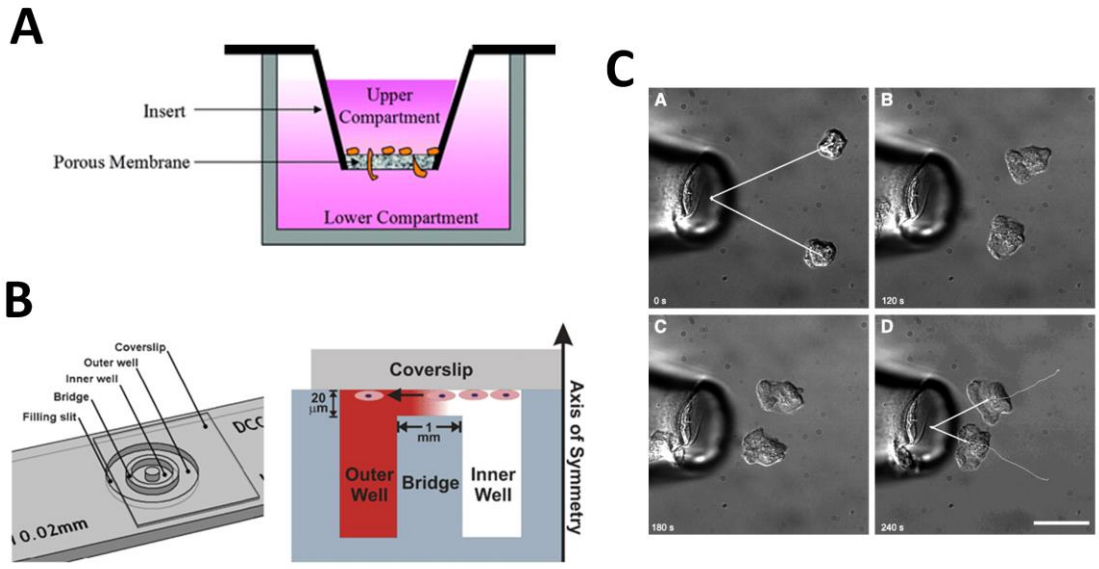

1.2 Overview of development of microfluidics

In the late 1970s, Terry *et al.* in Stanford University developed a miniature gas analysis system based on the principles of gas chromatography [37]. The device used photolithography and chemical etching techniques to make a sample injection valve and a 1.5-m-long separating capillary column on a 5-cm-diameter substrate silicon wafer. This remarkable device opened up the research field of microfluidics. However, the follow-up on this early device has been modest for a long time. Some other works in this period focused on developing on the fabrication of the micro components such as the micro valves, pumps, mixers and sensors [38-41]. Most of these early systems were fabricated by technologies derived from microelectronics – photolithography and etching in silicon and glass. The limited applications of this microfluidics were the chemical analysis using the methods such as capillary electrophoresis [42] and liquid chromatography [43].

Starting from 1990s, the microfluidics developed rapidly since more research groups realized the benefits of using microfluidics in their applications and joined the effort to develop this area. Many ideas from different fields of science started to converge at biological and chemical analysis on microscale. The publications increased sharply and can be roughly classified into two types: the first type was the development of fabrication techniques, including the new selections of materials and fabrication methods; the second type was the diverse applications of microfluidics in many subjects, including analytical chemistry and biochemistry [44], cell biology [45], drug discovery [46], clinical testing [47] and biosystems applications [48]. Microfluidic devices have shown a number of advantages in these applications: the ability to use very small quantities of samples and reagents, and to carry out separation and detections with high resolution and sensitivity;

low cost; and short times for analysis. In the remaining part of this section, I will introduce the fabrication methods of the microfluidics devices based on their materials and the diverse applications of microfluidics.

1.2.1 Fabrication of microfluidic devices based on the materials

1.2.1.1 Silicon and glass microfluidic devices

Most of the early microfluidic devices were fabricated in silicon and glass because they can take advantage of the technologies already existing in the microelectronics and microelectromechanical systems. Microfluidic structures in glass or silicon devices were usually fabricated with microfabriction methods, including several photolithography and etching steps, which are a direct adaptation of the processes developed by the semiconductor integrated-circuit industry [49]. The processes normally start with the deposition of metal or dielectric thin film onto a silicon wafer or glass substrate. A photolithography step then transfers a pattern or image from a photomask onto a photo-sensitive and etch-resistant photoresist coating deposited over the film. The patterned photoresist is used as a template and mask for the subsequent etch steps to pattern the thin film. Once the desired features are etched into silicon wafer or glass substrate, a bonding process is usually performed to attach a cover on top, forming the reaction chambers and fluid channels.

1.2.1.2 Polymer microfluidic devices

Although silicon and glass are attractive materials for fabricating microfluidic devices, the fabrication methods of these types of devices suffers from a large number of complex process steps, use of harmful wet chemistry reagents, and high cost. The introduction of polymer microfabrication technologies has opened new possibilities for

microfluidic applications. Polymers as substrate materials can avoid many of the above-mentioned fabrication challenges. They have a wide range of material properties: mechanical properties, optical characteristics, temperature stability, and resistance against chemicals, and can be biodegradable, and are normally low-cost.

The common fabrication methods of polymer devices include hot embossing, injection molding, and elastomer casting. The selection of methods is dependent on the materials. Hot embossing and injection molding are suitable for the thermoplastic and duroplastic polymers, while elastomeric polymer devices are usually fabricated using elastomer casting. The hot embossing microfabrication process is straightforward [50]. After fabrication of the master mold, it is mounted in the embossing system together with a planar polymer substrate. Both are heated to a temperature just above the Glass Transition Temperature of the polymer material. The pattern is then imprinted into the polymer by pressing the mold on the polymer substrate at certain pressure.

Inject molding is another widely used technology in the macroscopic world to fabricate polymer components, which has also been applied for the fabrication of microfluidic devices [51]. The process starts with the melt of raw polymer material. This melt is then transported forward toward the mold cavity. The molten material is then injected under high pressure into the evacuated cavity, which contains the mold insert as the master structure.

A process finding increasing use mainly in the academic world is casting of silicone based elastomers. Casting generally offers very flexible and low-cost access to planar microchannel structures and is therefore very well suited for rapid prototyping. In this microfabrication technique, a mixture of the elastomer precursor and its curing agent

are poured over the molding templates. These templates can be made by variable methods, such as silicon surface micromachining, lithographically patterning of a photoresist layer and might be surface modified for better mold release. After curing, the soft elastomer copy can simply be peeled off the mold and placed against a planar surface, for example, a glass slide, a plastic sheet, to form closed channels. Among the elastomers, polydimethylsiloxane (PDMS) has become the most widely used material for making microfluidic device in research labs owing to its suitable optical property, biocompatibility, low-cost, and fabrication control, therefore ideal for rapid prototyping of different designs [52].

1.2.1.3 Paper microfluidic devices

In 2007, Martinez *et al.* at used a photolithography technique to make a paper-based microfluidic channels [53]. They patterned paper to create well-defined, millimeter-sized channels, comprising hydrophilic paper bounded by hydrophobic polymer. By building microfluidic channels on paper, liquid flow is confined within the channels and can be guided in a controlled manner. After that, many paper-based microfluidic devices have been developed, providing a novel system for fluid handling and fluid analysis for a variety of applications including health diagnosis, environmental monitoring as well as food quality testing [54].

The reasons why paper becomes an attractive substrate for making microfluidic systems include: (1) it is a ubiquitous and extremely cheap cellulosic material; (2) it is compatible with many chemical/biochemical/medical applications; and (3) it transports liquids using capillary forces without the assistance of external forces [54]. Fabrication of paper-based microfluidic devices is based on patterning sheets of paper into hydrophilic

channels (paper) bounded by hydrophobic barriers. The patterning process defines the width and length of paper-based microfluidic channels; the thickness of the paper defines the height of the channel.

There are many techniques reported in the literature for fabricating paper-based microfluidic devices: (1) photolithography [53] (2) plotting with an analogue plotter [55] (3) ink jet etching [56, 57] (4) plasma treatment [58] (5) wax printing [59-61] (6) paper cutting [62, 63] (7) ink jet printing [64] (8) flexography printing [65] (9) screen printing [66] and (10) laser treatment [67]. The main application of paper-based microfluidic devices is to provide a low-cost, easy-to-use, and portable analytical platform for chemical and biochemical assays. However, the limitation of the paper microfluidic devices is that the limit of the detection is usually high, making them insufficient for the analysis of samples of very low concentration [54].

1.2.2 Microfluidic applications in chemistry

Microfluidic devices have been widely applied to protein and nucleic acids analysis [44]. Profiling proteomics is used to identify all of the proteins in a sample or to compare changes in protein expression between several samples. Due to the complexity of the proteome, accurate analysis requires a great deal of sample processing, including proteolytic digestion, followed by multidimensional separations and mass spectrometry. The traditional way to prepare sample for profiling proteomics typically requires hours-days and the process is tedious. In contrast, microfluidic devices have shown great promising in this field. For example, Liu *et al.* used surface adsorbed trypsin in micro channels to enable complete digestion in less than 5s [68]. Also, sample purification and concentration can be carried out in microfluidics [69].

Traditionally, enzymatic assays and immunoassays are performed in microtitre plates (plastic trays containing arrays of isolated wells). Microfluidic devices can perform enzymatic studies without interference between individual elements and consume small volumes of enzyme. Jiang *et al.* patterned antigens on a membrane via a microfluidic network, and then positioned the membrane under a microdilution network to carry out serially-diluted immunoassays to detect multiple antigens on the patterned surface [70]. This fluidic network enables the simultaneous quantitation of several molecules that vary widely in concentration. Wang *et al.* developed an integrated microfluidic solid-phase ELISA platform for rapid and ultrasensitive detection of proteins. The microwell-patterned assay chamber structure of the device significantly reduces the volume of chemifluorescent reaction, markedly improving the sensitivity and speed of ELISA. Martinez *et al.* developed a paper microfluidic device that can simultaneous detect glucose and protein in 5ul of urine [53].

Microfluidic devices have also been applied to protein crystallization, a process that serves as the basis for X-ray crystallography for determining the protein's three-dimensional structure. Zhou *et al.* developed a 3×52 array platform involving nanoliter dispensing for screening protein crystallization conditions [71].

The conventional biochemical DNA analysis requires several steps in common, including precise volume measurement of reagent and DNA-template solutions; mixing of solutions; controlled thermal reaction of the mixture; loading of the reaction products onto an electrophoresis device; and detection of reaction products. The complete process is time-consuming and labor-intensive. The required volume of reagent and samples is big and the expensive equipment makes the testing costly. However, all of these complex

processes can be performed in a single microfluidics device. Burns *et al.* developed such an integrated nanoliter DNA analysis device, which integrated fluidic channels, heaters, temperature sensors, and fluorescence detectors in a single device [72]. The device is capable of measuring aqueous reagent and DNA-containing solutions, mixing the solutions together, amplifying or digesting the DNA to form discrete products, and separating and detecting those products. In DNA analysis, the polymerase chain reaction (PCR) process is widely used as a molecular biological tool to replicate DNA, and can create copies of specific fragments of DNA by cycling through three temperature steps. However, the conventional PCR instruments usually have low ramping rate in the temperature range relevant for PCR, which results in long analysis time. Instead, as demonstrated in the first PCR chip by Northrup *et al.* [73, 74], the microfluidic-based PCR technologies have facilitated DNA amplification with much faster rates as the result of smaller thermal capacity and larger heat transfer rate between the PCR sample and temperature-controlled components.

1.2.3 Microfluidic applications in cell biology

Microfluidic devices provide an excellent platform for the sorting and culture of cells, and are an extremely useful tool for the investigation of cellular responses to various stimuli [45]. Advantages offered over traditional methods include cost-effectiveness, controllability, low volume, high resolution, and sensitivity.

Cell separation is a useful cell manipulation tool in the microfluidic device, capable of isolating cells of interest from a complex background. Various types of cell separation methods have been developed, based on mechanical forces, dielectrophoresis (DEP), optical interactions, magnetic interactions and biochemical interactions. Warkiani

et al. developed a slanted spiral microfluidics for the ultra-fast, label-free isolation of circulating tumor cells [75]. The technique utilizes the inherent Dean vortex flows present in curvilinear microchannels under continuous flow, along with inertial lift forces that focus larger circulating tumor cells against the inner wall. By using a single spiral microchannel with one inlet and two outlets, they have successfully isolated and recovered more than 80% of the tested cancer cell line cells spiked in 7.5 mL of blood within 8 min with high purity. For optical methods, fluorescent sorting in microfluidic devices have been demonstrated. Fu *et al.* developed a microfabricated fluorescence-activated cell sorter, which provides higher sensitivity and no cross-contamination at a lower cost [76]. The cells are manipulated with electro-osmotic flow. DEP is another excellent approach to sort cells. Viable from nonviable human lung cancer cells (A549-luc-C8) have been separated using DEP operating at 16 MHz [77].

For precision cell analysis and manipulation, it is often desirable to trap cells and culture them in defined locations. The trapping or patterning of cells in different locations in microfluidics can be divided into three types. The first method is the microcontact printing, which is a simple method for directly patterning biomolecules on surfaces. Inking a stamp is done by simply adsorbing proteins from solution onto the hydrophobic surface of a PDMS stamp. After the stamp is rinsed, dried, and placed in contact with a surface, adhesion forces cause proteins to transfer from the stamp to the printed surface. Chen *et al.* used this technology to culture cells in the confined micropatterned substrates that contains extracellular matrix-coated adhesive islands [78]. They found that the cell shape of the human and bovine endothelia cells was able to govern whether individual cells grow or die. The second method is to use the microfluidic channel to deposit the

cells and proteins onto surfaces. Chiu *et al.* developed a three-dimensional microfluidic system to pattern proteins and mammalian cells on a planar substrate [79]. The 3-D topology of the microfluidic network in the stamp makes this technique a versatile one to pattern multiple types of proteins and cells in complex, discontinuous structures on a surface. The third method is to use the topological structure to confine cells in a defined geometry. Lee *et al.* developed a nanoliter scale microbioreactor array for multiplexed quantitative cell biology [80]. An addressable 88 array of three nanoliter chambers was demonstrated for observing the serum response of HeLa human cancer cells in 64 parallel cultures. The individual culture unit was designed with a ‘‘C’’ shaped ring that effectively trapped the cell and decoupled the central cell growth regions from the outer fluid transport channels.

As mentioned before, cell migration is an essential phenomenon in a variety of biological processes. Microfluidic device is well suited for the cell migration studies due to its great ability to generate well-defined external stimulation environment. For example, Hsu *et al.* used a micropatterning technique to generate step changes of collagen surface density [9]. Due to haptotaxis, endothelial cells (ECs) developed focal adhesions and migrated into the area with higher surface density of collagen. In the same device, they also introduced different levels of fluid shear stress on ECs in the direction perpendicular to collagen stripes to investigate the interactions between haptotaxis and mechanotaxis. Their results suggest that shear stress beyond a certain threshold can be a predominant factor to determine the direction of EC migration. Physiological dcEF produced at the wound and electrical attraction of epithelial cells for wound recovery is well-known. Research towards better understanding the mechanisms of electrotaxis is an

important and rapidly growing area with direct relevance to wound care. Li *et al.* developed two microfluidic devices allowing controlled application of electric fields inside the microfluidic channel to study the lymphocyte electrotaxis [81]. Their results showed that anti-CD3/CD28 antibodies activated human blood T cells migrate to the cathode of the applied dcEF.

1.3 Overview of recent microfluidic-based chemotaxis studies

This section is based on the following publication: "**J.D. Wu,** X. Wu and F. Lin, "Recent developments in microfluidics-based chemotaxis studies". **Lab on Chip**. 2013, 13(13):2484-99.".

Compared with conventional cell migration assays as mentioned in the previous section [17, 34, 82, 83], microfluidic devices provide a new experimental platform for quantitative cell migration and chemotaxis studies under better controlled gradient conditions [84].

1.3.1 Microfluidic gradient generation

Microfluidic gradient-generating devices can be broadly categorized as: 1) flow-based devices; and 2) flow-free devices. The flow-based devices rely on laminar flow mixing in microfluidic channels to create highly controlled chemical gradient profiles. On the other hand, the flow-based devices require peripheral chemical perfusion and expose cells to shear forces. By contrast, the flow-free devices produce gradients by free diffusion of chemicals in a static fluidic environment; therefore, they are less dependent on external controls and the flow effect on cells is minimized. However, the flow-free devices are compromised for its flexibility of controlling gradient profiles. Therefore, both flow-based and flow-free devices require innovations to overcome their respective limitations. In this section, some recent new developments in microfluidic gradient generation are highlighted.

1.3.1.1 One-dimensional gradient generation

Most microfluidic devices generate one-dimensional (1-D) chemical gradients. The network gradient generators [85] are commonly used for chemotaxis studies [86, 87].

These devices can produce a well-defined 1-D gradient but require external fluid perfusion. To release the device from external perfusion, Gao *et al.* used gravity-based passive pumping to drive the fluid into the network channels for gradient generation [88] **(Fig. 1.2A)**. A pressure balancing circuit was added before the downstream network channels to balance inlet flows. The network channels create the required fluidic resistance to maintain the low flow rate over a long time. Recently, Xu *et al.* used commercial osmotic pumps for portable and long-term gradient generation [89]. Despite the attractive portability of these devices, they are limited to fixed flow rate or single use of the osmotic pumps.

In contrast to the designs to simplify fluid delivery, another approach aims at further realizing the potential of microfluidic network devices for flexibly generating different gradient profiles [90-98]. As one example in this direction, Wang *et al.* developed a microfluidic device that connects multiple upstream network modules to the downstream cell seeding chambers. Fluid delivery are modulated by on-chip valves to control input chemical configurations and fluidic path through the network module for flexible gradient generation in both soluble and surface-bound forms [91] **(Fig. 1.2B)**. Furthermore, an array of parallel micro-wells within the cell culture area was etched into the underlying glass coverslip. This feature selectively increases the chamber height at locations where cells reside, which help reduce flow-induced shear stress. On the other hand, these sophisticated features for controlling gradients and cells are compromised by the more complicated device fabrication for making on-chip valves and micro-wells.

Beta *et al.* reported a new method that combines a microfluidic device with the photochemical release of caged signalling molecules to generate tailored stimuli on the

length scale of single cells with subsecond switching time [99]. Such an approach enables spatiotemporal gradient stimulation with high resolution while it requires caged chemoattractant molecules and laser scanning.

While the flow-based devices provide the powerful feature for gradient control, it simplifies the physiological autocrine and paracrine effects among migrating cells and can cause shear stress to cells. In addition, it has been shown that the actual gradient across the cell in a flow-based device can significantly differ from the gradient in a smooth channel without cells [100].

In addition to the flow-based devices, various flow-free microfluidic devices were developed for generating 1-D gradients. Many flow-free devices require physical barriers such as membrane or gel to increase the fluidic resistance as a means to control chemical diffusion [89, 101, 102]. Although this method is useful, it also increases the complexity of the fabrication process and the time for gradient establishment. Berthier *et al.* developed a microfluidic device for gradient generation based on free chemical diffusion between the source and the sink through thin microfluidic channels [103]. Furthermore, a useful bypass channel with much larger dimensions than the gradient channel was designed to connect the source and the sink for balancing the pressure. Kong *et al.* employed a microfluidic device with a similar bypass bridge channel to investigate fibroblast chemotaxis in EGF gradient [104]. Despite the simplicity, these devices are more suitable for maintaining gradient over short-term.

Based on the similar principle, different ladder-shaped devices (i.e. two side channels connected by multiple thin parallel microgrooves) have formed a distinct class of flow-free microfluidic gradient generators [105-108]. In most of these devices, two

parallel channels are designed as perfect source and sink by continuous replenishment of chemicals. Horizontal microgrooves, which connect the two parallel source/sink channels, serve as the gradient channels. The ladder-shaped devices allow parallel gradient generation in a flow-free environment. The main limitations of these devices are the requirement of more complicated multi-depth channel fabrication and the limited gradient channel height required for gradient generation.

Instead of generating gradients in the thin microgroove channels, another class of microfluidic gradient device consisting of three parallel channels has been developed. Those three-channel devices typically consist of parallel side channels as the source and sink, which are connected to a center gradient channel through barrier structures. Some devices of this class use microgrooves as the barrier to connect the source/sink channels with the gradient channel [109-111]. Keenan *et al.* developed a variant of the three-channel device, in which an array of microjets (or microgrooves) were used to connect the two side channels and control the release of chemicals into the open cell culture reservoir [109] **(Fig. 1.2C)**. This device allows rapid variation of gradient profiles.

In addition to the microgroove-based approach, gels were introduced to the three-channel microfluidic device to enable controlled 1-D gradient generation [89, 112-117]. Cheng *et al.* developed a microfluidic gradient generator that consists of three parallel channels patterned on a piece of agarose gel [115] **(Fig. 1.2D)**. Source and sink chemical solutions flow through the two outer channels and the chemicals diffuse across the agarose gel into the center channel to form a linear gradient at the steady state.

Figure 1.2 Examples of 1-D microfluidic gradient generation.

(A) A standalone microfluidic network gradient generator using on-chip passive pumps and a flow balancing circuit [88]; (**B**) A microfluidic device that combines multiple upstream network modules, the downstream cell seeding chambers and on-chip pneumatic valves for flexible gradient generation [91]; **(C)** A microfluidic device for generating flow-free gradient in an open environment [109]; **(D)** An agarose gel-based microfluidic device for generating flow-free gradients [115].

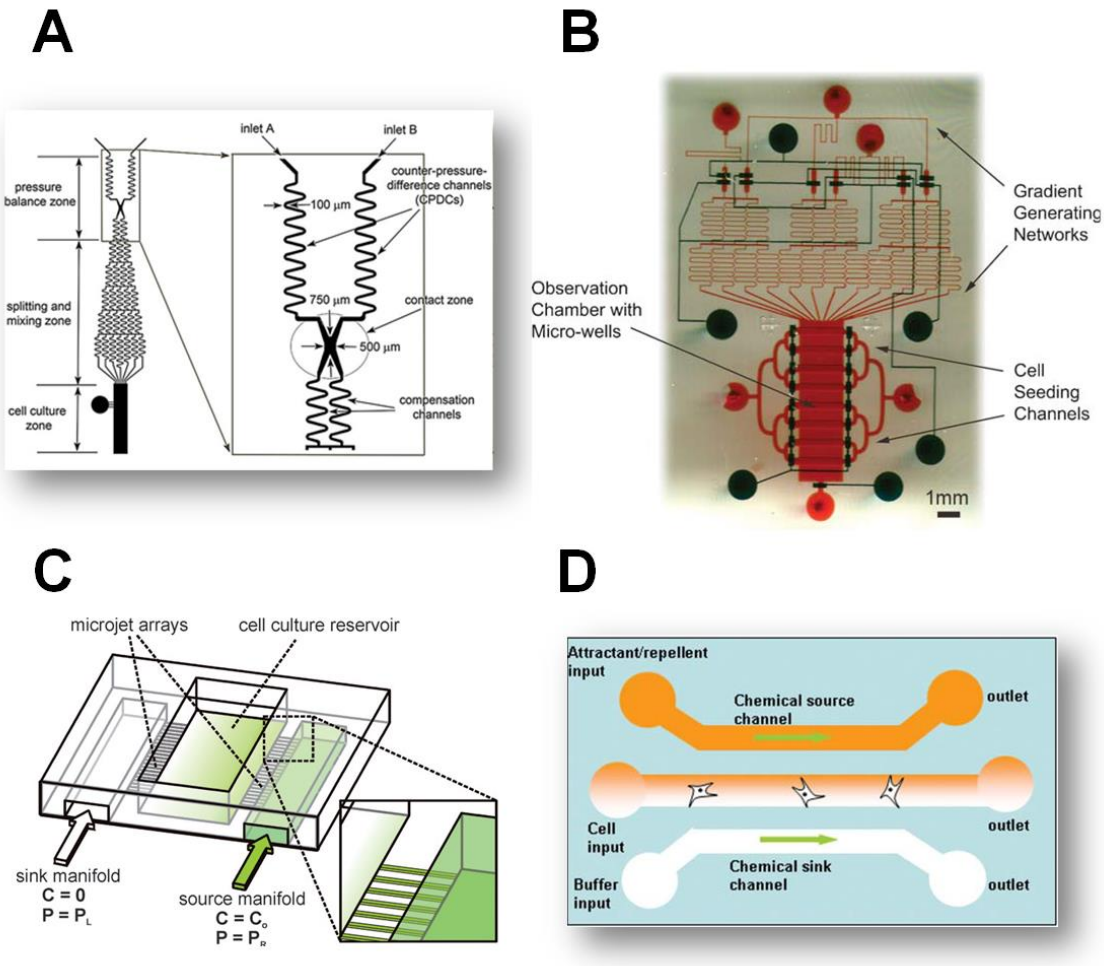

1.3.1.2 Two-dimensional gradient generation

Because a 1-D gradient simplifies the *in-vivo* chemical gradient environment, an increasing number of studies have been directed toward generating controlled gradients in a two-dimensional (2-D) plane using microfluidic devices [118-120]. Over recent years, innovations in developing new microfluidic devices for generating 2-D gradients with diverse approaches have shown promising progress. Atencia *et al.* developed a microfluidic palette, which can generate spatiotemporally controlled 2-D gradients [119] **(Fig. 1.3A & 1.3B)**. In this device, the gradient chamber and the chemical infusion channels are separated into different layers, so that multiple gradients can be generated and superimposed in the flow-free gradient chamber in a 2-D plane. Changing the chemical inputs can modify 2-D gradients in space and in time. The applicability of the developed device was demonstrated to study chemotactic response of bacteria *Pseudomonas aeruginosa* (*P. aeruginosa*) to glucose. Choi *et al.* presented a different method by introducing self-assembled microspheres to control chemical diffusion for rapid generation of superimposed multiple gradients in 2-D [120] **(Fig. 1.3C & 1.3D)**. The developed system was used to study preferential bacteria chemotaxis in multiple competing chemoattractant sources, and the results identified aspartate as the preferred chemoattractant over galactose and ribose. In addition, this device was used to demonstrate the dynamic control of bacteria positioning to sequential changes of chemical gradients from different angles in a 2-D plane. Other strategies for producing 2-D gradients include the floating gradient method reported by Qasaimeh *et al.* [121]; gradient generation in an open environment reported by Wright *et al.* [122]; and optical manipulation of chemical microsources reported by Kress *et al.* [123].

Figure 1.3 Examples of 2-D microfluidic gradient generation.

(A) The microfluidic palette device uses stacked multi-layer channels for generating 2-D gradients [119]; (**B**) Picture of superimposed gradients in the microfluidic palette device [119]; **(C)** The 2-D microfluidic gradient-generator incorporating self-assembled microspheres [120]; **(D)** Picture showing self-assembled microspheres at the chemical entrance to the gradient chamber [120].

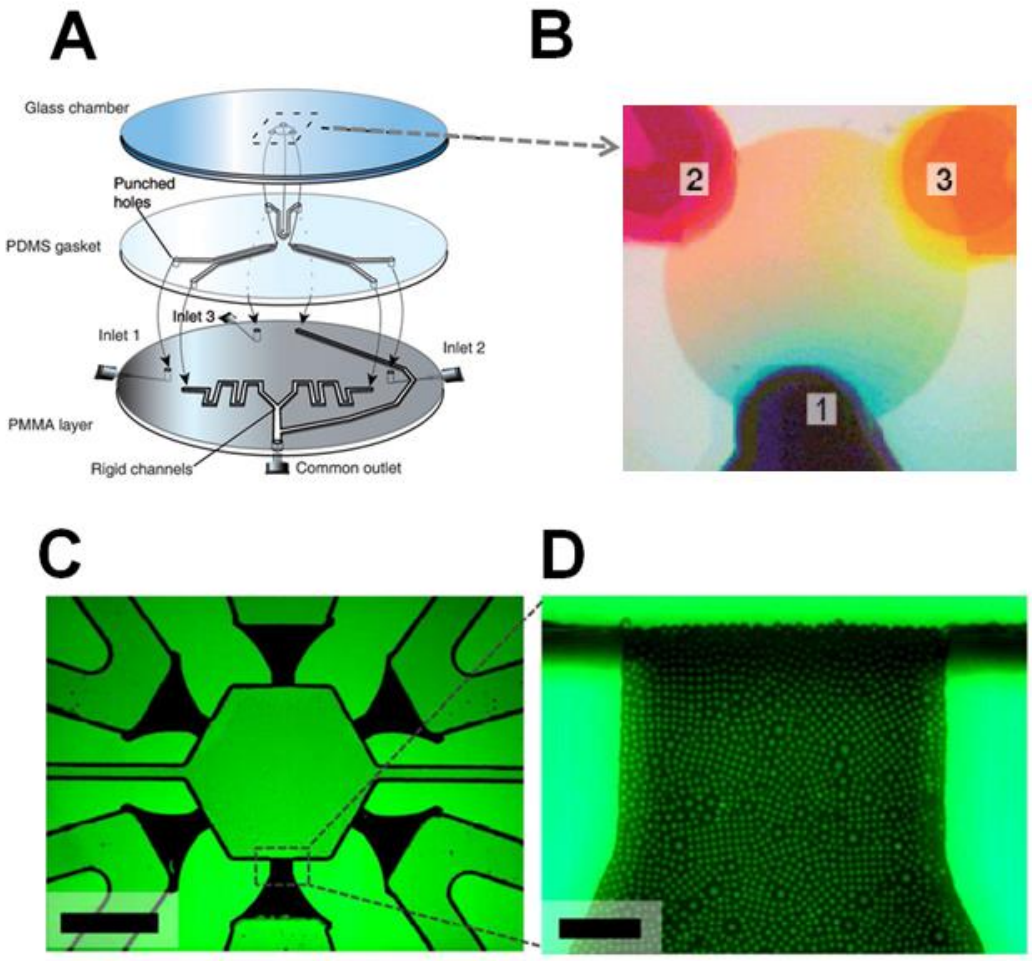

1.3.1.3 Three-dimensional gradient generation

Cells migrate in three-dimensional (3-D) tissue environments *in vivo*. Compared with cell migration in 1-D or 2-D gradients, in which cells adhere to a 2-D substrate, cell migration in a 3-D microenvironment requires the ability of cells to squeeze through ECM [124]. Therefore, it is important to develop microfluidics-based biomimetic approaches to study cell migration in 3-D environments. Many 3-D microfluidic devices were derived from 1-D gradient devices by incorporating 3-D ECM for gradient generation and cell migration [33, 105, 125-128]. For example, the ladder-shaped devices were modified for gradient generation in 3-D ECM [105, 127]. Saadi *et al.* extended the use of the ladder-shaped device to generate gradients in 3-D gels **(Fig. 1.4A)**. This method later was further developed to vary gradient profiles by adjusting the relative geometry of the microgroove channels on each side of the gradient channel [106]. Kim *et al.* reported a ladder-shaped device for 3-D gradient generation in a standard 96-well format [129]. As an alternative approach, Haessler *et al.* modified the 1-D agarose gel based three-channel device to allow 3-D cell migration applications **(Fig. 1.4B)**. In this device, agarose gel walls are used to control chemical diffusion from the source/sink channels to the center gradient channel, which contains cells in 3-D gel matrix [125]. The developed device was used to demonstrate murine dendritic cell chemotaxis to chemokine gradients. Although 3-D gradient devices provide more physiologically realistic environments for cell migration, further improvement and innovation are required to enable more flexible control of gradient generation.

Figure 1.4 Examples of 3-D microfluidic gradient generation.

(A) The microfluidic ladder device for gradient generation in 3-D gel [105]; (**B**) The microfluidic device with agarose gel walls to separate source/sink channels to the gradient channel for gradient generation in 3-D ECM [125].

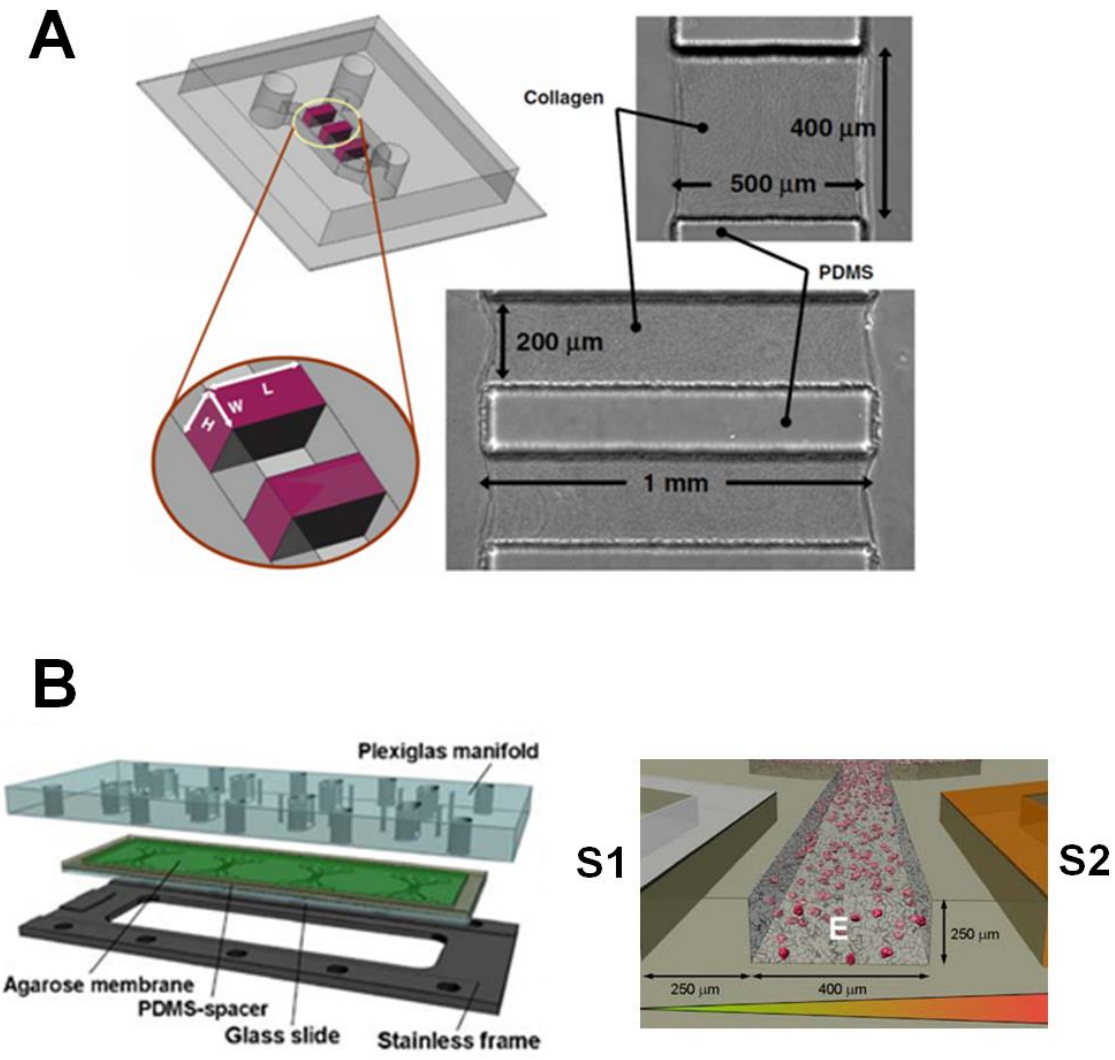

1.3.2 Chemotaxis studies based on cell types

Highly controlled chemical gradients in microfluidic devices offered a powerful research approach for studying gradient sensing and chemotaxis of different cell types. High motility cells such as bacteria and neutrophils were first tested in microfluidic gradient devices. In recent years, a broader range of cell types have been studied using microfluidic devices. In this section, we highlight recent microfluidic chemotaxis studies based on cell types.

1.3.2.1 Bacteria

Bacteria are able to measure chemical gradients towards favourable chemicals or away from unfavourable ones. Because bacteria swim in soluble medium, its migration is strongly influenced by flows. Both flow-based and flow-free microfluidic gradient-generating devices have been extensively used for bacteria chemotaxis studies.

Escherichia coli (*E. coli*) and *Salmonella typhimurium* (*S. typhi*) are closely related bacterium. Particularly, *E. coli* is well-studied as a model system for bacteria chemotaxis. Microfluidic devices have been used for chemotaxis studies of these bacteria cells [89, 113, 114, 130-134]. For example, Ahmed *et al.* characterized *E. coli* chemotaxis in steady single linear or non-linear gradient using a flow-free microfluidic device, and the experimental data are consistent with the established mathematical model [117]. In 1-D competing gradients produced in a flow-based microfluidic device that mimic the human gastrointestinal environment, Englert *et al.* showed that the quorum-sensing molecule autoinducer-2 preferentially induces chemotaxis of *E. coli* and thus represents a preferential signal for pathogen colonization in the gastrointestinal tract [135]. Kalinin *et al.* used a three-channel microfluidic device to demonstrate logarithmic

gradient sensing of *E. coli* cells [113]. Using a similar device, the same group examined *E. coli* migration in opposing gradients of methyl-aspartate and serine, and the results demonstrated the direct dependence of *E. coli* chemotaxis on the ratio of the respective receptor numbers (i.e. Tar/Tsr) for the two chemoattactants [114]. Kim *et al.* presented an agarose-gel based microfluidic method for testing preferential chemotaxis of *E. coli* cells to different chemoattractant sources [102]. Using the 2-D microfluidic gradient generator by incorporating self-assembled microspheres Choi *et al.* showed that *S. typhi* are more sensitive to aspartate than galactose or ribose in competing gradients of these chemoattractants [120],.

In addition to *E. coli* and *S. typhi*, chemotaxis of other bacteria cells was also studied using microfluidic devices. For example, Chen *et al.* and Jeong *et al.* examined *P. aeruginosa* chemotaxis using different microfluidic devices [136, 137]. Kim *et al.* demonstrated steering polystyrene beads by the attached chemotaxing *Serratia marcescens* (*S. marcescens*) cells using a three-channel microfluidic gradient device [112]. Moreover, several microfluidic chemical pulse injectors were employed to study the migratory responses of marine bacterium. Among them, Stocker *et al.* showed the accumulation response of *Pseudoalteromonas haloplanktis* (*P. haloplanktis*) cells to a nutrient pulse [138]; The same group further examined migratory responses of various marine microorganisms to nutrient patches including chemotactic responses of *P. haloplanktis* [139].

1.3.2.2 Dictyostelium discoideum

Aggregation of the social amoeba *Dictyostelium discoideum* forms a multicellular structure that is enabled by the migration of *Dictyostelium* cells towards a cAMP gradient

[140]. Like *E. coli*, *Dictyostelium* serves as a chemotaxis model system but for eukaryotic cells. Using a flow-based microfluidic gradient device, Fuller *et al.* showed that *Dictyostelium* chemotaxis depends on both the steepness and the local concentration of the cAMP gradient [141]. Skoge *et al.* studied the localization of intracellular chemotactic signaling molecules in *Dictyostelium* cells using microfluidic devices and the results help understand signaling amplification mechanisms for cell directional sensing [142]. Meier *et al.* applied a flow-based microfluidic device to study *Dictyostelium* cell responses to spatially alternating chemoattractant gradients [143]. The results showed the frequency-dependent ability of cells to adjust their orientation to switching gradients and furthermore the differential role played by PI3-Kinase in mediating cell reorientation during different stages of chemotactic aggregation. More recently, Ameselem *et al.* used microfluidics-based experimental data to assist in developing stochastic descriptions of *Dictyostelium* chemotaxis [144] and to test the theoretically predicted control of chemotaxis by signal-to-noise ratio [145].

1.3.2.3 Immune cells

Compared to bacteria or *Dictyostelium*, immune cells exhibit more diverse subset-dependent and tissue-specific chemotaxis patterns. Immune cells respond to a wide range of chemoattractants including bacteria-derived peptides, complement factors, lipid products and chemokines. Chemotaxis mediates various immune responses such as recruitment of neutrophils to sites of infection, and homing of dendritic cell and lymphocytes to specific tissues.

Neutrophils respond to bacterial-derived chemoattractants such as fMLP and tissue-derived chemoattractants such as IL-8 and LTB4. Herzmark *et al.* employed a

microchannel network and membrane valves for quantitative chemotaxis analysis of differentiated neutrophil-like HL-60 cells in fMLP gradients [94]. Liu *et al.* applied a switching gradient in a microfluidic device to study the role of PI3-Kinase for cell orientation and migration responses [97]. Instead of limiting cells to a single gradient channel, Ambravaneswaran *et al.* developed a microfluidic maze with co-existing migration paths to examine the directional decision-making behaviors of neutrophils [31]. Irimia *et al.* employed a previously developed microfluidic gradient device that allows fast gradient switching to provide experimental data for constructing an adaptive-control model for neutrophil chemotactic orientation [146]. Sackmann *et al.* presented a versatile microfluidic assay for rapid neutrophil chemotaxis analysis in both 2-D and 3-D environments [147]. The developed assay was validated to compare the adhesion and migration of neutrophils from chronically inflamed and wild-type mice.

Dendritic cell can take up antigens from inflamed tissue and traffic into T cell rich areas of secondary lymphoid organs through chemotaxis mechanisms. Several chemokines, including CCL19, CCL21 and CXCL12, have been implicated in mediating dendritic cell migration and trafficking in SLT. Ricart *et al.* employed a flow-based microfluidic device to examine dendritic cell chemotaxis in different single or combined chemokine gradients and to compare their relative chemoattraction [148]. The same group incorporated micropost arrays with the microfluidic network gradient device to study the traction force of dendritic cells during chemotaxis and chemokinesis [86]. The PDMS micropost arrays were fabricated on glass coverslips and bonded to the microfluidic gradient generator. Cells adhered to the microposts and the forces exerted by the cells on the microposts were measured by the displacements of the microposts. Using

a 3-D microfluidic gradient device, Haessler *et al.* demonstrated the stronger dendritic cell chemotaxis to CCL21 in competing gradients of CCL19 and CCL21 [149]. Also focusing on secondary lymphoid tissue-related chemokines, our group employed a simple flow-based microfluidic gradient generator to study the migration of activated human blood T cells in different CCL19 and CCL21 gradient configurations [21].

1.3.2.4 Stem cells, cancer cells and other tissue cells

Stem cells can uniquely give rise to different specialized cell types that construct functional tissues or organs. Therefore, it is important to characterize and understand the homing mechanisms of different stem cell types in tissues. Wong *et al.* analyzed the migration of neural stem cells under various chemical conditions using an agarose gel-based microfluidic device, and the results showed the effect of over-expression of epidermal growth factor receptors on cell motility [150]. Xu *et al.* used a portable flow-based microfluidic gradient device to monitor chemotaxis of bone marrow mesenchymal stem cells [89]. Our group studied the growth and migration of rodent adipose-derived stem cells to an EGF gradient using a simple flow-based microfluidic gradient generator [151].

Migration and chemotaxis of various cancer cells are largely responsible for the translocation and spread of tumors. Zhang *et al.* developed a microfluidic model that reconstitutes the principal components of blood vessels, including vessel cavity, endothelium, and perivascular matrix containing chemokines, to study the migration of salivary gland adenoid cystic carcinoma cell aggregates [152]. Mosadegh *et al.* employed the microfluidic network gradient generator to show the role of EGF for promoting breast cancer cell chemotaxis in a chemokine gradient [153].

Directed migration of tissue cell types is an important enabling process for their growth and assembly pertaining to specific biological and physiological functions. Barkefors *et al.* employed a flow-based microfluidic gradient device to investigate endothelial cell migration in response to hill-shaped gradients of vascular endothelial growth factor A and fibroblast growth factor 2 [154]. The results from quantitative gradient-region specific cell migration analysis helps better understand how endothelial cells approach growth factor sources and the corresponding shifting of migration phenotype of these cells. In another study using a flow-free microfluidic gradient device, Shamloo *et al.* investigated endothelial cell polarization and chemotaxis, with a focus on the distinct roles played by the absolute concentration and the gradient of vascular endothelial growth factor [110] . Kong *et al.* used a flow-free microfluidic gradient device with a unique bridge balancing channel to quantitatively characterize chemotactic responses and sensitivity of fibroblast to EGF gradients [104]. Wu *et al.* employed a three-channel microfluidic gradient device to demonstrate the differential requirement of lamellipodia for fibroblast chemotaxis and haptotaxis [155].

1.3.3 Chemotaxis studies in complex environments

Comparing to conventional cell migration assays, microfluidic devices are advantageous to flexibly manipulate complex spatiotemporal chemical gradients and construct defined geometric environments for cell migration.

Chemoattractant fields are presented to cells in complex spatiotemporal patterns in tissues, and cells can integrate and prioritize multiple chemotactic signals for effective navigation and positioning. Microfluidic devices can uniquely configure defined co-existing chemoattractant gradients and thus are well-suited for studying the complex

chemical guiding mechanisms. Ricart *et al.* employed a microfluidic network gradient-generator to study dendritic cell migration in competing chemokine gradients on a 2-D substrate [148]. The results showed that CCL19 is more effective for attracting dendritic cell migration than CCL21 or CXCL12. By contrast, Haessler *et al.* showed that cells preferentially migrate towards the CCL21 gradient over a competing CCL19 gradient in 3-D ECM using a flow-free microfluidic gradient device [149]. The opposite observations of the relative chemotactic potency between different chemokines for dendritic cell in these two studies possibly reflect different cell gradient sensing and migration mechanisms in 2-D substrates or in 3-D ECM. Our group employed a simple flow-based microfluidic gradient device to examine T cell migration in different single or combined CCL19 and CCL21 gradients that mimic different lymph node sub-region gradient profiles [21] **(Fig. 1.5A)**. Particularly, our results showed the interesting repulsive T cell migration in a combined field of CCL19 and CCL21. Together with mathematical modeling, our group proposed a dual CCR7 ligand mediated combinatorial guiding mechanism for T cell migration and trafficking in SLT. Besides lymphocytes and dendritic cells, some microfluidics-based approaches were also applied to study bacteria chemotaxis in co-existing chemoattractant gradients [102, 114, 120, 135]. These quantitative cell migration studies in co-existing gradients help understand the mechanisms for cell migration and trafficking in physiological contexts. Further studies in this direction require improved knowledge of gradient profiles in vivo.

During inflammation, immune cells navigate through complex tissues and traffic to the target site. Similarly, tumor cells from their primary site invade surrounding regions by migrating through complex tissue environments. Recently, microfluidic

devices were designed to engineer complex planar geometries for studying how cells make directional migration decisions. Ambravaneswaran *et al.* developed a microfluidic maze consisting of bifurcating channels to investigate the directional decision-making of neutrophils [31] **(Fig. 1.5B)**. The results show that neutrophils can undergo highly robust and efficient chemotactic navigation. Specifically, in complex maze-like channels, neutrophils are able to select the most direct route toward the chemoattractant source with high efficiency. The more effective chemoattractant gradient toward the short path experienced by neutrophils at the junction of the short and long path is suggested to assist cells to distinguish different paths and make directional migration decisions.

Physiological cell migration environments are often spatially confined. Such geometric confinement can be mimicked using microfluidic devices to examine its effect of on cell migration and chemotaxis. Fu *et al.* developed a device that consists of an array of microchannels mimicking the tight syncytium of endothelial cells that lines the capillaries, which are encountered by tumor cells during metastasis [156]. The study showed that nuclear deformation is a critical and rate-limiting step for transmigration of highly metastatic human breast cancer cells in the confined microfluidic channels. Tong *et al.* employed a microfluidic device, which can directly compare inherent migratory potential among multiple cell types [157] **(Fig. 1.5C)**. The results showed that physical confinement created by reduced microchannel dimensions can affect cell morphology and migration speed.

Microfluidic devices can be used to create controlled co-culture cell systems, which allow quantitative cell migration studies in physiologically-relevant environments that involve complex cell-ECM and cell-cell interactions. Zhang *et al.* developed a

microfluidic system, which mimics vessel cavity, endothelium, and perivascular matrix containing chemokines, to investigate the transendothelial invasion of tumor cells [152]. This developed system allows detailed analysis of the attachment and transendothelial invasion of tumor aggregates. Similarly, Han *et al.* presented a microfluidics-based inflammation model for quantitative measurements of neutrophil transendothelial migration (TEM) in a 3-D environment during inflammatory responses [158] (**Fig. 1.5D**). The developed microfluidic system incorporated 3-D ECM, concentration gradients of various inflammatory molecules including fMLP and IL-8, and a co-culture of endothelial cells and neutrophils.

Figure 1.5 Examples of microfluidic cell migration and chemotaxis studies in complex environments.

(A) T Cell migration studies in chemokine gradients mimicking a lymph node sub-region led to the proposed combinatorial guidance model for T cell trafficking in secondary lymphoid tissues [21]; **(B)** The chemotaxis assay for studying neutrophil directional decision-making in bifurcating microfluidic channels [31]; **(C)** The influence of microfluidic channel width on migrating human osteosarcoma cells morphology and speed [157]; **(D)** Microfluidic system for studying transmigration of neutrophils in response to different inflammatory chemoattractants in a dose-dependent and time-dependent manner [158].

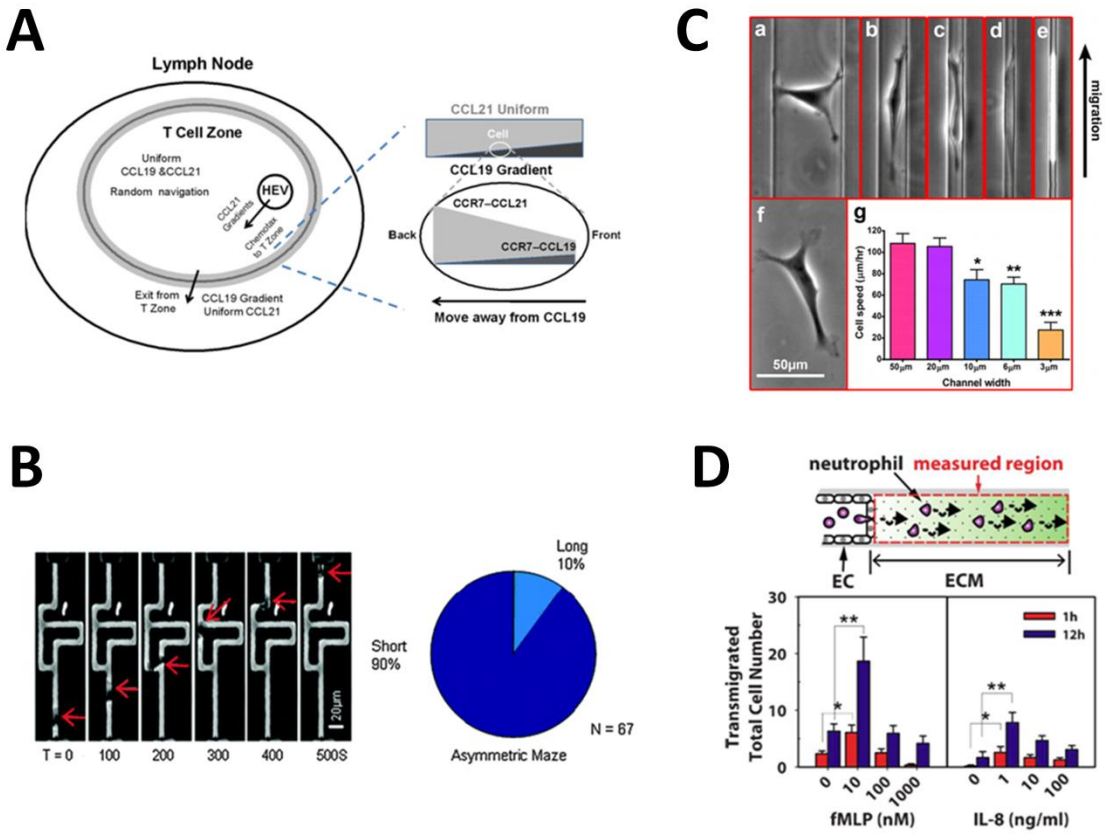

1.3.4 Chemotaxis studies with a medical or commercial application focus

More easily used microfluidic products and interfaces are required as microfluidics is increasingly accepted as a useful approach for cell migration and chemotaxis studies. In addition to basic research, microfluidic cell migration systems are extending their use to biomedical applications. Moreover, commercial microfluidic gradient devices and cell migration systems have been developed, suggesting the market potential of these products.

Butler *et al.* developed a simple microfluidic device to study the correlation of neutrophil motility to burn injury [26]. The device consists of a chemoattractant source channel connected to an array of side channels to allow gradient generation and neutrophil chemotaxis measurement for burn injured patients **(Fig. 1.6A)**. The results showed correlated neutrophil motility with the total burn surface area in patients 72 hours after burn injury **(Fig. 1.6B)**, suggesting the potential of microfluidic chemotaxis systems for clinically oriented studies. Towards this direction, various autoimmune diseases with implicated alteration of chemotaxis of neutrophils or other immune cell types may be targeted as potential diagnostic applications for microfluidic chemotaxis systems [159, 160].

To enable potential clinical applications, the problem of the current lengthy and interfering cell isolation procedures must be addressed to allow easier and reliable microfluidic chemotaxis experiments as well as faster test result reporting. Agrawal *et al.* developed a microfluidics-based method for directly capturing neutrophils from a drop of finger blood by flowing the blood sample to the neutrophil capturing adhesion molecule coated channel [161]. The captured neutrophils were subsequently used for chemotaxis

experiments on the same chip. A similar neutrophil capturing approach combined with automated cell tracking analysis was reported to be able to rapidly analyze neutrophil chemotaxis in a chronically inflamed mouse model [147].

Other important issues that need to be addressed for clinical applications include experimental throughput and automation to meet the requirement of rapid parallel testing of different conditions and samples. Berthier *et al.* reported a high-content neutrophil chemotaxis screening system for biomedical applications [103]. The developed system incorporated surface tension based passive pumps for chemical transport, allowing highly parallel gradient generation and chemotaxis testing **(Fig. 1.6C)**. The performance of this system was evaluated using cell samples from infants with severe and recurrent bacterial infections, and the results showed impairment of neutrophil chemotaxis to fMLP. These research advancements and commercialization suggest the practical future use of microfluidic chemotaxis systems in clinical settings.

Another commercialized microfluidic chemotaxis device is the µ-Slide developed by Ibidi [162]. The device can create chemical gradients in the gradient chamber based on controlled chemical diffusion between two volumetrically defined chemical chambers. The device follows an optimized operation protocol and uses specifically designed sealing plugs for controlled chemical filling and diffusion to maintain a stable gradient for a long period of time.

Finally, an integrated microfluidic cell migration system, the EZ-TAXIScan system, is commercially available. The key feature of this system is that it integrates live cell imaging modules with a microfluidic device to enable cell migration and chemotaxis experiments in a portable manner [163]. The system also allows high-throughput

chemotaxis experiments on a single chip, and includes automated data analysis software. Since its commercialization, a number of cell types have been tested for chemotaxis using this system [164-166].

Figure 1.6 Examples of application-driven microfluidic chemotaxis studies.

(A) The microfluidic device for testing motility of neutrophils from burn injured patients [26]; (**B**) Correlation between neutrophil motility 72 hours after burn injury to the total burn surface area [26]; **(C)** The high-content microfluidic chemotaxis device. The figure above the device picture (the inserted picture shows the liquid handling robot) shows the principle of surface tension based passive pumping for fluid infusion in the microfluidic device [103].

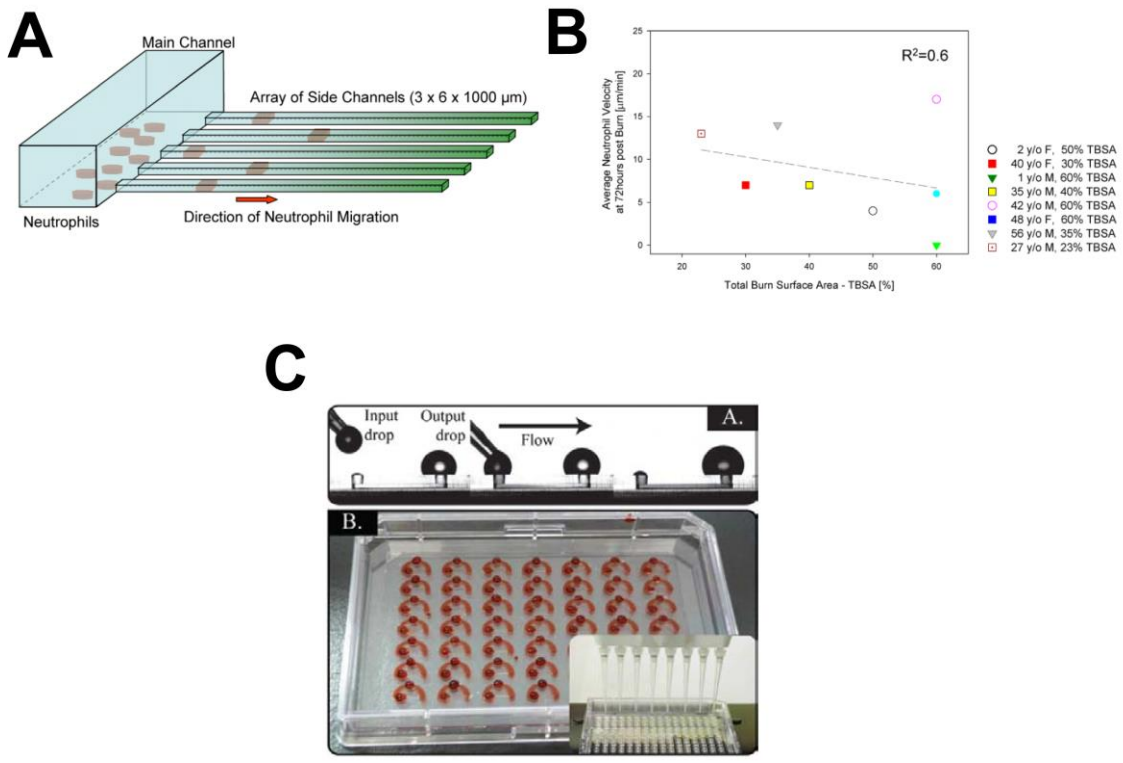

1.4 Overview of recent developments in microfluidic-based electrotaxis assays

This section is based on the following publication "J.D. Wu and F. Lin, Recent developments in electrotaxis assays. Advances in Wound Care, 2014, 3(2):149-155.".

Among the diverse guiding mechanisms, electrotaxis or galvanotaxis, cell migration in response to dcEF, can direct the migration of various cell types such as epithelial cells [12], endothelial cells [167], cancer cells [168] and immune cells [169]. Physiological dcEF produced at the wound and electrical attraction of epithelial cells for wound recovery is well-known. Research toward better understanding the mechanisms of electrotaxis is an important and rapidly growing area with direct relevance to wound care. Sophisticated *in-vitro* electrotaxis assays provide the important experimental platform for electrotaxis studies.

The dish-based assays are the current gold standard for *in-vitro* electrotaxis measurements and have been widely adapted to study electrotaxis of various cell types [168, 170, 171]. In addition, microfluidic devices, which can better control electric field applications and the cell migration environments, have been increasingly developed and used for electrotaxis research [172]. Despite the successful use of these experimental tools, it is challenging to effectively address more advanced scientific questions and meet higher technical requirements for the rapidly growing electrotaxis research. For example, parallel experiments are required to compare cell migration in different dcEF, thus allowing more efficient electrotaxis analysis and minimal variations among devices. Furthermore, electrotaxis analysis in 3-D environments is required to better simulate the situation in wound tissues. It is also important to analyze cell migration in response to

dcEF and other co-existing guiding signals, which occurs in wound healing. In addition to single cell electrotaxis, collective migratory behaviors of cell groups in response to dcEF, which is the migration mode of many relevant cell types in wound healing, need to be understood. Finally, it is of great interest to use electrotaxis for sorting applications. Research in these areas will require further development of electrotaxis assays to meet specific requirements.

Indeed, a number of new microfluidic-based electrotaxis assays have been recently reported, providing improved experimental throughput and capabilities for configuring more complex and physiologically relevant cell migration environments, and for sorting electrotactic populations. In addition, several previously developed assays have been used for studying collective electrotactic cell migration. These technological developments provide advanced experimental tools for electrotaxis research. In this section, we highlight some of these new developments.

1.4.1 Multi-fields assays

In most *in-vitro* electrotaxis assays, only single dcEF strength can be configured in each experiment and only one experiment can be done at a time. Therefore, observing cell responses in different conditions requires multiple experiments in a sequential manner. High throughput electrotaxis assays are needed for parallel electrotaxis experiments. Huang *et al.* developed a microfluidic electrotaxis device, which can generate multiple dcEF in a single microchannel [173]. The device consists of a straight microchannel with three consecutive segments of different width. Thus, three different dcEF can be generated in different segments. Using this device, electrotaxis of different lung cancer cell lines was compared and correlated with their metastatic potential.

However, different channel widths result in different flow speed, which can potentially complicate electrotaxis analysis due to flow-induced shear stress. To overcome this issue, Tsai *et al.* reported an improved microfluidic device, which can generate different dcEF with uniform flow speed (**Fig. 1.7A**) [174]. In this device, the main channel is divided into four segments without varying the channel width and each segment is connected to the cathode via a different channel path. Thus, different dcEF is generated in different segments with comparable internal flow speed. In addition to validating the developed device for testing electrotaxis of lung cancer cells, the device was further used to demonstrate and characterize cathode-directing electrotaxis of HSC-3 oral squamous cell carcinoma cells. Further development of microfluidic electrotaxis devices is expected to further increase the experimental throughput, and these devices can be applied to more effectively test electrotaxis of various cell types relevant to wound healing.

1.4.2 3-D assays

Currently, most of the electrotaxis experiments investigate cell migration on a 2-D substrate. However, cells can migrate in both 2-D and 3-D tissue environments *in vivo* and cell migration in 2-D and 3-D can be largely different. Compared with cell migration on a 2-D substrate, cell migration in a 3-D microenvironment requires the ability of cells to squeeze through ECM. Therefore, it is important to develop biomimetic approaches to study the effect of dcEF on cell migration over 3-D topology. Zhang *et al.* reported the use of 3-D matrigel for studying electrotaxis of human induced pluripotent stem (hiPS) cells [175]. The cells were mixed with matrigel followed by transference to the electrotactic chamber. The study showed that dcEF can stimulate and direct hiPS cell migration in 3-D. Sun *et al.* developed a 3-D scaffold to study electrotactic response of

lung cancer cells (**Fig. 1.7B**) [176]. A PDMS-based microfluidic device was used to generate uniformly sized bubbles in gelatin by injecting gelatin solution and nitrogen gas from two different inlets. The bubbles were then collected and the 3-D scaffold was formed by chemical cross linking and degassing. The pore size is well-controlled and uniform in the scaffold. Cells were easily seeded into the scaffolds using a pipette, and the scaffold was integrated into a polymethylmethacrylate (PMMA)-based electrotactic chamber for cell migration experiments. Using this device, different electrotactic cell migration was observed in 3-D comparing to it on a gelatin-coated 2-D substrate. Further optimization and development of 3-D electrotaxis assays will enhance their use for studying electrotaxis of relevant cell types in wound healing in more realistic ECM, which simulates wound tissues *in vivo*.

1.4.3 Co-existing fields assays

Diverse environmental signals such as chemical, electrical, and mechanical signals are presented to cells in a complex and co-existing manner to guide cell migration. Some examples include effective neutrophil navigation in co-existing chemical gradient arrays [177]; dendritic cell migration guided by co-existing soluble and surface bound chemokine gradients [178]. In wound healing, a combination of dcEF, chemical gradients and other cues provide co-existing guiding environments to direct the migration of relevant cell types at the wound. Interestingly, dcEF was suggested to override other guiding cues to direct cell migration in wound healing [2]. Improved knowledge of the competition between electrical and chemical guidance will help researchers better understand cell migration in electrochemical guiding environments and inspire new therapeutic applications by electrically manipulating cell migration. Li *et al.*

reported a microfluidic device that can configure co-existing chemical gradients and dcEF in a controlled manner **(Fig. 1.7C)** [179]. In this device, laminar flow mixing was used to maintain chemical gradients in the main channel with minimized disturbance by the dcEF applied from the side wells. Using this device, it was shown that T cells migrate more strongly toward the cathode of dcEF in the presence of a competing chemokine gradient under specific experimental conditions. Thus, external dcEF applications may be used clinically to manipulate the migration of relevant cell types over co-existing tissue produced chemical guiding factors for mediating wound healing. More recently, Song *et al.* developed a microfluidic device to monitor cellular migration in response to dcEF and fluid shear stress in single, simultaneous, and sequential modes [180]. In this device, constant dcEF in the microchannel is maintained by a feedback control loop. The developed device was used to study fibroblast migration in response to co-stimulating dcEF and fluid shear stress. While wound produced dcEF is well known, fluid shear stress can also be induced by interstitial fluid loss in the connective tissue toward the wound. Separate dcEF or flow stimulations induce electrotactic cell migration or migration along the flow direction respectively. Simultaneous dcEF and flow stimulations enhance directional cell migration. When dcEF and flow are applied sequentially, cell migration is affected by the applied stimulation as well as pre-existing stimulating conditions. Thus, electrotaxis of fibroblast under flow conditions may benefit wound healing comparing to electric field or fluid shear stress based guidance alone. These studies showed promise for investigating cell migration in complex multi-fields guiding environments in wound healing and motivate further development of electrotaxis assays to permit more advanced studies.

1.4.4 Electrotactic sorting

Caenorhabditis elegans (*C. elegans*) is a widely utilized model organism in biology research. Electrotaxis of *C. elegans* has been studied in direct current, alternating current or pulse electric fields [181-183]. Research using *C. elegans* often requires sorting worms by their stages or separating normal worms and mutants. Besides various existing sorting methods, electrotaxis provides a simple and effective way to sort *C. elegans*. Manière *et al.* demonstrated separation of normal worms from mutants by their electrotactic motility in electrophoresis agar gel [184]. The gel box is easy to fabricate and the method allows for sorting a large number of worms. Rezai *et al.* spatially separated different worms in a simple planar microchannel with a narrowed trap region based on the age-dependent or stage-dependent electrotactic responses of worms [185]. In addition, continuous sorting can be achieved in a parallel manner. Han *et al.* proposed another sorting strategy based on the size-dependent motility and electrotaxis of worms in a micro-structured channel [186]. This device features hexagonally arrayed microstructures. The study established the relationship between the worm size and the geometry of the environment, which was used to optimize the sorting performance. Integration of sorting and downstream analysis in an automated and high-throughput manner will lead to improved and broad future applications. Furthermore, the possibility of sorting cells based on electrotaxis should be explored. If successful, it will provide a method to identify and isolate cells with different electrotactic migration ability for both further basic electrotaxis research and tissue engineering applications.

1.4.5 Electrotaxis assays for studying collective cell migration

In wound healing, large epithelial sheets migrate collectively as a group in defined directions and maintain tight cell-cell adhesion. Li *et al.* adapted the dish-based electrotaxis assay to study electrotaxis of epithelial sheets [187]. The study showed that cells in monolayer migrated much more efficiently and directionally than isolated cells. Furthermore, E-cadherin mediated cell-cell adhesion is essential for collective electrotactic migration. A force sensing assay with PDMS pillar arrays was integrated into the electrotaxis chamber to measure traction force during cell migration (**Fig. 1.7D**). Using this assay, it is shown that the traction forces of the leading edge cells in an epithelial sheet orient with dcEF, leading collective electrotaxis. Further research toward better understanding electrotaxis of wound healing related cell types in their physiological group format will provide important scientific basis for deriving effective therapeutic strategies for wound healing. Successful use of existing cell migration assays for studying collective electrotaxis will certainly motivate development of more sophisticated assays to better suit the need of collective electrotaxis experiments.

Figure 1.7 Illustrations of new developments in electrotaxis assays.

(A) Illustration of the microfluidic device for generating multiple dcEF with uniform flow [174]; (**B**) Illustration of 3-D electrotaxis assay [176]; **(C)** Illustration of the microfluidic device for generating controlled co-existing dcEF and chemical gradients [179]; (**D**) Illustration of the traction force assay [187].

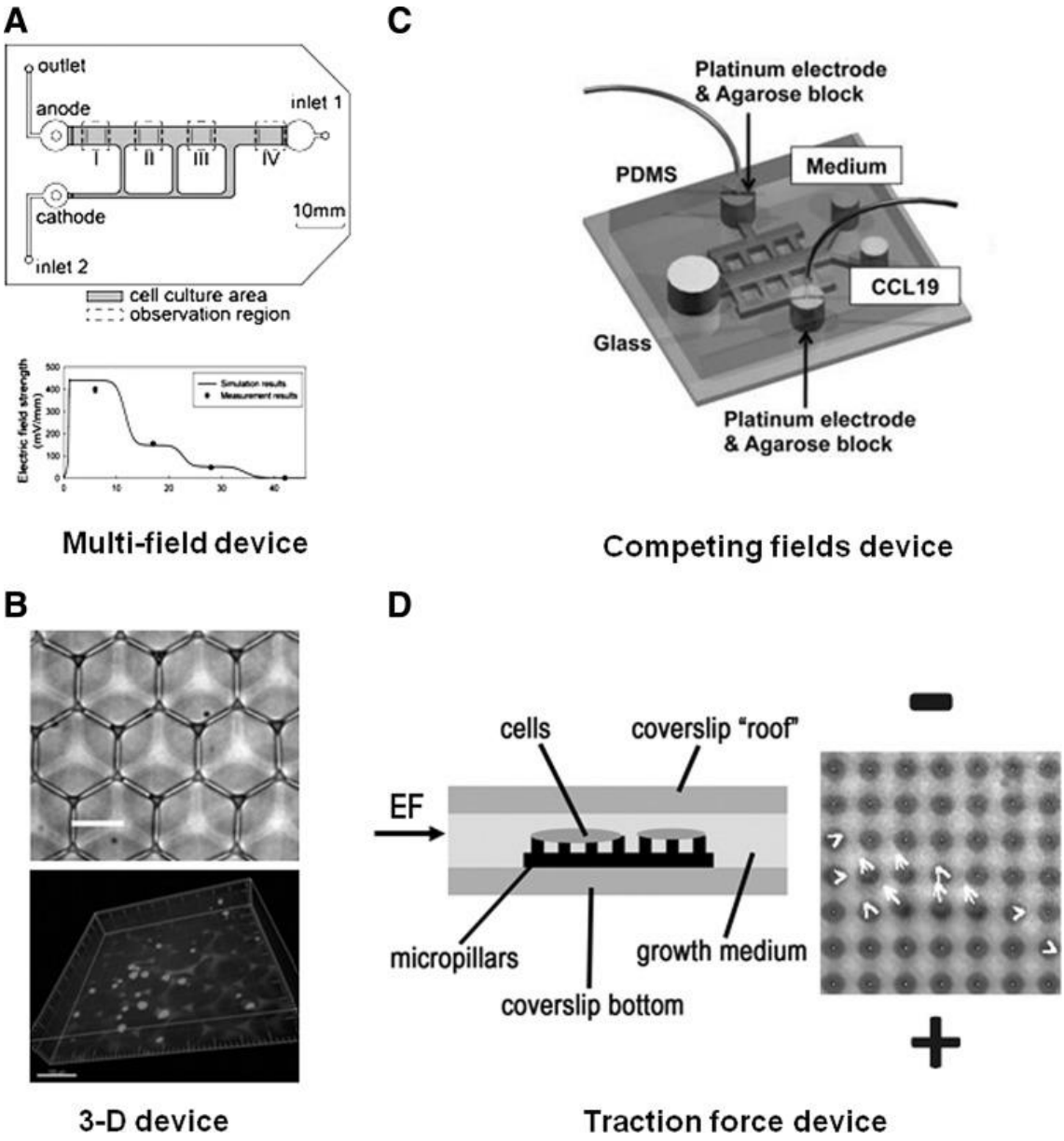

1.5 Neutrophil chemotaxis in chronic obstructive pulmonary disease

Chronic obstructive pulmonary disease (COPD) is one of the most common lung diseases resulting from narrowed airway that causes breath difficulty [188]. The long time exposure of lung to the noxious particles or gases, such as cigarette smoke, is regarded as the main causes for COPD. In 2002, COPD was the fifth leading cause of death worldwide and was predicted by World Health Organization to climb to the third in 2030. Spirometry is the current "gold standard" for COPD diagnosis, which measures the ratio of the forced expiratory volume in the first second to the forced vital capacity (FEV1/FVC) [189]. Currently there is no cure for COPD. The lifestyle changes such as quitting smoking and avoiding lung irritants can slow the progress of the disease. Some medicine treatments such as bronchodilators can help to relax the muscles around the airways and make breathing easier. Inhalation of steroids may help reduce airway inflammation in the patients with severe COPD.

Previous studies have shown an increased number of neutrophils in bronchial tissue of COPD patients and its correlation to the severity of airflow obstruction [188, 190-193]. Two chemoattractants of neutrophils, such as IL-8 and LTB4, has then been detected in sputum and BAL fluid from the patients. Further studies suggested that these two chemoattractants play important roles in recruiting neutrophils to the airways through chemotactic mechanisms that cause inflammation and tissue damage [194-197]. Genetic disorders such as Alpha-1 Antitrypsin Deficiency (A1AD) can also cause COPD and affects the disease progression [198]. The COPD patient's sputum induced neutrophil chemotaxis has been demonstrated *in vitro,* and is associated with COPD progression

[199]. Overall, the neutrophil chemotaxis plays a central role in COPD. Understanding the mechanisms involved will lead to the design of appropriate therapeutic strategies.

1.6 Motivation and outline of the thesis

Given the importance of chemical gradient directed cell migration and the suitability of microfluidic devices for cell migration studies in better controlled cellular environments, we are motivated to develop microfluidic devices to quantitatively characterize neutrophil chemotaxis for both research and clinical applications. Specifically, we focused on developing compact and easy-to-use microfluidic systems to characterize human neutrophil chemotaxis in single or overlapping gradients of chemoattractants. Furthermore, we proposed to apply the novel microfluidics-based approach to better characterize neutrophil chemotaxis induced by clinical sputum samples from patients with COPD and explore its potential for disease diagnosis and monitoring.

The thesis is organized as follows：Chapter 1 provides background information about directed cell migration and chemotaxis, development of microfluidics. Because our lab's research focuses on the investigation of cell response induced by soluble chemical field and electrical field using microfluidic devices and I have been involved in both studies. I also give an overview of the recent developments in microfluidic-based chemotaxis studies and electrotaxis assays in this chapter. These two parts are based on two of my published review papers. In addition, this chapter provides the background information of neutrophil chemotaxis in COPD. Finally, the chapter gives out the motivation and outline of this thesis.

Following the introduction chapter, Chapters 2-4 are sandwiched by three published and one submitted research publications. All these works aim to apply

microfluidic systems to investigate neutrophil chemotaxis in basic research and clinical applications. Chapter 2 describes a compact microfluidic system using a USB microscope for neutrophil migration studies. Chapter 3 describes a microfluidic platform for evaluating the relationship between neutrophil chemotaxis and COPD. Chapter 4 describes an all-on-chip method, including on-chip cell isolation, cell patterning, and cell chemotaxis, for testing neutrophil chemotaxis induced by fMLP and COPD patient's sputum. Finally, I conclude the thesis and discuss the future directions in Chapter 5. In the appendix, I described a method to develop a standalone gradient generator for chemotaxis studies which is used in Chapter 2, as well as a method for rapid fabrication of the microfluidic device using a desktop craft-cutter for cell migration studies. Some methodologies used in different chapters are similar such as neutrophil preparation and soft-lithography. I included full details of all the methodologies for each result chapter to ensure that sufficient and accurate methodological information is provided within each chapter and in consistence with my corresponding research publications.

Chapter 2

A compact microfluidic system for cell migration studies

This chapter is based on the following publication: "J.D. Wu, L.P. Ouyang, N. Wadhawana, J. Li, M. Zhang, S. Liao, D. Levin and F. Lin, A compact microfluidic system for cell migration studies, Biomedical Microdevices, 2014, 16(4): 521-528".

This part of work was performed in the first two years in my Ph.D study. We wanted to develop portable and low-cost imaging system to perform cell migration experiment and expected such a system can be further applied to point-of-care clinical applications. To simplify the complex setup of gradient generation using the traditional pump and tubing chemical infusion system, we also developed a standalone pump-free microfluidic gradient generator. The system was validated by testing neutrophil chemotaxis, a well-studied model for the eukaryotic cell chemotaxis. In this study, L.P. Ouyang, who was a graduate student at the University of Winnipeg, helped write the Matlab code to perform the cell counting analysis. I assembled the system, performed the cell migration experiments, did the manual tracking analysis, and wrote the manuscript for publication.

2.1 Overview

Microfluidic systems can better control cellular microenvironments and therefore are increasingly used for cell migration research. However, most existing systems are impractical to use without specialized facilities and researchers. In this chapter, I developed a compact USB microscope-based Microfluidic Chemotaxis Analysis System (UMCAS) to remove this barrier. This system integrates microfluidic devices, live cell

imaging, environmental control and data analysis to provide a solution for rapid microfluidic cell migration and chemotaxis experiments with real-time result reporting. This developed system was successfully validated by testing neutrophil chemotaxis.

2.2 Introduction

Cell migration is a fundamental process that is important for many physiological and pathological processes ranging from immune response to tissue development and to cancer metastasis [5, 200, 201]. Among the diverse environmental guiding mechanisms, chemical concentration gradients (i.e. chemoattractant gradients) can direct the migration of many cell types, a process termed chemotaxis [202]. Aside from the importance of chemotaxis in our understanding of fundamental cell biology, this mechanism has high potential to be targeted in therapeutic applications for cell migration related diseases and physiological problems due to its broad applicability, high diversity and specificity. For example, various adhesion and chemotactic molecules have been targeted clinically for treating autoimmune diseases [5] and altered neutrophil chemotaxis has been implicated in airway diseases and burn injury patients [26, 160].

Traditionally, chemotaxis is measured by Boyden chamber or transwell assays, and other conventional cell migration assays [17, 34, 35]. Rapid development of microfluidics enabled quantitative cell biology studies in well-controlled cellular microenvironments, and there is a growing trend of applying microfluidic devices and systems for cell migration and chemotaxis research [172, 203]. However, a major barrier that prevents microfluidic cell migration systems from becoming a common research tool in life science labs is its requirements of device fabrication capability, live cell imaging facilities, and the associated skills in researchers. Furthermore, the current gold standard,

single-cell tracking method for analyzing cell migration data (which in many cases is done manually) can extract quantitative parameters to evaluate the cell movement such as chemotactic index, cell migration angles, migration speed, motility coefficient, persistent migration time or distance, and mean square displacement. However, this process is time-consuming and labour-intensive, and often times the analysis outcomes vary depending on the availability of specialized software and the researchers' experience and judgement.

These above-mentioned limitations have been recognized by the microfluidics community and in recent years have motivated researchers to develop simple and easy-to-use systems for microfluidic cell migration and chemotaxis studies. Particularly, researchers have started exploring the use of webcams as compact and cheap microscopy systems for imaging tissues and cells [204, 205]. These systems were designed to fit into conventional incubators and thus are compatible for use with common life science research facilities. Additionally, the use of a cell phone camera for imaging tissues and cells was also explored [206]. However, such a system is not capable of monitoring live cell functions such as directional cell migration, which requires much more sophisticated controls. Although several automated particle tracking programs are freely-available to researchers [207], their performance significantly varies depending on image quality, cell density and morphology. Recently, a study reported the successful use of an automatic cell tracking program for analyzing neutrophil chemotaxis showed new promise in this area [147]. Furthermore, commercial products for microfluidic cell migration and chemotaxis studies have become available. For example, the µ-Slide Chemotaxis developed by ibidi (Germany) offers the microfluidic chemotaxis device with a standardized experimental protocol. However, performing the chemotaxis experiments

using this device relies on the availability of specialized imaging and cell culture facilities. To our best knowledge, the only system that integrates all components for microfluidic cell migration and chemotaxis experiments in a relatively portable manner is the EZ-TAXIScan system (ECI Inc., Japan). However, this system remains prohibitively expensive to many researchers.

Motivated by the need of a compact, integrated and inexpensive system to enable easy microfluidic chemotaxis experiments, we in this study developed a USB microscope-based Microfluidic Chemotaxis Analysis System (UMCAS). The UMCAS integrates microfluidic devices, live cell imaging, environmental control, and data analysis to provide an inexpensive and compact solution for rapid microfluidic cell migration and chemotaxis experiments with real-time result reporting. Furthermore, a smartphone-based module was developed for remote experiment data monitoring. The system was validated by testing neutrophil chemotaxis to an IL-8 gradient.

2.3 Materials and methods

2.3.1 System assembly

The detailed design of UMCAS is illustrated in **Fig. 2.1**. The basic system consists of a USB microscope (VMS-004D, 400X magnification, Veho, UK), a microscope stand with an adjustable XY stage and LED light illumination (DP-M06, Oriental Inspiration Limited Company), and a high lumina blue LED (Blue Rebel LED, 470nm, 700mA, LUXEON STAR LEDs). The stand holds the USB microscope vertically, providing position control for focus adjustment. The stand is connected to a computer (Windows XP or above, 1 GB free disk space and 1024 MB RAM is recommended, a Bluetooth adaptor is required for the remote monitoring module) via a

USB cable to power the intensity adjustable LED for cell imaging. The USB microscope is connected to the PC for image acquisition. The high lumina blue LED for gradient visualization is covered with a condenser lens to focus the light beam, and is in contact with an iron block as the heat sink. The blue LED is powered via an adaptor and is installed to a custom-machined angle adjusting arm sitting on an aluminum rotating base-ring, allowing 3-D position adjustment of the LED to best illuminate the microfluidic device for gradient visualization. In addition, a transparent heater (Minco, MN) was mounted on the stage contacting the microfluidic device for controlling the temperature during cell migration experiment. The heater is controlled by a sensorless temperature controller (Minco, MN) and the temperature was calibrated to 37 °C using a digital thermometer (VWR, Canada). The heater is powered via a custom-made adaptor. The assembled system is mounted to a polyethylene box with transparent and removable top and front covers for system protection and easy experiment setup. The box is installed with carrying handles and cable storage pocket. This completes the UMCAS assembly.

Figure 2.1 Illustration of the UMCAS.

(A) The setup of the whole system; (**B**) The imaging module; **(C)** The control and analysis software interface; **(D)** The smartphone application for real-time remote data monitoring.

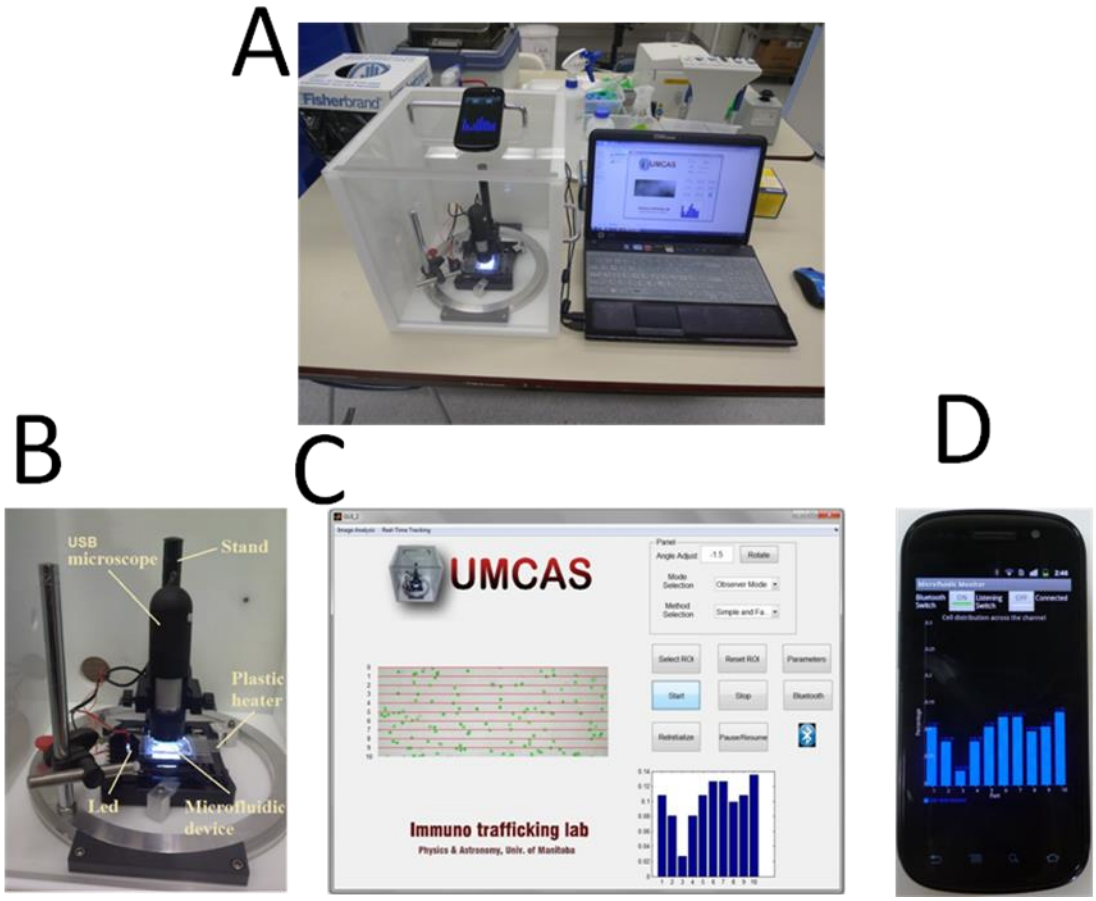

2.3.2 Microfluidic device preparation

A previously developed flow-based "Y" shape microfluidic device [10] and a flow-free microfluidic device [179] **(Appendix A.1)** were used to test the UMCAS. Both devices were fabricated using the standard optical lithography and soft-lithography method as detailed previously [10]. Briefly, the device was designed in Freehand 9.0 (Macromedia) and the design was printed to a transparency mask by a high-resolution printer with at least 2400 dpi resolution. The device masters were fabricated in The Nano Systems Fabrication Laboratory (NSFL) at the University of Manitoba. The design was patterned on a silicon wafer by contact photolithography with SU-8 photoresist (MicroChem, MA), yielding ~100 µm thickness. The PDMS replicas were then fabricated by molding PDMS (Dow Corning, MI) against the master. Chemical reservoirs were created by punching holes out of the PDMS using sharpened punchers. The PDMS replica was then plasma bonded to a 50 mm x 75 mm glass coverslide to complete the device fabrication.

2.3.3 Cell preparation

Human whole blood was obtained from healthy volunteers (in collaboration with The Clinical Institute of Applied Research and Education at Victoria General Hospital in Winnipeg, Manitoba, Canada, under an approved human ethics protocol). Peripheral blood mononuclear cells (PBMCs) were removed using standard gradient centrifugation method. The remaining content in the blood sample after PBMCs isolation was mixed with Dextran-500 to partially separate red blood cells (RBCs) to the bottom portion of the blood sample. The neutrophil enriched upper portion of the blood sample was transferred to a new tube and RBCs in the sample was further removed by hypotonic lysis for 30

seconds using 0.2% saline buffer. Isolated neutrophils were washed with 0.85% saline buffer 2 times and re-suspended in RPMI-1640 medium before experiments. Neutrophils were used for experiments within 8 hrs after isolation.

2.3.4 Experimental setup

Microfluidic devices were coated with fibronectin (0.25 mg/mL, BD Biosciences, MA) for one hour followed by 0.4% BSA blocking for another hour at room temperature before use. For loading human blood neutrophils to the fibronectin coated device with the above described coating protocol, we recommend adding cells at high concentration (e.g. ~10^7/mL in small volume) to efficiently settling enough cells in the channel. For the flow-free device, RPMI medium and IL-8 solution (12.5 nM in RPMI, R&D Systems) mixed with FITC-Dextran 10 kDa were added to the two side wells to allow gradient generation in the center channel by free chemical diffusion **(details are provided in Appendix A.1)**. For the "Y" shape device, the IL-8 solution and RPMI medium were infused into the device at 0.2 μL/min by syringe pumps to generate a flow-based gradient in the microfluidic channel. The device was placed on the heater and maintained at 37 ^{o}C. The gradient of FITC-Dextran (with similar molecular weight of IL-8) was visualized using the blue LED and the USB microscope. Cell migration in the microfluidic device was then imaged and recorded by the UMCAS.

2.3.5 Data analysis

2.3.5.1 Manual tracking analysis

As the reference method, time-lapse cell migration images acquired by the UMCAS were analyzed by single-cell tracking using the "Manual Tracking" plug-in in NIH ImageJ. The tracking data were then exported to Excel (Microsoft) and Origin

(OriginLab) for analysis using the previously established methods [10]. Specifically, the movement of cells was quantitatively evaluated by 1) the percentage of cells that migrated towards the gradient; 2) the Chemotactic Index (C.I.), which is the ratio of cell displacement toward the gradients to the total migration distance; and 3) the average speed (V), calculated as the ratio of total migration distance to the experiment period. Five independent cell migration experiments were performed for each condition tested. All parameters are presented as the average value ± standard error of the mean (SEM).

2.3.5.2 Cell distribution and digital scoring analysis

A custom program was developed in MATLAB for automated cell distribution analysis in real-time during the cell migration experiment and the program was integrated to the control program in the UMCAS **(Figure 2.1C)**. As illustrated in **Figure 2.2**, the region of interest (ROI) in the image was selected for analysis. Cells in the ROI were segmented from the background by applying a high-pass Gaussian filter and thresholding using specialized functions available in the MATLAB Image Processing Toolbox to smooth the image and enhance the contrast respectively. Morphology operations including erosion followed by dilation steps were applied to further reduce noise in the image.

The processed images were used for cell distribution analysis. Briefly, a search window (slightly bigger than the cell size) was defined to scan the entire image. During the scanning, the gray intensity of each pixel within the window was summed and compared to a threshold intensity to identify candidate cells. Then a refined search within the candidate cell-containing region was performed to locate the cell position by scanning the region with a search window for maximum total pixel intensity. Once a cell was

identified, the pixel intensity of the corresponding cell region was set to zero to avoid a duplicated search. The identified cells were counted in 10 equally spaced divisions across the channel width and along the chemical gradient direction. The cell count in each division was normalized to the total cell number and presented as a distribution histogram over the 10 divisions along the gradient.

Although clear biased initial cell distribution in the channel was disqualified for further analysis, variation of initial cell distribution among experiments and non-moving or flowing cells in the background were found to complicate the cell distribution analysis. To improve the comparison, the variation of cell distribution between the beginning and the end of the experiment was digitized. This digital scoring analysis was started by calculating the difference of normalized cell count between the end and the beginning of the experiment in each division. If the difference was > 0, the score was set to 1; if the difference was < 0, the score was set to -1. If the difference was = 0, the score was set to 0. Next, the scores for division 1-5 were added to calculate the left-side score (low IL-8 half of the channel), and the scores for division 6-10 were added to calculate the right-side score (high IL-8 half of the channel). Finally, the difference between the right-side score and left-side score were calculated to determine the final Chemotaxis Score.

Figure 2.2 Illustration of automated image and data analysis in the UMCAS.

(A-D) Illustration of automated cell-image processing for cell recognition. The original image and the image after each step of processing (i.e. Gaussian filter, thresholding and morphology operation) are shown; **(E-F)** Illustration of automated cell counting and distribution analysis. The identified cells in different divisions in the channel **(E)** and the corresponding cell number distribution in different divisions **(F)** are shown.

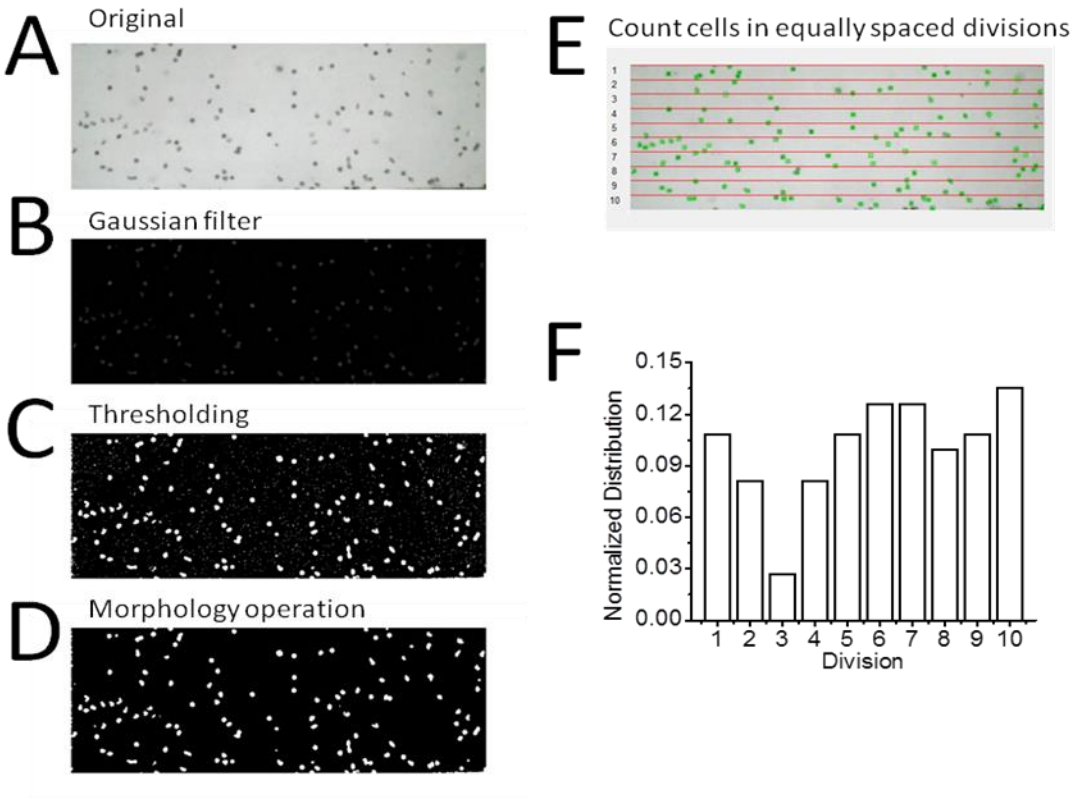

2.3.6 Remote data monitoring

The remote data-monitoring module was implemented based on the wireless communication between a custom-made application program installed in a smartphone (Nexus S, Google Company) and the UMCAS software operated in the laptop computer. The smartphone used ver. 2.3 of the Android operating system and was able to receive and plot the cell distribution analysis data wirelessly sent from the UMCAS software in real-time through the Bluetooth SPP protocol.

2.4 Results and discussion

2.4.1 Portability and cost comparison between traditional systems and the UMCAS

Traditional microfluidic cell migration systems require stationary imaging facilities within a research lab. In comparison, UMCAS was assembled into a box with the side dimension of ~50 cm and the total weight of ~10 kg. Two carrying handles were installed on the side of the box. A hole was drilled in the back of the box to allow cable connections from the UMCAS to the external laptop computer. A cable storage pocket was mounted next to the cable hole in the back of the box. The top and front windows of the box are transparent and removable. This design made the UMCAS truly portable and easy to set up the experiment. We verified the portability of the UMCAS by conveniently transporting the UMCAS to different rooms in our research building and to another lab located on the medical campus of our university (~30 min's drive from the University of Manitoba Fort Garry campus) and then successfully performing cell migration experiments using the UMCAS. There is significant room to further reduce the size and weight of the box by optimizing the box design and selecting lighter materials. If needs,

UMCAS can also be used without the box, which only weighs ~700 g and the system can be easily disassembled to be carried in a bag to a remote site for re-assembling and experiment. These improvements and alternative approaches will further increase the portability of the UMCAS.

The required imaging facility for traditional microfluidic cell migration systems typically includes a fluorescent microscope, a CCD camera, syringe pumps (if fluid perfusion is required for the microfluidic device) and a temperature control system. Based on our experience, these instruments will easily cost over $10,000 for a basic system configuration. By comparison, the total hardware cost for the current prototype version of UMCAS is less than $800 including material costs for the USB microscope, microscope stand, LED and heater/controller, plus the material and labour costs for making the box and assembling the system in the machine shop of the Department of Physics and Astronomy at the University of Manitoba. The computer, control software and smartphone are not included in the cost estimate. In the current prototype version of the UMCAS, a significant portion of the total cost (~60%) resulted from the initial costs of the custom-designed and fabricated box. This cost is expected to significantly reduce for duplicating the developed UMCAS with the established box design and fabrication/system assembly procedures, and by selecting more cost-efficient materials.

2.4.2 Validation of microscopy performance of the UMCAS

Gradient generation using the developed microfluidic devices was characterized by measuring FITC-Dextran 10 kDa gradient in the gradient channel. We used the blue LED in the UMCAS to excite FITC-Dextran in the device and imaged the FITC-Dextran gradient in the gradient channel using the USB microscope. The image showed clear

chemical gradient in the device (**Fig. A.1F)** and thus the system is effective to verify chemical gradient before performing chemotaxis experiment. On the other hand, due to the low resolution of the current model of USB microscope and non-uniform blue LED illumination, the measured gradient profile by UMCAS is not sufficient for quantitative characterization. Higher resolution USB microscopes with integrated LED illumination will further improve fluorescent imaging capability of the UMCAS.

To qualitatively validate the UMCAS for visualizing and correctly recognizing cells in the microfluidic device, we observed cells settled in the fibronectin-coated microfluidic channel by the USB microscope with integrated image processing in the UMCAS (as detailed in the Materials and Methods section). The UMCAS was able to resolve all cells in the channel with acceptable resolution for visualizing cell migration (**Fig. 2.2A**). The image quality was improved when we removed the Minco thermaclear heater between the stage and the device, which is known to reduce optical transparency by at least 30% (however, the Minco heater does not affect cell identification in this study). Other types of heaters that have less optical effect on cell imaging can also be considered (e.g. a temperature control box with circulating hot air or hot water can be incorporate). In addition, recent studies have reported the successful use of custom-modified webcam to allow improved optical adjustments for visualizing tissues and cells with relatively satisfying image quality [205]. A USB microscope at comparable cost but with higher resolution will further improve the image quality. These modifications can be included in the next version of the UMCAS to improve cell-imaging capability.

2.4.3 Validation of the UMCAS for neutrophil migration analysis

To validate the UMCAS for cell migration and chemotaxis studies, we performed migration experiments of human blood neutrophils over 20 min period using both flow-free microfluidic device and flow-based microfluidic device. In the flow-free device, the medium control, a uniform 12.5 nM IL-8 field, or a 12.5 nM IL-8 gradient were tested. The cell migration images were first analyzed by traditional single-cell tracking analysis. The results clearly show random cell migration in medium control and uniform IL-8, but strong chemotaxis toward the IL-8 gradient, as measured by the percentage of cells that moved toward the gradient and by the Chemotactic Index (**Fig. 2.3A & 2.3B**). As expected, cells migrated at higher speed in the uniform IL-8 or the IL-8 gradient compared with the medium control **(Fig. 2.3B)**. These results validated effective neutrophil migration and chemotaxis experiments in the UMCAS. The manual tracking analysis allowed visual inspection of the experiment to check if there was i) a significant change in the total cell number in the time-lapse images; ii) if there was significant bias in the initial cell distribution; and iii) if there were too many non-migrating cells or flowing cells in the background. These data were used to determine the suitability of the experiment for the automated cell distribution and digital scoring analysis.

To validate the real-time chemotaxis analysis in the UMCAS, automated cell distribution and digital scoring analysis in the UMCAS software were applied to the same neutrophil migration experiments. The results show that the image processing method can correctly identify and count cells in the microfluidic channel **(Fig. 2.2)**. To enable a rapid chemotaxis analysis report without single-cell tracking, we analyzed the cell distribution in equally space divisions across the gradient channel and along the gradient direction. Ideally, the shifted cell distribution toward the gradient will indicate chemotaxis.

However, the cell distribution analysis itself was often affected by the initial cell loading and the background non-migrating or flowing cells in the flow-free device. Therefore, we further developed a digital scoring method to compare the change of cell distribution over the experiment period in each division with the focus on the sign of change, but not the absolute change level. Furthermore, we summed up the digitized scores for the left-side divisions and the right-side divisions and then calculated the difference of the summed right-side score and the left-side score to enhance the comparison. This Chemotaxis Score gives the final readout of the analysis. Although this method did not necessarily reflect chemotaxis strength, it provided a simple way to distinguish random migration and chemotaxis in a relatively noisy system, as shown by the significantly higher Chemotaxis Score in IL-8 gradient compared to medium or uniform IL-8 control (**Fig. 2.3C**). These results are consistent with the manual tracking analysis: the chemotaxis score for the IL-8 gradient experiment is higher than it for the control experiments; manual tracking analysis shows that the percentage of chemotaxing cells and chemotactic index for the IL-8 gradient experiment is higher than it for the control experiments.

Figure 2.3 Neutrophil chemotaxis analysis in the flow-free device using the UMCAS. **(A)** Percentage of the cells migrated towards the gradient by manual cell tracking analysis; **(B)** C.I. and speed by manual cell tracking analysis; **(C)** Automated digital scoring analysis. The data are presented as average ± SEM. ** indicated that significance level was $p<0.01$. A minimum p-value of <0.05 was considered statistically significant. Five independent experiments were repeated for each condition.

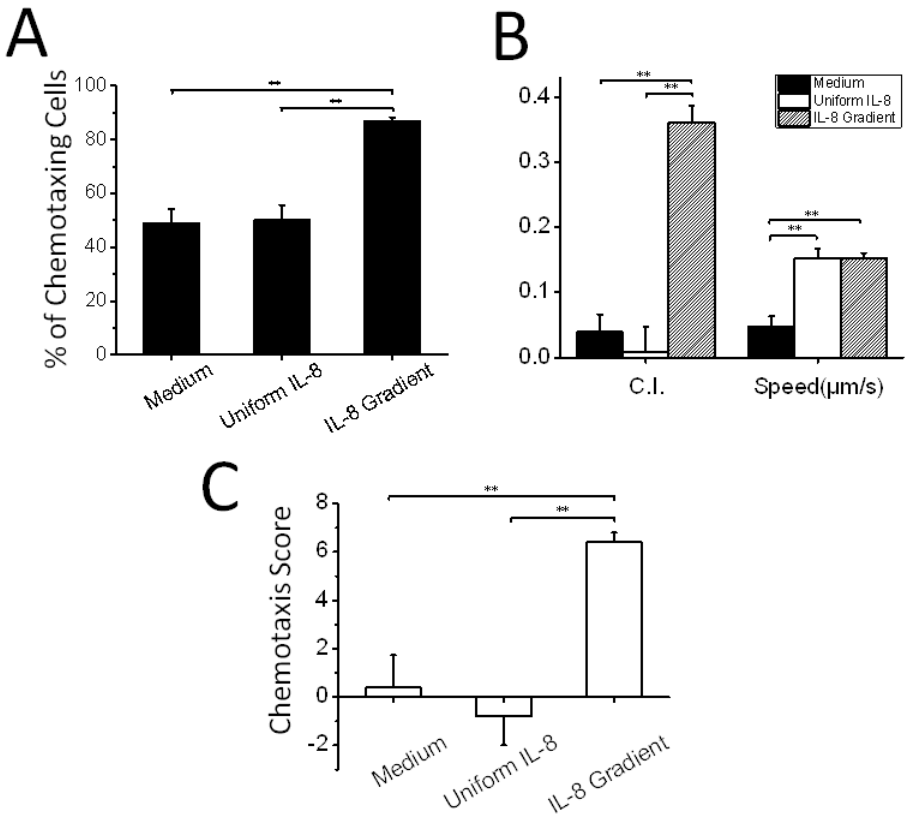

In addition to the flow-free device, we used the standard “Y” shape flow-based microfluidic gradient device to test neutrophil chemotaxis in the UMCAS. The results clearly show neutrophil chemotaxis to the IL-8 gradient (**Fig. 2.4**). As the background cells were better controlled in the “Y” shape flow-based device, we were able to perform automated cell tracking analysis (**Fig. 2.4E**), allowing more accurate and quantitative cell migration assessment in the UMCAS. As expected, the cells tend to migrate towards the flow direction, which is consistent with the literature [100, 208]. The use of a syringe pump significantly affects the compactness and cost of UMCAS. In this regard, gravity flow-based devices without the requirement of external pumps have been reported [88].

The automated cell analysis data in the UMCAS can be transmitted to a smartphone for real-time display within the Bluetooth signal transmission range using the remote data-monitoring module (**Fig. 2.1**). This added feature can be useful for researchers to more flexibly obtain updated experimental results. Further developing this module by engaging a central server will enable long-range remote data monitoring.

In addition to PDMS microfluidic devices, we fabricated a plastic microfluidic device using a previously developed craft-cutting method [209]. This method allows easy, fast and inexpensive device fabrication of flexible designs within 30 min using a desktop craft-cutter comparing to PDMS devices that require lengthy mask fabrication by photolithography and subsequent soft-lithography process. Gradient generation and neutrophil chemotaxis in the craft-cut plastic device were successfully demonstrated **(Appendix A.2).**

Figure 2.4 Cell distribution and tracking analysis of neutrophil chemotaxis in the "Y" shape device.

Cell image captured by the UMCAS at the 0th min (**A**) and the 20th min (**C**) of the chemotaxis experiment to an IL-8 gradient. Corresponding normalized cell distribution at the 0th min (**B**) and the 20th min (**D**); (**E**) Cell tracks (normalized to a common origin).

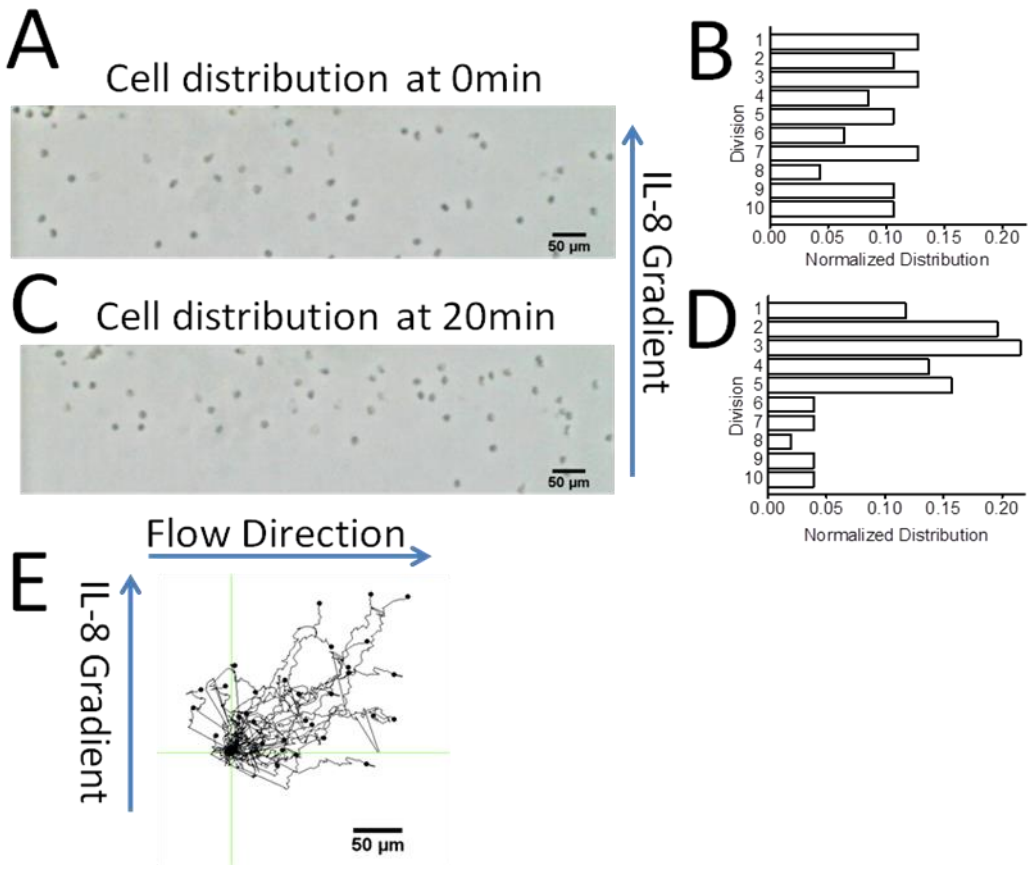

2.5 Conclusion

In conclusion, the UMCAS integrates all necessary components required for carrying out microfluidic chemotaxis experiments in a compact manner with the added features of real-time data analysis and wireless remote data monitoring, thus offering a full practical solution for microfluidics-based cell migration and chemotaxis analysis without the requirement of specialized facilities and research skills.

The developed UMCAS system has advantages in ease of operation, portability and cost efficiency comparing to existing systems. In addition, the UMCAS is compatible with different customized microfluidic devices (e.g. PDMS and glass devices with both flow-based and flow-free based gradient generation) and has high potential for further reduction of system size and cost. The main limitations of the current version of UMCAS are its low imaging capability (not suitable for high-resolution cell imaging and quantitative fluorescence microscopy) and simple environment control (no CO2 and humidity control). These limitations can be readily improved upon further development of UMCAS. We envision that this developed system will find broad applications in cell migration and chemotaxis research.

Chapter 3

A microfluidic platform for evaluating neutrophil chemotaxis induced by sputum from COPD patients

This chapter is based on the following publications:

"J.D. Wu, C. Hillier, P. Komenda, R. Lobato de Faria, D. Levin, M. Zhang and F. Lin, A microfluidic platform for evaluating neutrophil chemotaxis induced by sputum from COPD patients, PLoS ONE, 2015 May 11;10(5):e0126523".

"J.D. Wu, L.P. Ouyang, M. Zhang, S. Liao, C. Hillier, P. Komenda, R.L. de Faria and F. Lin, Assessing neutrophil chemotaxis in COPD using a compact microfluidic system, The 36th Annual International Conference of the IEEE Engineering in Medicine and Biology Society (EMBC'14), Chicago, U.S.A., August 26-30, 2014."

This part of work was performed in the middle period of my Ph. D. study. During that time, I gained enough knowledge of using microfluidic devices to perform the cell migration experiments. I wanted to further apply these technologies to investigate deeper biological questions. Meantime, the collaboration between our lab and the local hospital was established. So I took this opportunity to quantitatively study the relationship between neutrophil chemotaxis and COPD. We used both a traditional microfluidic system and the compact system described in Chapter 2 to perform this study. In addition, we developed an easier and more stable standalone microfluidic gradient generator compared the one described in Chapter 2. In this study, I performed the experiment, analyzed the data, and wrote the manuscript for publication.

3.1 Overview

Chronic Obstructive Pulmonary Disease (COPD) is a common lung disease characterized by breathing difficulty as a consequence of narrowed airways. Previous studies have shown that COPD is correlated with neutrophil infiltration into the airways through chemotactic migration. However, whether neutrophil chemotaxis can be used to characterize and diagnose COPD is not well established. In this chapter, we developed a microfluidic platform for evaluating neutrophil chemotaxis to sputum samples from COPD patients. Our results show increased neutrophil chemotaxis to COPD sputum compared to control sputum from healthy individuals. The level of COPD sputum induced neutrophil chemotaxis was correlated with the patient's spirometry data. The cell morphology of neutrophils in a COPD sputum gradient is similar to the morphology displayed by neutrophils exposed to an IL-8 gradient, but not a fMLP gradient. In competing gradients of COPD sputum and fMLP, neutrophils chemotaxis and cell morphology are dominated by fMLP.

3.2 Introduction

Neutrophils are the 'first responders' to the site of inflammation and play important roles in the human innate immune system [210]. Chemotaxis, a process whereby cells migrate toward a chemical concentration gradient, critically mediates neutrophil recruitment in tissues [211]. The biological mechanisms of neutrophil chemotaxis are highly complex and involve sophisticated cellular machinery for gradient sensing and migration [22]. Neutrophils express multiple chemoattractant receptors and can respond to individual chemoattractant gradients or their combinations [29]. Terminal chemoattractants, such as fMLP, and intermediate chemoattractants, such as IL-8, trigger hierarchical chemotactic signaling and define distinct migration characteristics in

neutrophils [212]. IL-8 can induce bi-directional migration of neutrophils in a dose-dependent manner [30]. Furthermore, spatiotemporal variations of IL-8 gradient profiles result in different migratory responses of neutrophils [30]. Taken together, neutrophil chemotaxis is coordinated by complex environmental factors. Changes of these factors can modulate cell migration patterns and their associated physiological outcomes.

Indeed, disorders of neutrophil chemotaxis are associated with various diseases such as asthma, chronic obstructive pulmonary disease (COPD), sepsis, diabetes, and kidney failure [28, 196, 213-215]. Among them, COPD is one of the most common lung diseases resulting from narrowed airways that cause breathing difficulty [188]. Long-term exposure of lungs to noxious particles or gases, such as cigarette smoke, is considered to be the main cause for COPD [188]. In 2002, COPD was the fifth leading cause of death worldwide and the World Health Organization (WHO) has predicted that COPD will become the third leading cause of death by 2030 [93]. Spirometry, which measures the ratio of the forced expiratory volume in the first second to the forced vital capacity (FEV1/FVC), is the current "gold standard" for COPD diagnosis [189]. The main limitation of spirometry is that it requires patient cooperation, which can be difficult for patients with severe conditions, or if the patients are unable to follow the procedures [94]. Secretions of chemotactic factors such as IL-8 and LTB_4 in the airways recruit neutrophils, leading to inflammation and tissue damage [160, 194-197]. Neutrophil chemotaxis induced by sputum of COPD patients has been demonstrated *in vitro*, and is associated with COPD progression [199]. Measurement of neutrophils, or the level of chemotactic factors responsible for recruiting neutrophils, in the patient's sputum have been proposed as new diagnostic markers for COPD [196]. Thus, it is of great interest to

further assess neutrophil chemotaxis to the sputum of COPD patients as a means of diagnosing COPD at the cellular function level.

Previous neutrophil chemotaxis studies in COPD were based on traditional cell migration assays, such as the transwell assay and the under-agarose assay [160, 198]. Variations among these cell migration assays, and their common limitation in gradient control, has made it difficult to obtain reliable chemotaxis measurements, and in some cases has lead to contradictory results [199, 216]. Clinical factors such as the patient's medical history and condition, methods of sample acquisition and processing, and the choice of control reference further complicate the interpretation of the chemotaxis results. Microfluidic devices provide a powerful new experimental tool for quantitative single cell migration and chemotaxis analysis owing to their ability to configure well-defined chemical concentration gradients, as well as having advantages in miniaturization, low reagent consumption, real-time visualization of cell migration, and high throughput [10, 13, 105, 217-219]. Indeed, microfluidic devices have been widely used for studying neutrophil migration and chemotaxis [13]. In addition to research applications to better understand the biological mechanisms underlying neutrophil chemotaxis [22, 32], several studies have reported the use of microfluidic devices for testing neutrophil chemotaxis with clinical samples for different disease models such as burn injury and chronic inflammation [26, 147]. Most recently, a microfluidic system was successfully used to rapidly test neutrophil chemotaxis from a drop of blood for asthma diagnosis [219].

In the present study, we developed a new microfluidic platform for evaluating neutrophil chemotaxis to the sputum samples from COPD patients. This platform allowed us to quantitatively characterize COPD sputum induced neutrophil chemotaxis.

Furthermore, we employed this system to assess the potential of neutrophil chemotaxis as a new clinical measure for COPD that may enable future point-of-care applications.

3.3 Materials and methods

3.3.1 Sputum sample preparation

Ethics approval for obtaining sputum samples from COPD patients and healthy subjects (Protocol number: J2012:140) was granted by the Joint-Faculty Research Ethics Board at the University of Manitoba. Informed consent form was obtained from all participants. Spontaneous sputum samples were collected from COPD patients (based on spirometry and physician diagnosis) and healthy control subjects at the Seven Oaks General Hospital in Winnipeg, Manitoba, Canada. For this initial proof-of-concept study, sputum samples from a small cohort of total 5 COPD patients and 5 healthy control subjects were used. The clinical descriptors of the participants are summarized in Table 1. The sputum samples were transferred to 1.5mL Eppendorf tubes and mixed with an equal volume of 0.1% dithiothreitol (Fisher Scientific). The samples were vortexed and placed in a water bath at 37 °C for 15minutes (min) to homogenize them. The samples were then centrifuged at 2800rpm for 10min. The supernatants were collected and centrifuged again at 3000rpm for 5min to completely remove cellular components. The supernatants were stored at -80 °C before use. The supernatants were diluted by 10X in migration medium (RPMI-1640 with 0.4% BSA) for chemotaxis experiments.

3.3.2 ELISA for measuring IL-8 concentration in sputum samples

The IL-8 concentration in the sputum samples was measured using a commercial ELISA kit (Cedarlanelabs, ON) and a multi-plate reader at 450nm (Synergy 4 HT). Each sputum sample was assayed in duplicate.

3.3.3 Neutrophil preparation

To reduce the variation of neutrophils among different donors, we used the neutrophils from one third-party healthy blood donor for each set of cell migration experiments. Ethics approval for obtaining blood samples from healthy human donors (Protocol number: J2009:030) was granted by the Joint-Faculty Research Ethics Board at the University of Manitoba. Informed consent form was obtained from all participants. Peripheral blood mononuclear cells (PBMCs) were removed using standard gradient centrifugation method. The remaining contents of the blood samples after PBMCs removal were mixed with Dextran-500, which partially separates the red blood cells (RBCs) to the bottom portion of the blood sample. The neutrophil enriched upper portion of the blood sample was transferred to a new tube and RBCs in the sample were further removed using a RBC lysis buffer (BioLegend, CA). Isolated neutrophils were washed with RPMI-1640 for 2 times and re-suspended in RPMI-1640 medium before experiments. Neutrophils were used for experiments within 8 hours (hrs) after isolation.

3.3.4 Microfluidic device preparation

The microfluidic device was fabricated in Polydimethylsiloxane (PDMS) (Dow Corning, MI) using the standard photolithography and soft-lithography methods. Briefly, the device pattern was designed in Freehand (Macromedia) and the design was printed to a transparency film as the photomask. The design was then patterned in SU-8 photoresist (MicroChem, MA) on a silicon wafer by UV exposure through the photomask. The photoresist pattern was used as a positive mold to make PDMS replicas. Holes (5mm diameter) were punched out of PDMS as solution wells and the outlet. The cell migration channel is 350μm in width and 100μm in height. The PDMS replica was then plasma

bonded to a glass slide. The microfluidic device was coated with fibronectin (0.25 mg/mL, BD Biosciences, MA) for 1 hr followed by a 0.4% BSA blocking step for another hour at room temperature to prevent non-specific binding.

3.3.5 Chemotaxis experiment setup

After seeding neutrophils onto the fibronectin-coated microfluidic channel, the two inlet wells of the device were filled with 100 μL of chemoattractant-containing migration medium and the migration medium alone (RPMI-1640 with 0.4% BSA) respectively. Then the outlet well was emptied. The pressure difference between the inlet and outlet wells establishes flows of the solutions from the inlet wells into the channels. Mixing of the flows generates a gradient of chemoattractant in the microfluidic channel **(Fig. 3.1A & 3.1B)**. The gradient was calibrated by adding FITC-Dextran 10 kDa to one of the solutions and measuring the fluorescent profile. The device was placed under an inverted microscope (Nikon Ti-U) with an environmental control enclosure chamber (InVivo Scientific) to maintain the temperature of the microscope stage at 37 °C. Differential interference contrast (DIC) time-lapse images of cell migration were captured every 10 seconds (s) for 15-20 min.

3.3.6 Data analysis

3.3.6.1 Cell migration analysis

The neutrophil migratory behaviors in different conditions were analyzed by previously established manual tracking methods [10]. Specifically, the individual cell trajectories were obtained using the “Manual Tracking” plug-in in NIH ImageJ. The movement of cells was quantitatively evaluated by 1) C.I., which is the ratio of cell displacement toward the gradient to the total migration distance; and 2) the average speed

(V), calculated as the ratio of total migration distance to the experiment period. At least 3 independent experiments were performed for each condition and at least 50 cells were tracked for each experiment.

3.3.6.2 Cell morphology analysis

We calculated the cell's aspect ratio using Fiji, an image processing package for ImageJ. Briefly, the cell boundary was segmented, and the best fitting ellipse of the cell boundary was calculated. The aspect ratio was calculated as the ratio of the major axis to the minor axis of the best fitting ellipse.

All parameters are presented as the average value ± SEM. Statistical analyses were performed with Student's *t*-test (for two samples) and ANOVA (for more than two samples). $p < 0.05$ (*) is considered significantly different.

3.4 Results

3.4.1 Development of a simple microfluidic chemotaxis device

A simple microfluidic device was developed for rapid and quantitative test of neutrophil chemotaxis in this study **(Fig. 3.1A).** The following features of this device make it suitable for chemotaxis testing in this study: 1) This device generates controlled and stable chemical gradient based on continuous laminar flow mixing in the main gradient channel. The gradient generation principle is similar to the previously characterized "Y" shape microfluidic gradient generator [10]; 2) This device does not require external pumps for fluid infusion. The flows are maintained by the pressure difference between the source inlet wells and the outlet well. Thus, this standalone device allows simple experiment setup, rapid gradient generation and chemotaxis testing; and 3) Similar to a previously reported design [88], this device uses a pressure balance zone to

stabilize the flows from different source inlet wells. This design makes the downstream gradient generation insensitive to the variation in solution volume of the source inlet wells. Therefore, the requirement of assay operation accuracy is reduced. Compared to the previous design that uses a complicated downstream network of microfluidic channels, the current design is significantly simplified by using simple zigzag channels before and after the pressure balance zone. This design allows faster gradient generation.

We monitored the gradient stability in the main gradient channel by measuring the fluorescent intensity profile of FITC-dextran over 2 hrs. Our results show that a gradient was generated within the first minute after adding the solutions to the source inlet wells and was stable over the 2 hr period, which is sufficient for the neutrophil chemotaxis experiment **(Fig. 3.1B).** When a known chemoattractant, or the supernatant of a COPD patient sputum, was added to one of the inlet wells, it generated a chemoattractant gradient in the downstream gradient channel. Our results show clear neutrophil chemotaxis to the gradient **(Fig. 3.1C & 3.1D).** The chemotaxis results will be described in the following sections.

Figure 3.1 Illustration of the microfluidic device for testing neutrophil chemotaxis. **(A)** Illustration of the microfluidic gradient generator with a pressure balance zone. Red and blue dyes were injected into the device for visualization of the channels; **(B)** The fluorescent image of the FITC-Dextran gradient in the mirofluidic channel and the corresponding gradient profiles at different time points; **(C)** A representative image of neutrophils in a COPD sputum gradient in the microfluidic channel at the end of the 20min migration experiment; **(D)** The corresponding cell tracks for the experiment in **(C)**.

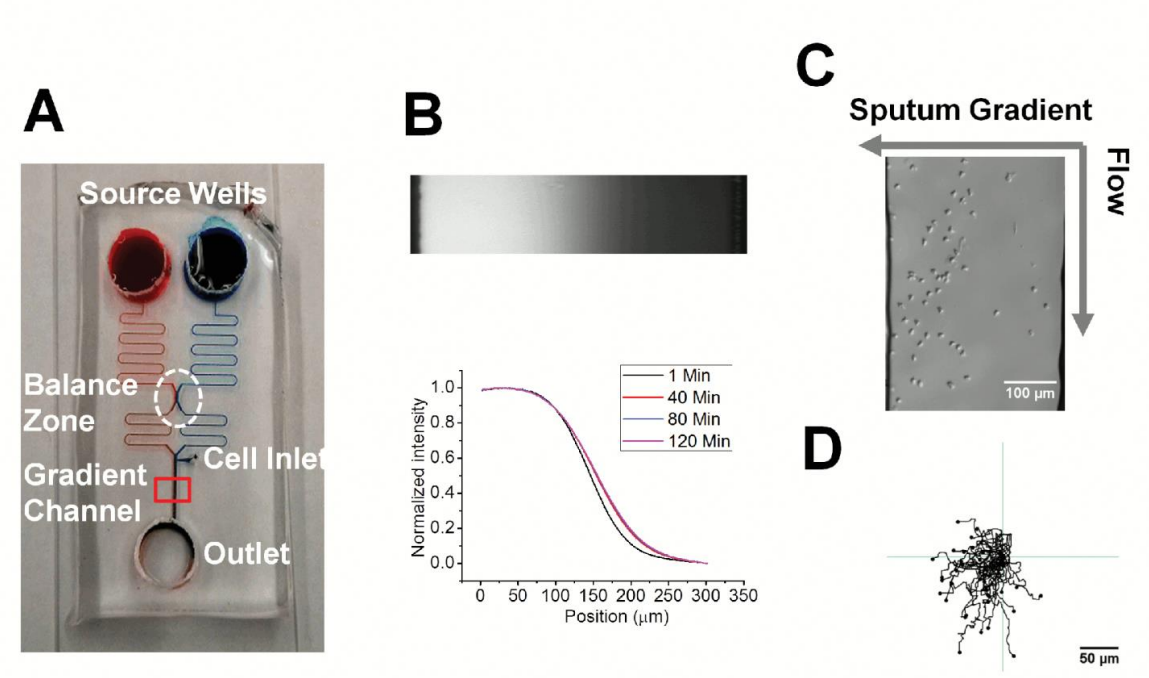

3.4.2 Characterizations of neutrophil chemotaxis to known chemoattractants using the microfluidic device

We validated the developed microfluidic device by testing neutrophil chemotaxis to single and competing gradients of recombinant chemoattractants IL-8 (10 nM) and fMLP (100 nM). These selected IL-8 and fMLP concentrations were demonstrated to induce neutrophil chemotaxis and a clear dominating effect of fMLP over IL-8 in directing neutrophil migration in competing gradients of these two chemoatttractants [29, 32, 177]. In single IL-8 or fMLP gradients, neutrophils showed strong chemotaxis towards the gradient as measured by the C.I. **(Fig. 3.2A).** In competing gradients of IL-8 and fMLP that were configured in the opposite directions, neutrophils preferentially migrated towards fMLP **(Fig. 3.2A)**. This result is consistent with previous reports that demonstrated the dominant neturophil chemotaxis toward fMLP over IL-8 [177], and the underlying signaling hierarchy of fMLP over IL-8 in directing neutrophil chemotaxis [212]. The migration speed was comparable in all conditions **(Fig. 3.2A).**

In addition to directionality and motility measurements of neutrophil migration, we further compared the morphology of chemotaxing cells in different IL-8 and fMLP gradient conditions. In single IL-8 gradient, cells displayed a narrower cell front and an elongated tail **(Fig. 3.2B).** By contrast, in single fMLP gradients, cells displayed a wide cell front without clear formation of a tail **(Fig. 3.2B).** These observations are consistent with the previous reports in the literature [220]. Consistently, in competing gradients of IL-8 and fMLP, the cell morphology was similar to those displayed in single fMLP gradients **(Fig. 3.2B)**. The cell morphological difference was characterized by the aspect ratio measurement **(Fig. 3.2C).**

Considering all the data, the microfluidic device was successfully validated with respect to measuring neutrophil chemotaxis in different gradient conditions with satisfying fidelity.

Figure 3.2 Neutrophil migration in different IL-8 and fMLP fields in the microfluidic device.

(A) C.I. and migration speed in different IL-8 and fMLP fields**; (B)** Representative images of cell morphology in different IL-8 and fMLP fields; **(C)** Aspect ratio of cells in different IL-8 and fMLP gradients. Positive C.I. indicates cell migration towards the chemoattractant source labeled on the top; negative C.I. indicates cell migration towards the chemoattractant source labeled at the bottom.

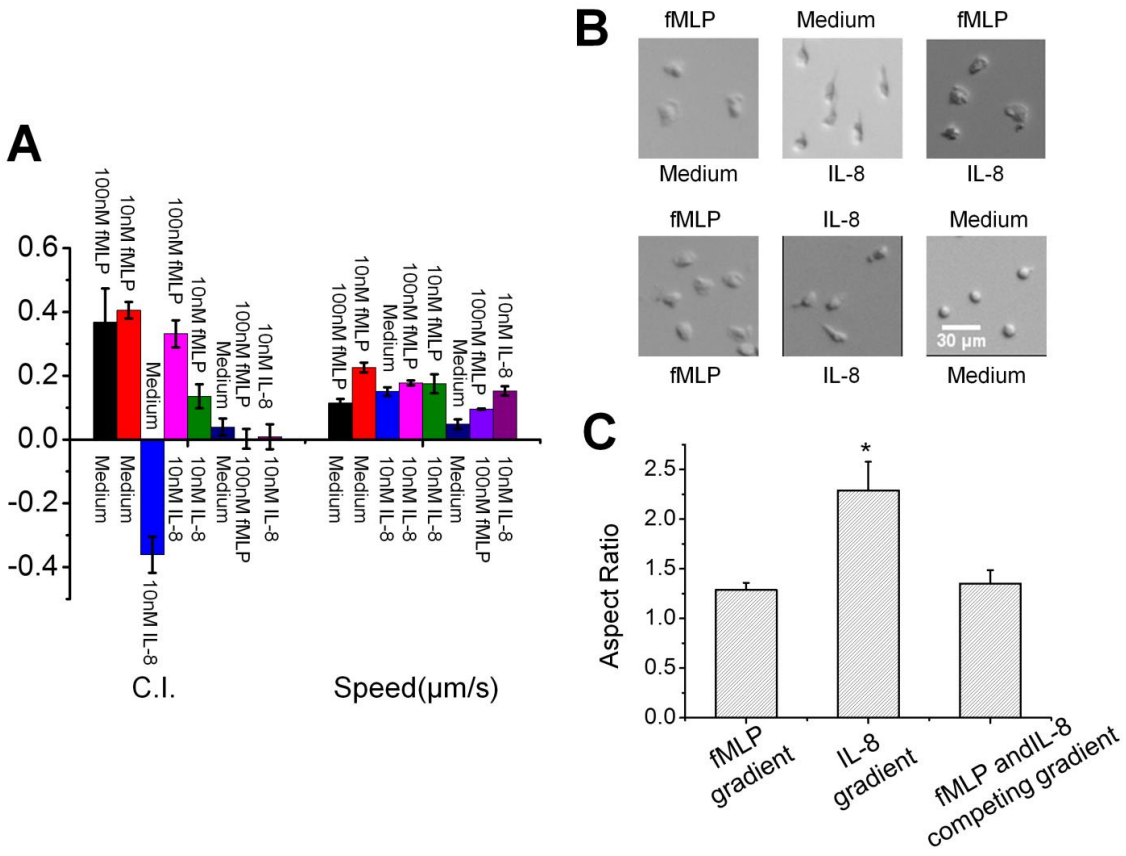

3.4.3 Characterizations of neutrophil chemotaxis to sputum from COPD patients and healthy control subjects using the microfluidic device

We then used the microfluidic device to test neutrophil chemotaxis to sputum from COPD patients versus healthy control individuals. Our results showed that single COPD sputum gradients and single healthy control sputum gradients induced strong neutrophil chemotaxis as measured by the C.I. **(Fig. 3.3A).** The levels of C.I. generated in response to the COPD sputum gradients were significantly higher compared with the levels of C.I. generated by the healthy control sputum gradients **(Fig. 3.3A).** The migration speed is comparable **(Fig. 3.3A).** These results suggest that neutrophil chemotaxis to a sputum gradient measured in our microfluidic device can distinguish COPD patients and healthy control subjects.

We further tested neutrophil chemotaxis in competing gradients of fMLP versus sputum from COPD patients or healthy control individuals. In competing gradients of fMLP and the COPD sputum, neutrophils preferentially migrated towards the fMLP gradient **(Fig. 3.3A).** Similarly, in competing gradients of fMLP and the healthy control sputum, neutrophils also preferentially migrated towards the fMLP gradient **(Fig. 3.3A).** The migration speeds were comparable **(Fig. 3.3A).** Following the same analysis method as in the previous section, we compared the cell morphology in different sputum gradients. Our results revealed that the cell morphology in single COPD or healthy control sputum gradients was similar to the morphology of cells in IL-8 gradients **(Fig. 3.3B).** In competing gradients of fMLP and sputum (COPD or healthy control), the cell morphology was similar to that of cells exposed to single fMLP gradients **(Fig. 3.3B).** The cell morphology differences in different gradient conditions were quantitatively

characterized by measuring the cell's aspect ratio **(Fig. 3.3C).** Collectively, these results suggest that neutrophil chemotaxis to sputum may be induced by different levels of tissue-derived chemoattractants such as IL-8 in the sputum. Consistently, ELISA measurements showed significantly higher IL-8 levels in COPD sputum than that in the healthy control sputum (i.e. average 3.58 ± 0.41 times higher), which is in conceptual agreement with previous reports in the literature [196].

Figure 3.3 Neutrophil migration in different sputum (COPD or healthy control) and fMLP fields.

(A) C.I. and migration speed in different sputum and fMLP fields; **(B)** IL-8 concentration in COPD sputum (n=3) and healthy control sputum (n=3)**; (C)** Representative images of cell morphology in different sputum and fMLP fields. **(D)** Aspect ratio of cells in different sputum and fMLP gradients. Positive C.I. indicates cell migration towards the chemoattractant source labeled on the top; negative C.I. indicates cell migration towards the chemoattractant source labeled at the bottom.

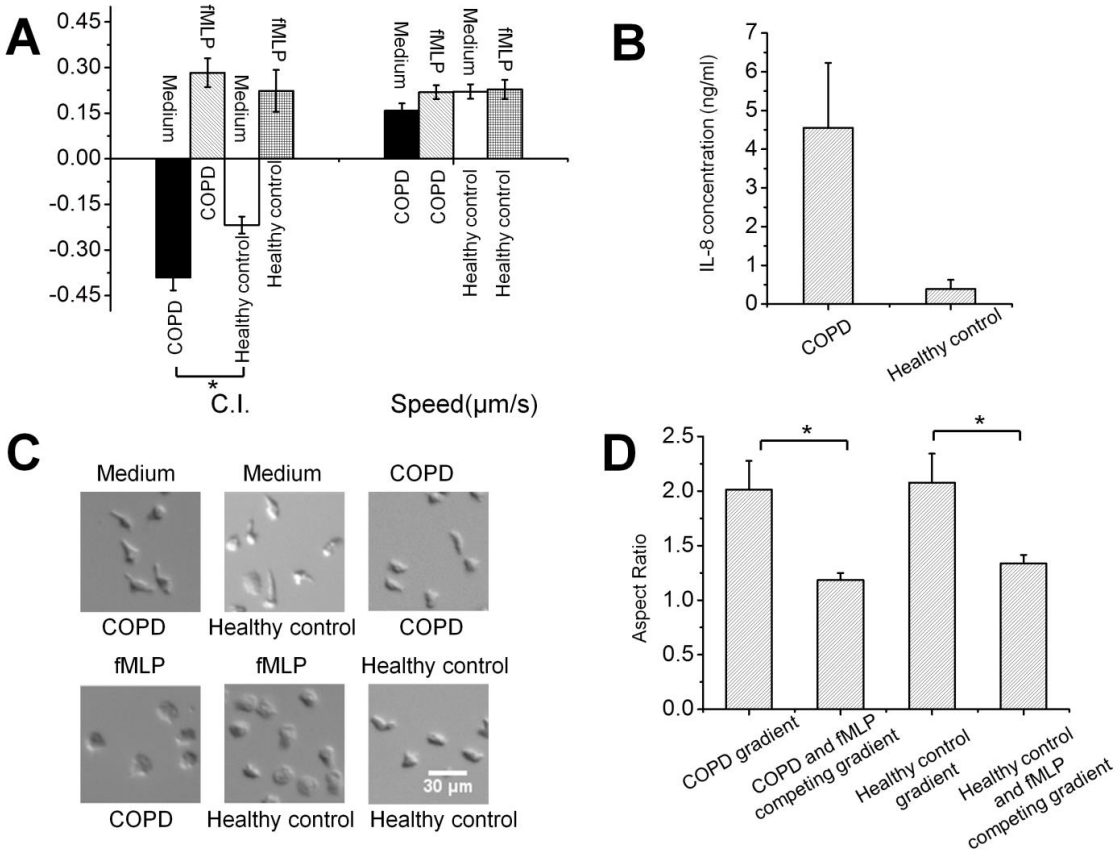

3.4.4 Characterizations of neutrophil chemotaxis to sputum from COPD patients and healthy control subjects using the compact microfluidic system

In addition to use the traditional microfluidic system to test the clinical samples, we then applied the previously developed USB microscope-based Microfluidic Chemotaxis Analysis System (UMCAS) (Details in Chapter 2) to assessing neutrophil chemotaxis in COPD **(Fig. 3.4A & 3.4B)**. Our results showed that UMCAS is effective for measuring neutrophil chemotaxis to sputum sample from COPD or healthy control patients. The sputum from both COPD patients and healthy control patients induced neutrophil chemotaxis **(Fig. 3.4C & 3.4D).** C.I. is relatively higher for COPD sputum induced neutrophil chemotaxis than it induced by healthy control sputum **(Fig. 3.4D).** The cell speed is more comparable under both conditions **(Fig. 3.4D).** The comparison of C.I. and cell speed between COPD and healthy control using the compact system is consistent with those using the traditional microscope described in section 3.4.3. Because of the limited resolution of the UMCAS, we didn't compare the cell morphology. The current results demonstrated the practical use of UMCAS for clinically-oriented research while further efforts are required to assess the potential of neutrophil chemotaxis as a clinical biomarker at the cellular function level for COPD.

Figure 3.4 Illustration of neutrophil chemotaxis in COPD using a compact microfluidic system.

(A) A picture of UMCAS; **(B)** An example of microfludic chemotaxis device and the cell image; **(C)** Cell tracks in the COPD sputum gradient from one representative experiment using UMCAS; **(D)** Comparison of Chemotaxis Index and migration speed between COPD and healthy control from all experiments. *, indicates that the significance level was $p < 0.05$.

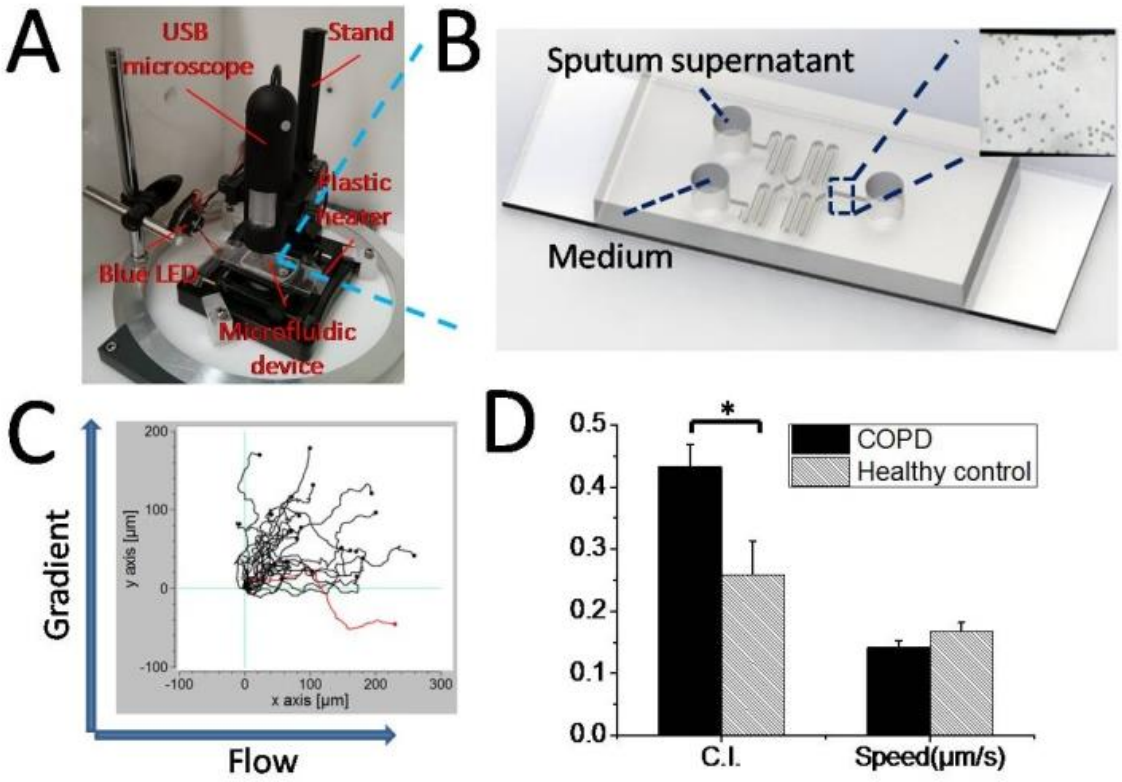

Finally, we attempted to search for possible correlations between different neutrophil chemotaxis parameters (i.e. C.I. and the migration speed), and between the neutrophil chemotaxis parameters and the conventional COPD diagnosis parameter (i.e. the spirometry data). The clinical descriptors and chemotaxis measurements for the COPD patients in this study are summarized in **Table 3.1.** Our results show no correlation between C.I. and the speed for cells in the same experiment **(Fig. 3.5A)** or for different COPD **patients (Fig. 3.5B & Table 3.1).** Interestingly, 4 out of the total 5 COPD patients showed clear correlation between C.I. and FEV1/FVC (R=0.93) **(Fig. 3.5C)**. Specifically, increased C.I. is correlated with decreased FEV1/FVC. The patient who did not follow this correlation has a younger age, a low FEV1/FVC as well as a low C.I. However, no correlation between the cell migration speed and FEV1/FVC is found **(Fig. 3.5D).**

Figure 3.5 Correlations between neutrophil chemotaxis parameters and spirometry data.

(A) No correlation is found between C.I. and migration speed in COPD sputum gradient from a single representative experiment; **(B)** No correlation is found between C.I. and migration speed from different COPD sputum samples; **(C)** Correlation between C.I. and FEV1/FVC. The dashed ellipse highlights the data with significant correlation; **(D)** No correlation is found between the migration speed and FEV1/FVC. The error bars indicate SEM.

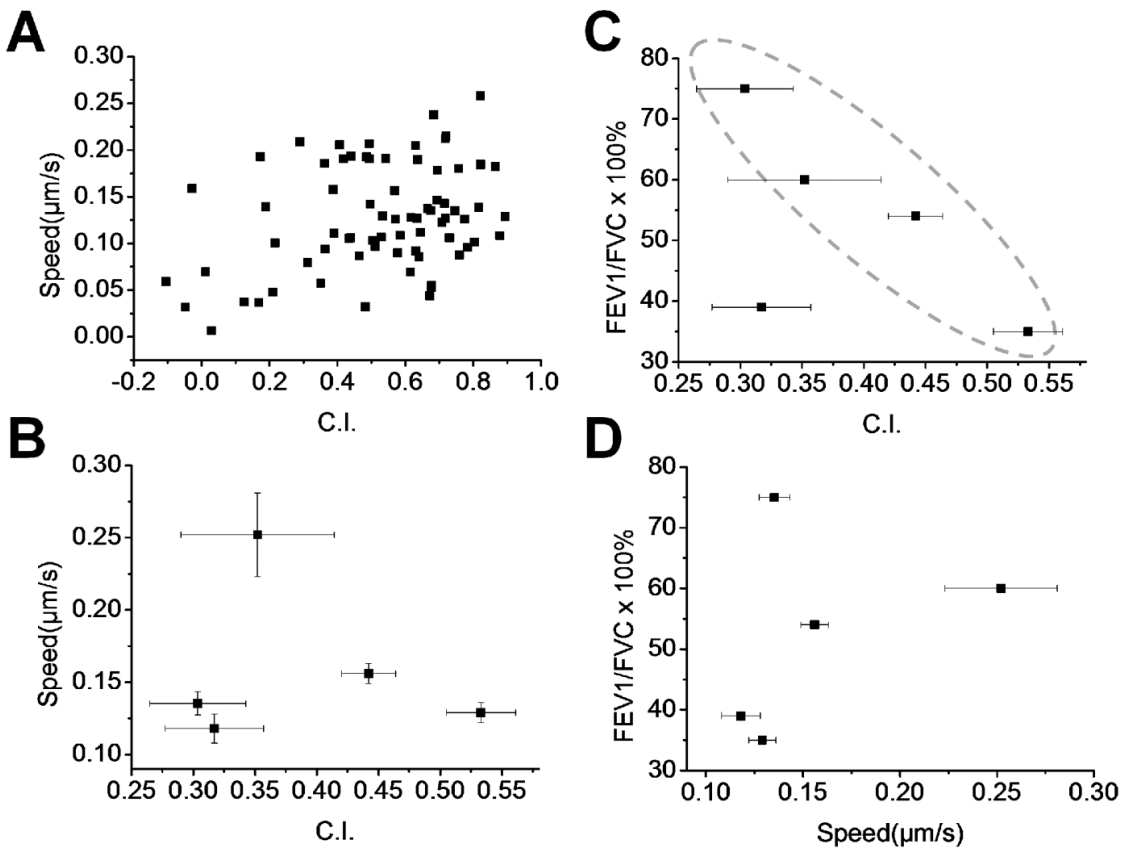

Table 3.1 The clinical descriptors and the chemotaxis measurements of the COPD patients and healthy control subjects in this study.

	Age	Gender	FVC (L)	FEV1 (L)	FEV1/FVC (x100%)	C.I.(SEM)	Speed (μm/s)(SEM)
COPD patients	74	F	1.68	0.59	35	0.533(0.028)	0.129(0.007)
	72	F	1.93	1.05	54	0.442(0.022)	0.156(0.007)
	57	F	1.89	0.73	39	0.317(0.040)	0.118(0.010)
	63	M	2.6	1.56	60	0.352(0.062)	0.252(0.029)
	67	F	1	0.75	75	0.304(0.039)	0.135(0.008)
Healthy control subjects	41	M	NA	NA	NA	0.298(0.020)	0.154(0.006)
	53	M	NA	NA	NA	0.144(0.013)	0.212(0.005)
	26	M	NA	NA	NA	0.265(0.045)	0.277(0.017)
	29	F	NA	NA	NA	0.191(0.045)	0.272(0.028)
	64	F	NA	NA	NA	0.194(0.031)	0.192(0.011)

3.5 Discussion

Previous microfluidics-based clinical studies focused only on testing the changes in the migration and chemotaxis of a patient's neutrophils to defined chemoattractants as a result of disease [199, 216]. In this study, and for the first time, we established an effective microfluidic platform for quantitative analysis of neutrophil chemotaxis to COPD sputum samples. This is also the first time that clinical samples from chronic disease patients were used as chemoattractant source for microfluidics-based chemotaxis studies. Therefore, our results better reflect the migration and chemotaxis properties of neutrophils under pathological conditions.

Furthermore, our test results provide quantitative evidence, at the single cell level, for significantly different levels of neutrophil chemotaxis to sputum from COPD patients versus healthy control subjects. Our data also provide a range of quantitative characterizations of neutrophil migration and chemotaxis to COPD sputum, including directionality, motility, and cell migratory morphology. In addition to directly quantifying neutrophil chemotaxis to sputum, competition of sputum and defined chemoattractants in directing neutrophil migration provides another complementary measurement. These results offer a panel of quantitative descriptors based on neutrophil chemotaxis to discriminate COPD and non-COPD samples, and suggest the important chemotactic factors in the sputum sample responsible for neutrophil chemotaxis.

In contrast to an intriguing earlier study that studied neutrophil chemotaxis for asthma diagnosis using a microfluidic device [219], our results show an interesting correlation between the C.I. of neutrophils to the sputum versus spirometry data of COPD patients. This suggests a possible correlation between neutrophil chemotaxis and the

severity of COPD, and the potential of using the chemotaxis characteristics to identify COPD in a particular stage. Further testing with a larger cohort is required to clarify this correlation. In addition, it will be very interesting to investigate the potential diagnostic value of this new microfluidics-based test by correlating neutrophil chemotaxis to the patient's medical history, such as the exacerbation record to improve disease group classification, risk prediction, and treatment strategy [221].

Microfluidic analysis of neutrophil chemotaxis has been recently demonstrated for successful diagnosis of asthma [219]. Our study provides another example of successful use of a microfluidic platform for diagnosis of inflammatory lung disease, by assessing neutrophil chemotaxis. These two studies suggest the promise of new biomarkers at the cellular function level for disease diagnosis and monitoring. On the other hand, microfluidic cell analysis often requires specialized research facilities, such as microfabrication and live cell microscopy labs, as well as highly-skilled personnel to perform the experiments and analyze the data. These requirements present significant challenges for adopting microfluidic methods for a routine test in clinical settings. To overcome these limitations, recent studies have demonstrated the promise of practical point-of-care applications based on microfluidic chemotaxis analysis [147]. In this direction, on-chip capture of neutrophils directly from a drop of blood, based on specific antibody or adhesion molecules for recognizing neutrophils, has been demonstrated [161, 222]. The captured cells can be directly used for chemotaxis analysis in the same microfluidic chip, which significantly reduces the current lengthy process for cell isolation and requires only minimal amounts of blood for each test. Pump-free standalone microfluidic gradient devices have been employed to minimize the requirement of

external instrument controls, such as syringe pumps or other pressure sources. The microfluidic gradient generator used in this study provides highly controlled flow-based chemical gradients without external fluid perfusion instrument. It has the advantage in fast generation of stable gradients compared with free diffusion-based standalone microfluidic gradient devices [13, 101]. The relatively simple and compact design of this device has the scaling potential to enable high-throughput tests on a single chip by integrating multiple test units in parallel. In addition, various image analysis methods have been developed to allow automated single cell tracking analysis, thus eliminating the need for lengthy and laborious post-experiment tracking analysis and permit instant result report [147].

To ultimately enable point-of-care test, the entire microfluidic system including microfluidic device, gradient generation and calibration, on-chip cell capturing, environmental control, chemotaxis experiment, image acquisition and automated data analysis and result reporting should be integrated to meet the requirements in portability, cost factor, ease-of-operation and reliability for clinical use. Toward this direction, we have previously reported a compact microfluidic chemotaxis analysis system (i.e. UMCAS) with most of the above listed features and demonstrated its effective use for measuring neutrophil chemotaxis to an IL-8 gradient [223]. This UMCAS system was effectively used to test neutrophil chemotaxis to sputum samples and the results are consistent with the results in this study using traditional microscopy. Therefore, the microfluidic chemotaxis system has the potential for on-site clinical COPD diagnosis.

In the current study, we used neutrophils from a third-party healthy blood donor to compare their chemotaxis to different sputum samples from CODP or non-COPD

patients. It has also been reported that neutrophil from COPD patients in different stages will have different chemotaxis behaviors [199]. Similar effect was also reported in other neutrophil chemotaxis mediated lung diseases such as asthma [224]. Therefore, chemotaxis of neutrophils from COPD or non-COPD patients to relevant chemoattractants such as IL-8 and LTB4 should be compared. It will also be important to further compare chemotaxis of neutrophils from COPD or non-COPD patient to their own sputum samples, which will determine if there is any patient specific response. Previous studies using conventional cell migration assays have also showed that neutrophil chemotaxis to the sputum from COPD patient with A1AD is higher comparing to the sputum from non-A1AD COPD patients [198]. The developed microfluidic method can be readily used to quantitatively assess the effect of A1AD under better controlled experimental conditions, which may enable discrimination of COPD patients with or without genetic disorders.

In conclusion, our study demonstrated for the first time successful use of a microfluidic system for assessing neutrophil chemotaxis to clinical samples from COPD patients, and suggested the potential of this new method to assist COPD diagnosis and monitoring at the point-of-care.

Chapter 4

An all-on-chip method for testing neutrophil chemotaxis induced by fMLP and COPD patient's sputum

This chapter is based on the following manuscript: "J.D. Wu, C. Hillier, P. Komenda, R. Lobato de Faria, S. Santos, D. Levin, M. Zhang and F. Lin, An all-on-chip method for testing neutrophil chemotaxis induced by fMLP and COPD patient's sputum, Technology, accepted 2016".

This part of the work was performed during the last two years of my Ph. D. study. In all the previous experiments, we separated the cells using the traditional centrifugation method, which is a lengthy and complex process. In order to enable the on-chip neutrophil isolation from few volumes of whole blood, I have tried several methods including using P-selectin as capture molecules and using DI water to lyse the RBCs and lymphocytes in a short time while neutrophils are still alive. None of these methods gave satisfactory results. Then in the autumn of 2014, we got a new magnetic neutrophil isolation kit for negative neutrophil selection directly from whole blood (EasySep Direct). I wondered if we could integrate this kit into our microfluidic device to enable neutrophil isolation and chemotaxis in a same chip. This idea was successfully validated in this paper. I performed the experiments, analyzed the data, and wrote the manuscript for journal publication.

4.1 Overview

Neutrophil migration and chemotaxis is a fundamentally important biological process and has direct relevance to various health problems. Microfluidic devices provide

useful experimental tools for quantitative analysis of neutrophil chemotaxis in controlled microenvironments. However, such experiments often require specialized research facilities and lengthy cell preparation from large amount of blood. In this chapter, we report a new, yet simple, all-on-chip method for magnetic isolation of untouched neutrophils directly from small volumes of blood, followed by chemotaxis testing on the same microfluidic device. Furthermore, we incorporated a cell-docking structure to the microfluidic device for better control of the cells' initial positions before the chemotaxis test and for improved data analysis. The whole experiment can be done in less than 25 minutes. We successfully validated this method by testing neutrophil chemotaxis to both purified chemoattractant (i.e. fMLP) and clinical samples (sputum from patients with Chronic Obstructive Pulmonary Disease). Thus, the "all-on-chip" method can be a useful tool for research and clinical applications that require rapid and accurate chemotaxis testing of untouched neutrophils.

4.2 Introduction

Directional cell migration plays important roles in many biological processes and diseases such as host defense, tissue generation and metastactic cancers [5, 200, 201]. Among the various environmental guiding mechanisms [17, 171], chemical gradient can direct the migration of different cell types by chemotaxis. Neutrophils are an important type of white blood cells that play a crucial role in host defense. Its immune functions rely critically on chemotaxis [225]. Neutrophils are a well-established cell model for studying cell migration and chemotaxis [17, 22], and neutrophil chemotaxis has been targeted for disease oriented research [26, 219, 226] . Traditionally, neutrophils are isolated by density gradient centrifugation based method [227], which is time-consuming,

requires large amounts of blood, and can cause cell activation and damage. Magnetic cell isolation method can further enrich neutrophils from the polymorphonuclear (PMN) fraction of the blood [228]. However, the magnetic method typically still requires centrifugation and has higher reagent cost. Nevertheless, traditional neutrophil isolation methods are widely used for different cell migration assays.

Compared with conventional cell migration assays, microfluidic devices provide useful experimental tools for quantitative cell migration and chemotaxis analysis in well-controlled chemical gradients [13]. Various microfluidic gradient devices have been developed and applied to neutrophil chemotaxis analysis [13]. In particular, several studies have demonstrated neutrophil migration testing directly from blood by integrating on-chip neutrophil isolation with adhesion-based neutrophil capturing or geometric confinement [161, 219, 229]. Recently, a new magnetic neutrophil isolation kit for negative neutrophil selection directly from whole blood has been developed (EasySep Direct) [230]. In this study, our primary objective was to integrate the EasySep Direct kit with a microfluidic device for all-on-chip neutrophil chemotaxis testing directly from blood. The useful features of this method include: 1) isolation of neutrophils at high purity directly from whole blood; 2) the enabling of rapid neutrophil chemotaxis experiments directly from a small amounts of blood using small volumes of cell isolation reagents; and 3) the enabling of on-chip chemotaxis testing using negatively selected neutrophils, which avoids possible activation and damage during traditional cell isolation processes. Two types of microfluidic devices were developed in this study. A previously reported microfluidic gradient generator (i.e. type I device) [226] was adapted to validate the cell isolation method. The type II device integrated a cell-docking structure so that the

cells are aligned next to the gradient channel and therefore the subsequent cell migration in response to the applied chemoattactant gradient can be easily and more accurately quantitated. To validate this method, we tested neutrophil chemotaxis to fMLP, a well-known neutrophil chemoattractant, and to sputum from patients with COPD, which has been shown to attract neutrophils [160].

4.3 Materials and methods

4.3.1 Microfluidic device preparation

The preparation of the microfluidic chemotaxis device has been previously described [226]. Briefly, the master of the microfluidic device was fabricated using the standard photolithography method. Two types of master were fabricated. The type I device was fabricated using a single layer photolithography method. The pattern was designed using AutoCAD software and printed onto a transparency film as the photomask. SU-8 photoresist (~ 60 μm thick) was spin coated on a silicon wafer. The pattern design was transferred to the photoresist by UV-exposure through the photomask. The type II device with the cell-docking structure was fabricated using a two-layer photolithography method [231]. A first layer of SU-8 (~ 4 μm) pattern was fabricated on the silicon wafer. Then another layer of SU-8 (~ 60 μm thick) pattern was aligned on the top of the first layer. The polydimethylsiloxane (PDMS) replica of the pattern was fabricated by the standard soft-lithography method [226]. Holes (4 mm diameter) for the two chemical inlet wells and one outlet well were punched out of the PDMS replica. Then the PDMS replica was plasma bonded to a glass slide to complete the microfluidic device assembly. The thin ~ 4 μm channel in the type II device was designed to pattern cells by preventing cells from entering the gradient channel before the gradient is applied.

The microfluidic channel was coated with fibronectin for one hour followed by BSA blocking for another hour in room temperature before cell migration experiments.

4.3.2 Collection of sputum and blood samples

The sputum samples from COPD patients were collected at the Seven Oak General Hospital in Winnipeg Manitoba (Canada). Research Ethics Board approval was obtained from the University of Manitoba. Supernatant from the sputum was prepared following the protocol as described previously [226]. The supernatant was used as chemoattractants for neutrophil chemotaxis experiments. Blood samples from healthy donors were collected at the Victoria General Hospital in Winnipeg under a separate approved human research ethics protocol.

4.3.3 On-chip cell isolation, cell migration experiment and analysis

The type I microfluidic device and the experimental procedures for the all-on-chip neutrophil chemotaxis testing are illustrated in **Fig. 4.1**. The microfluidic device follows the same design we reported previously [226], but the area near the outlet was specially shaped to allow easy attachment of the magnets. The serpentine input channel in each side is 60 mm long and 200 μm wide. The gradient channel is ~6mm long and 350 μm wide. This device allows rapid generation of chemical gradient in the microfluidic channel for chemotaxis experiments in a pump-free manner.

For on-chip neutrophil isolation, 10 μL of whole blood was added into a 1.5 mL Eppendorf tube. Then 2 μL of antibody cocktail and the magnetic particles (Ab-MP) from the neutrophil isolation kit for negative neutrophil selection (EasySep™ Direct Human Neutrophil Isolation Kit, STEMCELL) were added to the tube and mixed with the blood. The blood-Ab-MP mixture was incubated at room temperature for 5 minutes.

Two small magnetic disks (5 mm diameter and 1 mm thick (CAT# 44202-1, Indigo Instruments) were vertically attached to the two sides of the outlet well. The medium in the inlet and outlet wells was aspirated before loading the blood-Ab-MP mixture. Two microliters of the blood-Ab-MP mixture was loaded to the center of the outlet well using a pipette tip. The magnetically-conjugated cells moved to the side walls of the outlet well, driven by the magnetic force, while neutrophils were free to enter and settle on the fibronectin-coated gradient channel. Then chemoattracatant solution (prepared in RPMI-1640 with 0.4% BSA) and the medium were added to the inlet wells. Two chemoattractant solutions were used: 1) 100nM fMLP; 2) 10X diluted supernatant of the sputum from COPD patients. Because of the pressure difference between the inlets and outlet of the gradient channel, the solutions flowed into the gradient channel and a concentration gradient of the chemoattractant was generated based on laminar flow mixing. FITC-Dextran 10kDa (Sigma-Aldrich, MO; final concentration 5 μM in RPMI-1640) was added to the chemoattractant solution to verify gradient formation by measuring the fluorescent intensity profile in the channel. At this point, the magnets were removed from the device, and flow prevented cells in the outlet well from entering the channel.

Figure 4.1 Illustration of the all-on-chip method for neutrophil chemotaxis analysis using the type I device.

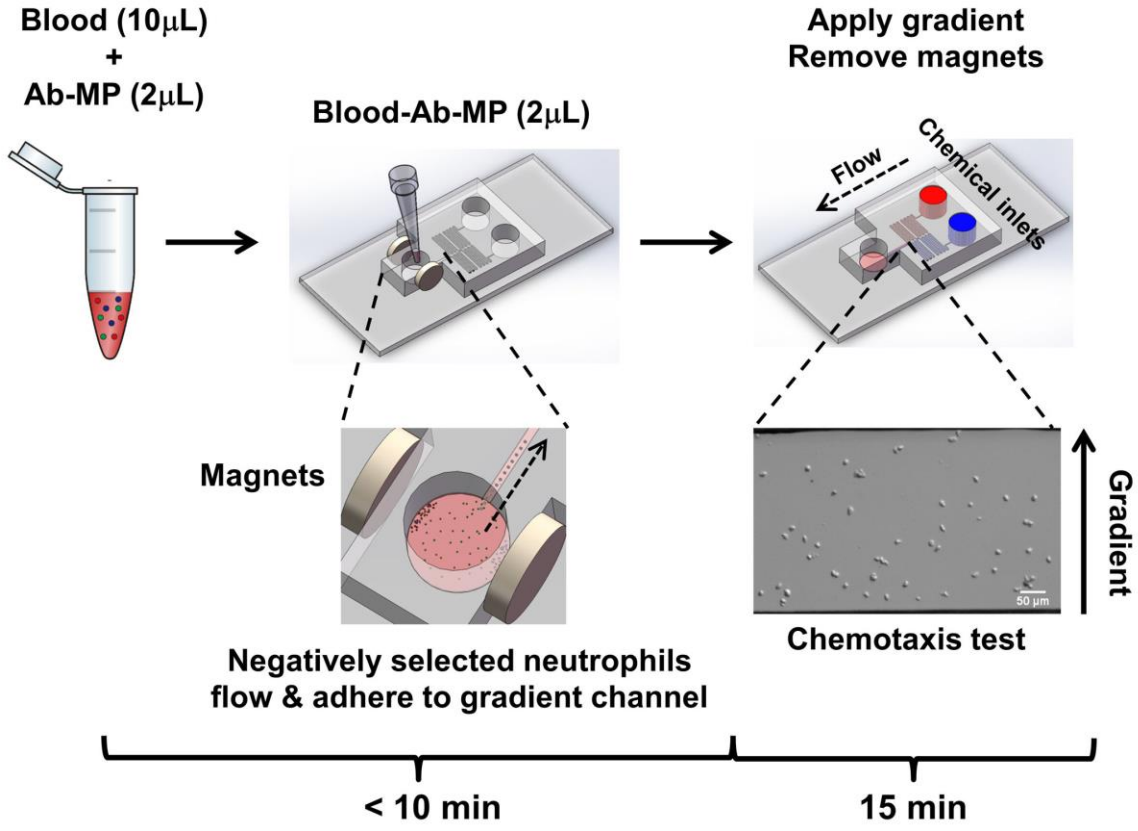

The type II device is illustrated in **Fig. 4.2.** The dimensions of the gradient channels are similar to the type I device except the width of the gradient channel of the type II device is 280 μm. The gradient generation method and cell isolation procedures were similar to those described for the type I device. To test the stability of the gradient, we measured the fluorescence intensity profile of FITC-Dextran in the gradient channel. The results showed stable gradient profile over an hour, which is sufficiently long for the cell migration experiment in this study (**Fig. 4.2E)**. Instead of isolating cells from the outlet as in the type I device, the magnetic cell isolation takes place through a separate cell-loading port and channel on one side of the gradient channel. The cell-loading channel connects to the cell-docking region. All the inlets and outlet were emptied before loading the blood. However, medium remains inside the cell loading channel and the bottom of the cell loading port. A few microliters of blood-Ab-MP mixture was added to the cell loading port and mixed with the medium. The isolated neutrophils flowed into the cell docking region driven by the pressure flow between the cell loading port and the gradient channel inlets/outlet. The cells were trapped and aligned next to the gradient channel in the cell-docking regions because of larger cell size comparing to the ~4 μm high docking channel.

Cell migration was recorded by time-lapse imaging at 6 frames per minute using a Nikon Ti-microscope with an environmental control chamber to maintain the temperature at 37 °C throughout the experiment. After the experiments, 10-100 individual cells from the time-lapse images for each experiment were tracked to calculate quantitative cell migration parameters including C.I. and migration speed using the established method [10]. C.I. is the ratio of cell displacement toward the gradient to the total migration

distance. The migration speed is the ratio of total migration distance to the experiment period. The cell morphology analysis was performed by measuring the aspect ratio following the previously described method [226]. Basically, the aspect ratio was calculated as the ratio of the long axis and short axis of the best fitting ellipse of the cell contour. Because the cells were patterned with the same starting position relative to gradient in the type II device, we analyzed the cell migration distance along the direction of the gradient into the gradient channel as a measure of chemotaxis.

Figure 4.2 Illustration of the all-on-chip method for neutrophil chemotaxis analysis using the type II device.

(**A**) Illustration of the type II device; (**B**) The enlarged view of the cell-docking structure; (**C**) The dimension of the gradient channel and the cell-docking structure (unit: μm); (**D**) The image of patterned cells before and after applying the gradient; (**E**) The gradient profile at different time points in type II device. Note the 0^{th} min indicates a few minutes after the medium and the chemoattractant solution were added to the inlets.

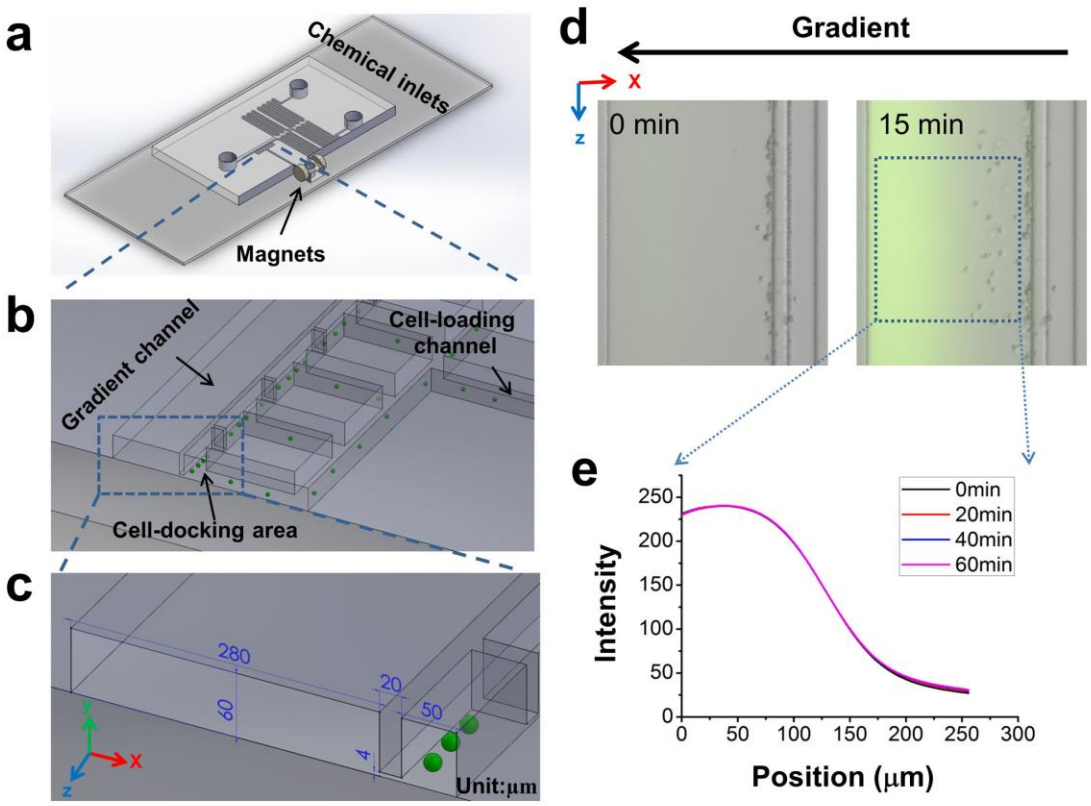

4.3.4 Cell staining and imaging

Cells (isolated by the on-chip method) in the microfluidic channel were fixed with methanol and then stained by 1:20 diluted Giemsa stain solution (Rowley Biochemical) [232]. Then the stained cells were washed with deionized water and imaged by an inverted light microscope. In a separate experiment, cells (isolated by the on-chip method) in the microfluidic channel were stained with FITC-conjugated anti-CD66b antibody (CAT# 10419, STEMCELL) for cell surface CD66b expression followed by 2X PBS wash and imaging with a fluorescence microscope.

4.3.5 Statistical analysis of the data

At least three independent experiments were performed for each condition for all experiments. All parameters are presented as the average ± SEM. Statistical analyses were performed using Student's *t*-test. $p < 0.05$ (*) was considered significantly different.

4.4 Results

4.4.1 Characterizations of on-chip neutrophil isolation

First, we verified that without using the microfluidic device, the EasySep Direct kit enabled isolation of polymorphonuclear (PMN) cells at high purity (i.e. >95%) from larger volumes of blood, as shown by the standard flow cytometric analysis (**Fig. 4.3A**). Next, we validated the on-chip method by on-chip Giemsa staining (**Fig. 4.3B**) and CD66b staining (**Fig. 4.3C).** The Giemsa staining showed typical ring-shaped and lobe-shaped nuclei feature of the neutrophils. The CD66b staining also showed positive result. These results suggested that the on-chip isolation method enabled effective isolation of PMN cells at high purity (near 100%) from much smaller volumes of blood. Because the on-chip method starts from very small volumes of blood, the amount of isolation reagent

is also significantly reduced (i.e. 25-fold less than the standard bulk isolation with the EasySept Direct kit), while still providing enough cells for the subsequent chemotaxis experiments in the same device. The whole on-chip cell isolation can be completed in less than 10 minutes.

Figure 4.3 Validation of cell isolation.

(**A**) Forward Scatter (FSC) *vs* Side Scatter (SSC) plot from flow cytometry shows high purity of PMN cells by standard bulk cell isolation using the EasySep Direct kit; (**B**) Giemsa staining images (60X) of the cells in the microfluidic channel isolated using the on-chip method; (**C**) DIC images, CD66b-FITC staining images and merged images (10X) of the cells in the microfluidic channel isolated using the on-chip method.

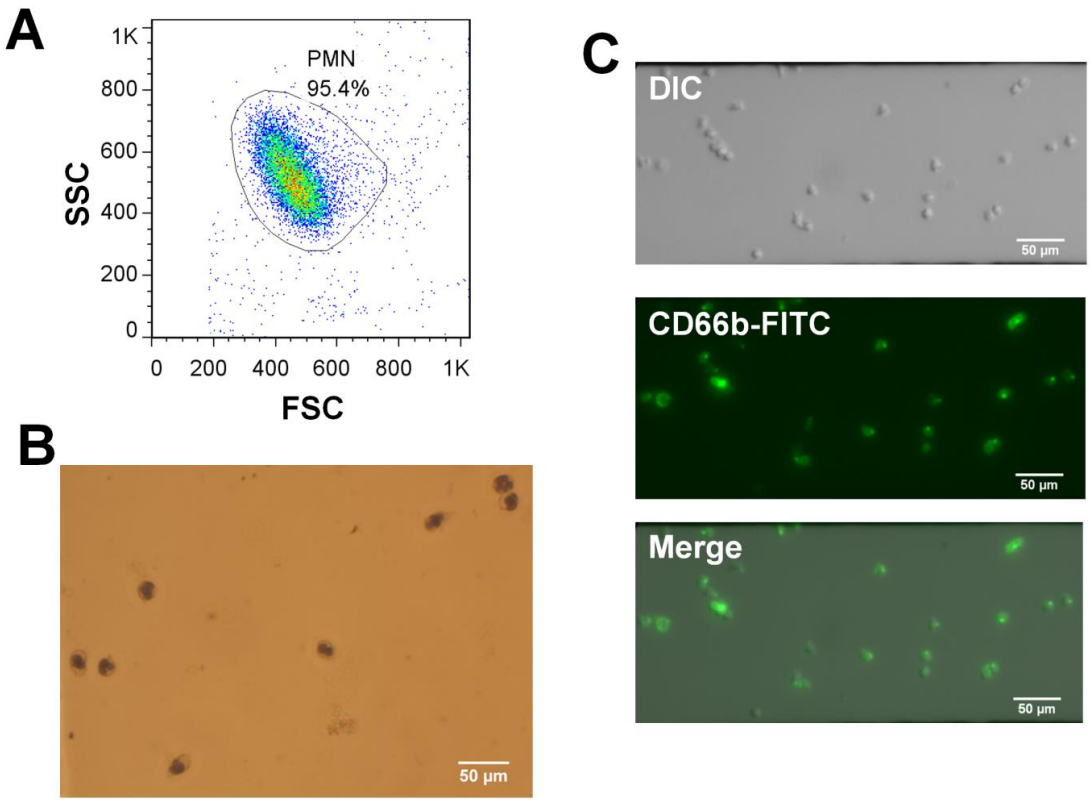

4.4.2 Direct on-chip testing of neutrophil migration to fMLP and sputum from COPD patient using the type I device

We next validated the type I device by testing neutrophil chemotaxis to a well-known chemoattractant, fMLP. After the on-chip cell isolation, a 100 nM fMLP gradient or medium flow alone as the control was applied to the cells in the gradient channel, and cell migration was recorded for 15 minutes. Because the cell migration experiment was immediately following the on-chip cell isolation in the same device, the whole experiment from blood to chemotaxis testing was done in less than 25 minutes. C.I. and migration speed in the fMLP gradient were significantly higher compared to the medium control, thus clearly demonstrating chemotaxis to fMLP using this all-on-chip method (**Fig. 4.4A**). This result is consistent with the previous result using the traditional isolation method as described in section 3.4.2.

We previously demonstrated neutrophil chemotaxis induced by sputum from COPD patients using a similar microfluidic device and the traditional cell isolation method [226]. This study suggested the potential of microfluidics-based neutrophil chemotaxis test for clinical COPD diagnosis. However, the lengthy traditional cell isolation method and the associated requirements in facility, as well as cost and skills, present a major bottleneck for clinical applications. We believe the all-on-chip method provides a rapid and cost effective solution. To further validate the on-chip method, we evaluated neutrophil chemotaxis to COPD sputum. Our results clearly demonstrated neutrophil chemotaxis and motility induced by COPD sputum, as shown by the C.I. and migration speed **(Fig. 4.4A)**. Compared with the medium control, both CI and cell speed in the fMLP and COPD sputum gradient are much higher. These results demonstrate the

chemoattractant gradient stimulated neutrophil chemotaxis. Furthermore, CI but not cell speed in the fMLP gradient is higher than it in the COPD sputum gradient. These results are in qualitative agreement with our previous study using a similar type of device [226]. However, the underlying biological mechanisms require further investigation. The quantitative cell migration parameters in different sets of experiments can also depend on the chemoattractant doses, blood donors and COPD sputum samples. Consistent with our previous results using the traditional cell isolation method [226], we found elongated cell morphology (higher aspect ratio) in the COPD sputum but fan-shape cell morphology in the fMLP gradient (lower aspect ratio) using the on-chip method **(Fig. 4.4B)**. Consistent with our previous work [226], the cell morphology in the COPD sputum is similar to it in the IL-8 gradient, suggesting that neutrophil chemotaxis to the COPD sputum gradient is mainly induced by tissue-derived chemoattractants such as IL-8 in the sputum. The observed difference in cell morphologies induced by different chemoattractant gradients requires further investigation to explore the underlying mechanisms.

Figure 4.4 Validation of neutrophil chemotaxis to a fMLP gradient and a COPD sputum gradient using the on-chip method in the type I device.

(A) Comparison of C.I. and migration speed in the medium control, a 100nM fMLP gradient, and a COPD sputum gradient; **(B)** Comparison of cell morphology in the COPD sputum gradient and the fMLP gradient using the on-chip method.

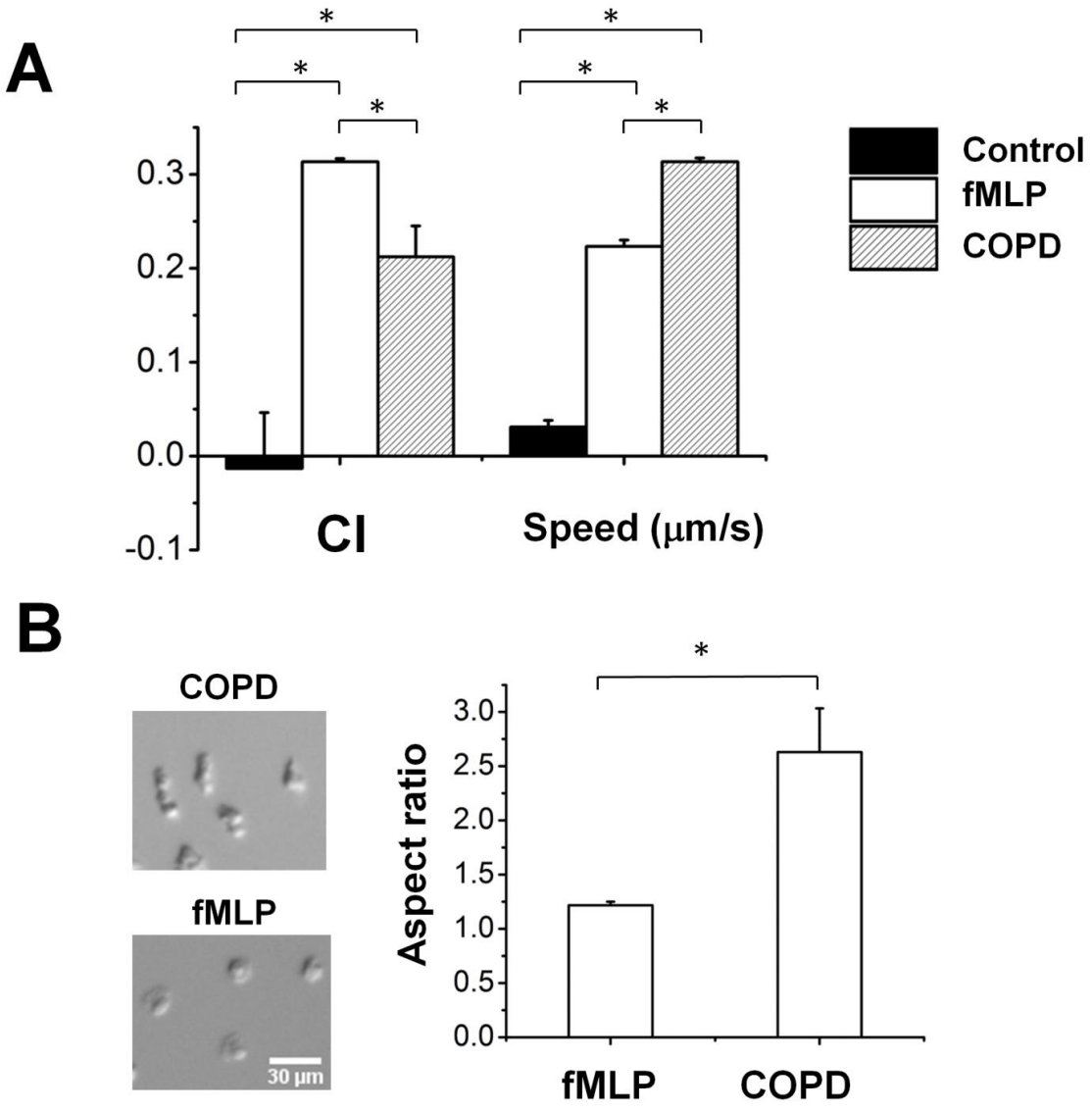

4.4.3 Direct on-chip testing of neutrophil migration to fMLP and sputum from COPD patient using the type II device

In some experiments using the type I device, we found the cells could not attach well to the fibronectin coated channel under flow. Furthermore, in the type I device, there is no control of the cells' initial positions in the channel relative to the gradient, which complicates the accuracy of the chemotaxis analysis. To overcome these limitations, we further developed a type II device by incorporating cell-docking structures. As shown in **Fig. 4.2D**, the cells isolated from the whole blood were successfully trapped in the cell-docking area. The stuff outside the docking area and stuck at the edge of gradient channel should be some broken cells and debris, which is observed to have limited affection to the cell migration. After the on-chip cell isolation, the cells were exposed to the medium flow, and the cell migration was recorded for 15 minutes as the control. During this period, very few cells crossed the barrier and moved into the gradient channel **(Fig. 4.5A)**. Then a 100 nM fMLP gradient was applied to the gradient channel. Many more cells responded quickly and migrated into the gradient channel **(Fig. 4.5A)**. Similarly, the cells showed migratory response to the COPD sputum gradient in the type II device (**Fig. 4.5A)**. The results show higher CI and migration speed in the fMLP gradient than those in the COPD sputum gradient (**Fig. 4.5C)**. In addition, cells migrated a longer distance toward the fMLP gradient than the COPD sputum gradient over the 15 minutes experiment (**Fig. 4.5D)**. This observation indicates the more persistent chemotactic migration of neutrophils to the fMLP gradient and is consistent with the higher CI in the fMLP gradient than the COPD sputum gradient in both the type I device and the type II device (**Fig. 4.4A & 4.5C**). The variations of quantitative cell migration parameter

comparison between the type I and type II device in this study can be in part due to neutrophils from different blood donors. In addition, the initial cell alignment in the low concentration region of the chemoattractant gradient in the type II device is believed to cause the significantly higher CI but lower cell speed, and different cell speed comparison between the fMLP gradient and the COPD sputum gradient comparing to the type I device without initial cell alignment.

Figure 4.5 Validation of neutrophil chemotaxis to a fMLP gradient and a COPD sputum gradient using the on-chip method in the type II device.

(A) Comparison of cell distribution in the medium control, a 100nM fMLP gradient, and a COPD sputum gradient at the 0^{th} minute and the 15^{th} minute after applying the gradient; **(B)** Illustration of the analysis of the cell migration distance. The green line denotes the edge of the gradient channel. The orange line denotes the cell migration distance towards the gradient direction; (**C**) Comparison of CI and migration speed in a 100nM fMLP gradient and a COPD sputum gradient; **(D)** The averaged cell migration distance into the gradient channel along the direction of the gradient in a 100nM fMLP gradient and a COPD sputum gradient.

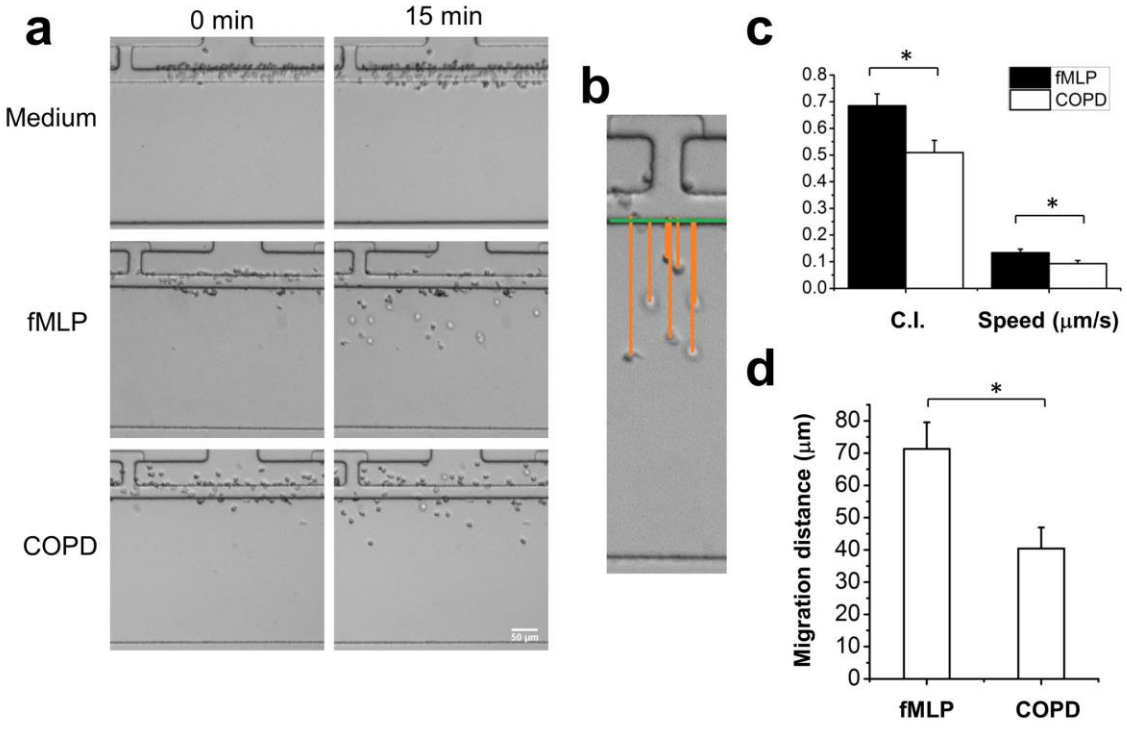

4.5 Conclusion

In this study, we demonstrated a simple, effective, and robust all-on-chip method for testing neutrophil chemotaxis. Previously, we used a similar microfluidic device to study neutrophil chemotaxis to sputum from COPD patients using both traditional microscopy-based method and a portable imaging system [226, 233]. However, the traditional cell preparation method significantly limits the efficiency of neutrophil chemotaxis experiment and makes it difficult to run the test in clinical settings. The developed all-on-chip method effectively removed this bottleneck. The previous cell chemotaxis analysis using the simple gradient generator is complicated by the un-controlled initial cell positions in the gradient [226], and we have recently shown that cell migration is sensitive to the cell's current and previous gradient exposure [234]. To this end, the integrated cell-docking function in the type II device provides an effective solution and the cell migration distance analysis permits easy chemotaxis quantification without cell tracking. It will be interesting and useful to further compare the quantitative chemotaxis parameters between traditional cell isolation method and the on-chip method. Collectively, the "all-on-chip" method provides a useful tool for research and clinical applications that require rapid and accurate chemotaxis testing of untouched neutrophils. Similar methods can be applied to other cell types upon availability of the corresponding magnetic cell isolation kits.

Chapter 5

Conclusion and outlook

Compared with the traditional investigation tools, the microfluidic platform offers a well-controlled, repeatable method for creating stable concentration profiles so that the cell migration experiments can be performed accurately and efficiently. In this thesis, we developed several microfluidic devices and systems for investigating neutrophil chemotaxis for both research and clinical applications. We provided a complete solution with minimum complexity and maximum efficiency for performing a cell migration experiment, including on-chip cell isolation from few microliters of whole blood, standalone microfludidic gradient generator, compact imaging system, and rapid data analysis. We successfully validated these systems by testing the neutrophil chemotaxis to single or competing gradients of well-known chemoattractants such as IL-8 and fMLP. Furthermore, we for the first time applied a microfluidic system to investigate the neutrophil chemotaxis induced by the sputum from patients with COPD, suggesting the use of this method as a potential diagnosis tool and biomarker for COPD.

The works described in this thesis are worthy of further study in many directions. For example, the compact microfluidic system UMCAS described in Chapter 2 has plenty of room for further improvement. With the technology development, smart phones now can offer great imaging quality and calculation ability. Our lab recently has started a project to develop smart phone based microfluidic system, which uses the camera in the smart phone as the imaging component to observe the cell migration in the microfluidic device. A prototype system has been developed and successfully validated by performing the neutrophil migration experiments. Further work will be conducted to

enable the real time cell migration analysis in the smart phone. Compared with UMCAS, the smart phone microfluidic system has advantages of being smaller in size and eliminates of the use of an external computer for data analysis.

Although we have shown some interesting relationships between the sputum-induced neutrophil chemotaxis and COPD, further testing with a larger cohort is required to clarify this correlation. In addition, it will be very interesting to investigate the sputum-induced neutrophil chemotaxis using the patient's own blood cells. These experiments can be much more easily performed using the all-on-chip method described in Chapter 4 and it has the potential to be performed at point-of-care. Furthermore, more direct isolation kits from whole blood for other cell types have been developed, such as T-cell subsets and NK cells. All these cell types have great importance in migration related basic and clinical researches. The all-on-chip method can be easily adapted for the study of these cell types.

In additional to the immune cell migration experiments, the microfluidic devices with the cell docking structure described in Chapter 4 can be applied to some low-speed migration cells. Our lab has validated this device for cancer cell and stem cell migration. Another potential application of this device is for chemotactic separation of chemotactic cells and non-chemotactic cells since these two types of cells can be separated by the cell docking structure in the channel.

For the basic research aspects, further efforts will be required to better understand the underlying biological mechanism in cell migration at the molecular level. Many current chemotactic signaling pathway researches still reply on the use of the traditional migration assay, possibly due to the requirement of specialized skills of using

microfluidic devices. By integrating the cell biology approaches and the microfluidic technologies developed in this thesis, we can further test signaling mechanisms for neutrophil chemotaxis, such as activation of G proteins, their downstream effectors PLC and PI-3 kinase, the activation of small GTPases of the Rho family, and new pathways may be identified.

Another direction is to combine the microfluidic and the mathematic tools to build better physical models to represent the cell migration. Our lab has developed a microfluidic device to characterize neutrophil migration under spatially varying profiles of interleukine-8 gradients. Our results show that neutrophils display a transition from chemotaxis to flowtaxis when they migrate across the steep gradient interface, and the relative efficiency of this transition depends on the cell's chemotaxis history. We are now working on a mathematic model based on the G-protein and ligand-receptor dynamics and attempting to explain the memory effect in the experimental findings. Currently, there are not many studies working on collective cell chemotaxis compared with the single cell migration. The cell cluster has shown interesting different chemotaxis behaviors [235]. We can further extend the developed microfluidic systems into this area.

For the clinical aspects, many other diseases have been report to be highly correlated to the disorder of neutrophil chemotaxis, such as bacterial sepsis or diabetes. Better understanding the mechanism and relationship of cell chemotaxis in diseases using the microfluidic system will provide new insights in monitoring and curing these diseases.

References

1. J. Adler, *Chemotaxis in bacteria.* Science, 1966. **153**(3737): p. 708-716.
2. M. Zhao, *Electrical fields in wound healing—An overriding signal that directs cell migration.* Seminars in Cell & Developmental Biology, 2009. **20**(6): p. 674-682.
3. H. Seppä, G. Grotendorst, S. Seppä, E. Schiffmann, and G.R. Martin, *Platelet-derived growth factor in chemotactic for fibroblasts.* The Journal of cell biology, 1982. **92**(2): p. 584-588.
4. J. Condeelis, R.H. Singer, and J.E. Segall, *The great escape: when cancer cells hijack the genes for chemotaxis and motility.* Annu. Rev. Cell Dev. Biol., 2005. **21**: p. 695-718.
5. A.D. Luster, R. Alon, and U.H. von Andrian, *Immune cell migration in inflammation: present and future therapeutic targets.* Nat Immunol, 2005. **6**(12): p. 1182-90.
6. S.D. Kobayashi, J.M. Voyich, C. Burlak, and F.R. DeLeo, *Neutrophils in the innate immune response.* ARCHIVUM IMMUNOLOGIAE ET THERAPIAE EXPERIMENTALIS-ENGLISH EDITION-, 2005. **53**(6): p. 505.
7. J.V. Stein and C. Nombela-Arrieta, *Chemokine control of lymphocyte trafficking: a general overview.* Immunology, 2005. **116**(1): p. 1-12.
8. S. Li, P. Butler, Y. Wang, Y. Hu, D.C. Han, S. Usami, J.-L. Guan, and S. Chien, *The role of the dynamics of focal adhesion kinase in the mechanotaxis of endothelial cells.* Proceedings of the National Academy of Sciences, 2002. **99**(6): p. 3546-3551.

9. S. Hsu, R. Thakar, D. Liepmann, and S. Li, *Effects of shear stress on endothelial cell haptotaxis on micropatterned surfaces.* Biochemical and biophysical research communications, 2005. **337**(1): p. 401-409.

10. F. Lin and E. Butcher, *T cell chemotaxis in a simple microfluidic device.* Lab Chip, 2006. **6**(11): p. 1462-9.

11. K.E. McCormick, B.E. Gaertner, M. Sottile, P.C. Phillips, and S.R. Lockery, *Microfluidic devices for analysis of spatial orientation behaviors in semi-restrained Caenorhabditis elegans.* PloS one, 2011. **6**(10): p. e25710.

12. M. Zhao, C.D. McCaig, A. Agius-Fernandez, J.V. Forrester, and K. Araki-Sasaki, *Human corneal epithelial cells reorient and migrate cathodally in a small applied electric field.* Current eye research, 1997. **16**(10): p. 973-984.

13. J. Wu, X. Wu, and F. Lin, *Recent developments in microfluidics-based chemotaxis studies.* Lab on a Chip, 2013. **13**: p. 2484-2499.

14. R.M. Macnab and D. Koshland, *The gradient-sensing mechanism in bacterial chemotaxis.* Proceedings of the National Academy of Sciences, 1972. **69**(9): p. 2509-2512.

15. A. Bagorda and C.A. Parent, *Eukaryotic chemotaxis at a glance.* Journal of cell science, 2008. **121**(16): p. 2621-2624.

16. P. Fisher, R. Merkl, and G. Gerisch, *Quantitative analysis of cell motility and chemotaxis in Dictyostelium discoideum by using an image processing system and a novel chemotaxis chamber providing stationary chemical gradients.* The Journal of cell biology, 1989. **108**(3): p. 973-984.

17. S. Zigmond, *Ability of polymorphonuclear leukocytes to orient in gradients of chemotactic factors.* J Cell Biol, 1977. **75**(2 Pt 1): p. 606-16.

18. M. Panaro and V. Mitolo, *Cellular responses to FMLP challenging: a mini-review.* Immunopharmacology and immunotoxicology, 1999. **21**(3): p. 397-419.

19. H.N. Fernandez, P.M. Henson, A. Otani, and T.E. Hugli, *Chemotactic response to human C3a and C5a anaphylatoxins I. Evaluation of C3a and C5a leukotaxis in vitro and under simulated in vivo conditions.* The Journal of Immunology, 1978. **120**(1): p. 109-115.

20. E.J. Fernandez and E. Lolis, *Structure, function, and inhibition of chemokines.* Annual review of pharmacology and toxicology, 2002. **42**(1): p. 469-499.

21. S. Nandagopal, D. Wu, and F. Lin, *Combinatorial guidance by CCR7 ligands for T lymphocytes migration in co-existing chemokine fields.* PloS one, 2011. **6**(3): p. e18183.

22. N.L. Jeon, H. Baskaran, S.K. Dertinger, G.M. Whitesides, L. Van De Water, and M. Toner, *Neutrophil chemotaxis in linear and complex gradients of interleukin-8 formed in a microfabricated device.* Nature biotechnology, 2002. **20**(8): p. 826-830.

23. J. Palmblad, C.L. Malmsten, A. Uden, O. Radmark, L. Engstedt, and B. Samuelsson, *Leukotriene B4 is a potent and stereospecific stimulator of neutrophil chemotaxis and adherence.* Blood, 1981. **58**(3): p. 658-661.

24. S. Perez-Patrigeon, B. Vingert, O. Lambotte, J.-P. Viard, J.-F. Delfraissy, J. Thèze, and L.A. Chakrabarti, *HIV infection impairs CCR7-dependent T-cell chemotaxis independent of CCR7 expression.* AIDS, 2009. **23**(10): p. 1197-1207.

25. R.A. Clark and H.R. Kimball, *Defective granulocyte chemotaxis in the Chediak-Higashi syndrome.* Journal of clinical investigation, 1971. **50**(12): p. 2645.

26. K.L. Butler, V. Ambravaneswaran, N. Agrawal, M. Bilodeau, M. Toner, R.G. Tompkins, S. Fagan, and D. Irimia, *Burn injury reduces neutrophil directional migration speed in microfluidic devices.* PloS one, 2010. **5**(7): p. e11921.

27. J.C. Alves-Filho, A. de Freitas, F. Spiller, F.O. Souto, and F.Q. Cunha, *The role of neutrophils in severe sepsis.* Shock, 2008. **30**(7): p. 3-9.

28. M. Manouchehr-Pour, P. Spagnuolo, H. Rodman, and N. Bissada, *Impaired neutrophil chemotaxis in diabetic patients with severe periodontitis.* Journal of dental research, 1981. **60**(3): p. 729-730.

29. F. Lin, C.M.-C. Nguyen, S.-J. Wang, W. Saadi, S.P. Gross, and N.L. Jeon, *Neutrophil migration in opposing chemoattractant gradients using microfluidic chemotaxis devices.* Annals of biomedical engineering, 2005. **33**(4): p. 475-482.

30. D. Irimia, S.-Y. Liu, W.G. Tharp, A. Samadani, M. Toner, and M.C. Poznansky, *Microfluidic system for measuring neutrophil migratory responses to fast switches of chemical gradients.* Lab on a Chip, 2006. **6**(2): p. 191-198.

31. V. Ambravaneswaran, I.Y. Wong, A.J. Aranyosi, M. Toner, and D. Irimia, *Directional decisions during neutrophil chemotaxis inside bifurcating channels.* Integrative Biology, 2010. **2**(11-12): p. 639-647.

32. F. Lin, C.M.-C. Nguyen, S.-J. Wang, W. Saadi, S.P. Gross, and N.L. Jeon, *Effective neutrophil chemotaxis is strongly influenced by mean IL-8 concentration.* Biochemical and biophysical research communications, 2004. **319**(2): p. 576-581.

33. V.V. Abhyankar, M.W. Toepke, C.L. Cortesio, M.A. Lokuta, A. Huttenlocher, and D.J. Beebe, *A platform for assessing chemotactic migration within a spatiotemporally defined 3D microenvironment.* Lab on a Chip, 2008. **8**(9): p. 1507-1515.

34. S. BOYDEN, *The chemotactic effect of mixtures of antibody and antigen on polymorphonuclear leucocytes.* J Exp Med, 1962. **115**: p. 453-66.

35. D. Zicha, G. Dunn, and G. Jones, *Analyzing Chemotaxis Using the Dunn Direct-Viewing Chamber*. 1997. p. 449-457.

36. H. Hayashi, O. Aharonovitz, R.T. Alexander, N. Touret, W. Furuya, J. Orlowski, and S. Grinstein, *Na+/H+ exchange and pH regulation in the control of neutrophil chemokinesis and chemotaxis.* American Journal of Physiology - Cell Physiology, 2008. **294**(2): p. C526-C534.

37. S.C. Terry, J.H. Jerman, and J.B. Angell, *A gas chromatographic air analyzer fabricated on a silicon wafer.* Electron Devices, IEEE Transactions on, 1979. **26**(12): p. 1880-1886.

38. P. Gravesen, J. Branebjerg, and O.S. Jensen, *Microfluidics-a review.* Journal of Micromechanics and Microengineering, 1993. **3**(4): p. 168.

39. H. Van Lintel, F. Van de Pol, and S. Bouwstra, *A piezoelectric micropump based on micromachining of silicon.* Sensors and actuators, 1988. **15**(2): p. 153-167.

40. S. Shoji, M. Esashi, and T. Matsuo, *Prototype miniature blood gas analyser fabricated on a silicon wafer.* Sensors and actuators, 1988. **14**(2): p. 101-107.

41. K.Y. Ng, J. Shajii, and M.A. Schmidt. *A liquid shear-stress sensor fabricated using wafer bonding technology*. in *Solid-State Sensors and Actuators, 1991.*

Digest of Technical Papers, TRANSDUCERS '91., 1991 International Conference on. 1991.

42. A. Manz, D.J. Harrison, E.M.J. Verpoorte, J.C. Fettinger, A. Paulus, H. Lüdi, and H.M. Widmer, *Planar chips technology for miniaturization and integration of separation techniques into monitoring systems: Capillary electrophoresis on a chip.* Journal of Chromatography A, 1992. **593**(1–2): p. 253-258.
43. A. Manz, Y. Miyahara, J. Miura, Y. Watanabe, H. Miyagi, and K. Sato, *Design of an open-tubular column liquid chromatograph using silicon chip technology.* Sensors and Actuators B: Chemical, 1990. **1**(1–6): p. 249-255.
44. K.i. Ohno, K. Tachikawa, and A. Manz, *Microfluidics: applications for analytical purposes in chemistry and biochemistry.* Electrophoresis, 2008. **29**(22): p. 4443-4453.
45. G. Velve-Casquillas, M. Le Berre, M. Piel, and P.T. Tran, *Microfluidic tools for cell biological research.* Nano Today, 2010. **5**(1): p. 28-47.
46. S. Giselbrecht, T.J. Huang, K. Lange, A. Manz, and P. Neuzil, *Revisiting lab-on-a-chip technology for drug discovery.* Nature Reviews Drug Discovery, 2012. **11**(8): p. 620+.
47. S.K. Sia and L.J. Kricka, *Microfluidics and point-of-care testing.* Lab on a Chip, 2008. **8**(12): p. 1982-1983.
48. S. Neethirajan, I. Kobayashi, M. Nakajima, D. Wu, S. Nandagopal, and F. Lin, *Microfluidics for food, agriculture and biosystems industries.* Lab on a Chip, 2011. **11**(9): p. 1574-1586.

49. M. Madou, *Fundamentals of microfabrication: the science of miniaturization*. 2002: CRC press.

50. H. Becker and U. Heim, *Hot embossing as a method for the fabrication of polymer high aspect ratio structures.* Sensors and Actuators A: Physical, 2000. **83**(1): p. 130-135.

51. R.M. McCormick, R.J. Nelson, M.G. Alonso-Amigo, D.J. Benvegnu, and H.H. Hooper, *Microchannel Electrophoretic Separations of DNA in Injection-Molded Plastic Substrates.* Analytical Chemistry, 1997. **69**(14): p. 2626-2630.

52. G.M. Whitesides, *The origins and the future of microfluidics.* Nature, 2006. **442**(7101): p. 368-373.

53. A.W. Martinez, S.T. Phillips, M.J. Butte, and G.M. Whitesides, *Patterned paper as a platform for inexpensive, low-volume, portable bioassays.* Angewandte Chemie International Edition, 2007. **46**(8): p. 1318-1320.

54. X. Li, D.R. Ballerini, and W. Shen, *A perspective on paper-based microfluidics: current status and future trends.* Biomicrofluidics, 2012. **6**(1): p. 011301.

55. D.A. Bruzewicz, M. Reches, and G.M. Whitesides, *Low-Cost Printing of Poly(dimethylsiloxane) Barriers To Define Microchannels in Paper.* Analytical Chemistry, 2008. **80**(9): p. 3387-3392.

56. K. Abe, K. Suzuki, and D. Citterio, *Inkjet-Printed Microfluidic Multianalyte Chemical Sensing Paper.* Analytical Chemistry, 2008. **80**(18): p. 6928-6934.

57. K. Abe, K. Kotera, K. Suzuki, and D. Citterio, *Inkjet-printed paperfluidic immuno-chemical sensing device.* Analytical and Bioanalytical Chemistry, 2010. **398**(2): p. 885-893.

58. X. Li, J. Tian, T. Nguyen, and W. Shen, *Paper-Based Microfluidic Devices by Plasma Treatment.* Analytical Chemistry, 2008. **80**(23): p. 9131-9134.

59. Y. Lu, W. Shi, L. Jiang, J. Qin, and B. Lin, *Rapid prototyping of paper-based microfluidics with wax for low-cost, portable bioassay.* Electrophoresis, 2009. **30**(9): p. 1497-1500.

60. E. Carrilho, A.W. Martinez, and G.M. Whitesides, *Understanding Wax Printing: A Simple Micropatterning Process for Paper-Based Microfluidics.* Analytical Chemistry, 2009. **81**(16): p. 7091-7095.

61. Y. Lu, W. Shi, J. Qin, and B. Lin, *Fabrication and Characterization of Paper-Based Microfluidics Prepared in Nitrocellulose Membrane By Wax Printing.* Analytical Chemistry, 2009. **82**(1): p. 329-335.

62. E.M. Fenton, M.R. Mascarenas, G.P. López, and S.S. Sibbett, *Multiplex Lateral-Flow Test Strips Fabricated by Two-Dimensional Shaping.* ACS Applied Materials & Interfaces, 2008. **1**(1): p. 124-129.

63. W. Wang, W.-Y. Wu, and J.-J. Zhu, *Tree-shaped paper strip for semiquantitative colorimetric detection of protein with self-calibration.* Journal of Chromatography A, 2010. **1217**(24): p. 3896-3899.

64. J.L. Delaney, C.F. Hogan, J. Tian, and W. Shen, *Electrogenerated Chemiluminescence Detection in Paper-Based Microfluidic Sensors.* Analytical Chemistry, 2011. **83**(4): p. 1300-1306.

65. J. Olkkonen, K. Lehtinen, and T. Erho, *Flexographically Printed Fluidic Structures in Paper.* Analytical Chemistry, 2010. **82**(24): p. 10246-10250.

66. W. Dungchai, O. Chailapakul, and C.S. Henry, *A low-cost, simple, and rapid fabrication method for paper-based microfluidics using wax screen-printing.* Analyst, 2011. **136**(1): p. 77-82.

67. G. Chitnis, Z. Ding, C.-L. Chang, C.A. Savran, and B. Ziaie, *Laser-treated hydrophobic paper: an inexpensive microfluidic platform.* Lab on a Chip, 2011. **11**(6): p. 1161-1165.

68. Y. Liu, H. Lu, W. Zhong, P. Song, J. Kong, P. Yang, H.H. Girault, and B. Liu, *Multilayer-Assembled Microchip for Enzyme Immobilization as Reactor Toward Low-Level Protein Identification.* Analytical Chemistry, 2005. **78**(3): p. 801-808.

69. A.R. Wheeler, H. Moon, C.A. Bird, R.R. Ogorzalek Loo, C.-J.C.J. Kim, J.A. Loo, and R.L. Garrell, *Digital Microfluidics with In-Line Sample Purification for Proteomics Analyses with MALDI-MS.* Analytical Chemistry, 2004. **77**(2): p. 534-540.

70. X. Jiang, J.M. Ng, A.D. Stroock, S.K. Dertinger, and G.M. Whitesides, *A miniaturized, parallel, serially diluted immunoassay for analyzing multiple antigens.* Journal of the American Chemical Society, 2003. **125**(18): p. 5294-5295.

71. X. Zhou, L. Lau, W.W.L. Lam, S.W.N. Au, and B. Zheng, *Nanoliter Dispensing Method by Degassed Poly(dimethylsiloxane) Microchannels and Its Application in Protein Crystallization.* Analytical Chemistry, 2007. **79**(13): p. 4924-4930.

72. M.A. Burns, B.N. Johnson, S.N. Brahmasandra, K. Handique, J.R. Webster, M. Krishnan, T.S. Sammarco, P.M. Man, D. Jones, D. Heldsinger, C.H. Mastrangelo,

and D.T. Burke, *An Integrated Nanoliter DNA Analysis Device.* Science, 1998. **282**(5388): p. 484-487.

73. M.A. Northrup, M. Ching, R. White, and R. Watson. *DNA amplification with a microfabricated reaction chamber*. in *Transducers*. 1993.

74. M.A. Northrup, C. Gonzalez, and D. Hadley, *A MEMS-based miniature DNA analysis system*. 1995. Medium: ED; Size: 6 p.

75. M.E. Warkiani, G. Guan, K.B. Luan, W.C. Lee, A.A.S. Bhagat, P. Kant Chaudhuri, D.S.-W. Tan, W.T. Lim, S.C. Lee, P.C.Y. Chen, C.T. Lim, and J. Han, *Slanted spiral microfluidics for the ultra-fast, label-free isolation of circulating tumor cells.* Lab on a Chip, 2014.

76. A.Y. Fu, C. Spence, A. Scherer, F.H. Arnold, and S.R. Quake, *A microfabricated fluorescence-activated cell sorter*. Nature biotechnology, 1999. **17**(11): p. 1109-1111.

77. C.-H. Tai, S.-K. Hsiung, C.-Y. Chen, M.-L. Tsai, and G.-B. Lee, *Automatic microfluidic platform for cell separation and nucleus collection.* Biomedical microdevices, 2007. **9**(4): p. 533-543.

78. C.S. Chen, M. Mrksich, S. Huang, G.M. Whitesides, and D.E. Ingber, *Geometric control of cell life and death.* Science, 1997. **276**(5317): p. 1425-1428.

79. D.T. Chiu, N.L. Jeon, S. Huang, R.S. Kane, C.J. Wargo, I.S. Choi, D.E. Ingber, and G.M. Whitesides, *Patterned deposition of cells and proteins onto surfaces by using three-dimensional microfluidic systems.* Proceedings of the National Academy of Sciences, 2000. **97**(6): p. 2408-2413.

80. P.J. Lee, P.J. Hung, V.M. Rao, and L.P. Lee, *Nanoliter scale microbioreactor array for quantitative cell biology.* Biotechnology and bioengineering, 2006. **94**(1): p. 5-14.

81. J. Li, S. Nandagopal, D. Wu, S.F. Romanuik, K. Paul, D.J. Thomson, and F. Lin, *Activated T lymphocytes migrate toward the cathode of DC electric fields in microfluidic devices.* Lab on a Chip, 2011. **11**(7): p. 1298-1304.

82. R.D. Nelson, P.G. Quie, and R.L. Simmons, *Chemotaxis Under Agarose: A New and Simple Method for Measuring Chemotaxis and Spontaneous Migration of Human Polymorphonuclear Leukocytes and Monocytes.* J Immunol, 1975. **115**(6): p. 1650-1656.

83. A. Lohof, M. Quillan, Y. Dan, and M. Poo, *Asymmetric modulation of cytosolic cAMP activity induces growth cone turning.* J. Neurosci., 1992. **12**(4): p. 1253-1261.

84. S. Kim, H.J. Kim, and N.L. Jeon, *Biological applications of microfluidic gradient devices.* Integr Biol (Camb), 2010. **2**(11-12): p. 584-603.

85. N.L. Jeon, S.K.W. Dertinger, D.T. Chiu, I.S. Choi, A.D. Stroock, and G.M. Whitesides, *Generation of Solution and Surface Gradients Using Microfluidic Systems.* Langmuir, 2000. **16**(22): p. 8311-8316.

86. Brendon G. Ricart, Michael T. Yang, Christopher A. Hunter, Christopher S. Chen, and Daniel A. Hammer, *Measuring Traction Forces of Motile Dendritic Cells on Micropost Arrays.* Biophysical journal, 2011. **101**(11): p. 2620-2628.

87. S.-J. Wang, W. Saadi, F. Lin, C. Minh-Canh Nguyen, and N. Li Jeon, *Differential effects of EGF gradient profiles on MDA-MB-231 breast cancer cell chemotaxis.* Experimental Cell Research, 2004. **300**(1): p. 180-189.

88. Y. Gao, J. Sun, W.-H. Lin, D.J. Webb, and D. Li, *A compact microfluidic gradient generator using passive pumping.* Microfluidics and nanofluidics, 2012. **12**(6): p. 887-895.

89. X. Zhu, G. Si, N. Deng, Q. Ouyang, T. Wu, Z. He, L. Jiang, C. Luo, and Y. Tu, *Frequency-Dependent Escherichia coli Chemotaxis Behavior.* Physical Review Letters, 2012. **108**(12): p. 128101.

90. K. Campbell and A. Groisman, *Generation of complex concentration profiles in microchannels in a logarithmically small number of steps.* Lab on a Chip, 2007. **7**(2): p. 264-272.

91. C. Joanne Wang, X. Li, B. Lin, S. Shim, G.-l. Ming, and A. Levchenko, *A microfluidics-based turning assay reveals complex growth cone responses to integrated gradients of substrate-bound ECM molecules and diffusible guidance cues.* Lab on a Chip, 2008. **8**(2): p. 227-237.

92. G.A. Cooksey, C.G. Sip, and A. Folch, *A multi-purpose microfluidic perfusion system with combinatorial choice of inputs, mixtures, gradient patterns, and flow rates.* Lab on a Chip, 2009. **9**(3): p. 417-426.

93. D. Amarie, J.A. Glazier, and S.C. Jacobson, *Compact microfluidic structures for generating spatial and temporal gradients.* Anal Chem, 2007. **79**(24): p. 9471-7.

94. P. Herzmark, K. Campbell, F. Wang, K. Wong, H. El-Samad, A. Groisman, and H.R. Bourne, *Bound attractant at the leading vs. the trailing edge determines*

chemotactic prowess. Proceedings of the National Academy of Sciences, 2007. **104**(33): p. 13349.

95. K. Lee, C. Kim, B. Ahn, R. Panchapakesan, A.R. Full, L. Nordee, J.Y. Kang, and K.W. Oh, *Generalized serial dilution module for monotonic and arbitrary microfluidic gradient generators.* Lab on a Chip, 2009. **9**(5): p. 709-717.

96. K. Lee, C. Kim, Y. Kim, B. Ahn, J. Bang, J. Kim, R. Panchapakesan, Y.K. Yoon, J.Y. Kang, and K.W. Oh, *Microfluidic concentration-on-demand combinatorial dilutions.* Microfluidics and nanofluidics, 2011. **11**(1): p. 75-86.

97. Y. Liu, J. Sai, A. Richmond, and J. Wikswo, *Microfluidic switching system for analyzing chemotaxis responses of wortmannin-inhibited HL-60 cells.* Biomedical microdevices, 2008. **10**(4): p. 499-507.

98. S. Paliwal, P.A. Iglesias, K. Campbell, Z. Hilioti, A. Groisman, and A. Levchenko, *MAPK-mediated bimodal gene expression and adaptive gradient sensing in yeast.* Nature, 2007. **446**(7131): p. 46-51.

99. C. Beta, D. Wyatt, W.J. Rappel, and E. Bodenschatz, *Flow photolysis for spatiotemporal stimulation of single cells.* Analytical Chemistry, 2007. **79**(10): p. 3940-3944.

100. C. Beta, T. Fröhlich, H.U. Bödeker, and E. Bodenschatz, *Chemotaxis in microfluidic devices—a study of flow effects.* Lab Chip, 2008. **8**(7): p. 1087-1096.

101. V.V. Abhyankar, M.A. Lokuta, A. Huttenlocher, and D.J. Beebe, *Characterization of a membrane-based gradient generator for use in cell-signaling studies.* Lab on a Chip, 2006. **6**(3): p. 389-393.

102. M. Kim and T. Kim, *Diffusion-based and long-range concentration gradients of multiple chemicals for bacterial chemotaxis assays.* Anal Chem, 2010. **82**(22): p. 9401-9.

103. E. Berthier, J. Surfus, J. Verbsky, A. Huttenlocher, and D. Beebe, *An arrayed high-content chemotaxis assay for patient diagnosis.* Integrative Biology, 2010. **2**(11-12): p. 630-638.

104. Q. Kong, R.J. Majeska, and M. Vazquez, *Migration of connective tissue-derived cells is mediated by ultra-low concentration gradient fields of EGF*. Experimental Cell Research, 2011. **317**(11): p. 1491-1502.

105. W. Saadi, S.W. Rhee, F. Lin, B. Vahidi, B.G. Chung, and N.L. Jeon, *Generation of stable concentration gradients in 2D and 3D environments using a microfluidic ladder chamber.* Biomed Microdevices, 2007. **9**(5): p. 627-35.

106. B. Mosadegh, C. Huang, J.W. Park, H.S. Shin, B.G. Chung, S.K. Hwang, K.H. Lee, H.J. Kim, J. Brody, and N.L. Jeon, *Generation of stable complex gradients across two-dimensional surfaces and three-dimensional gels.* Langmuir, 2007. **23**(22): p. 10910-10912.

107. D. Irimia, G. Charras, N. Agrawal, T. Mitchison, and M. Toner, *Polar stimulation and constrained cell migration in microfluidic channels.* Lab on a Chip, 2007. **7**(12): p. 1783-1790.

108. J. Atencia, G.A. Cooksey, and L.E. Locascio, *A robust diffusion-based gradient generator for dynamic cell assays.* Lab on a Chip, 2012. **12**(2): p. 309-16.

109. T.M. Keenan, C.W. Frevert, A. Wu, V. Wong, and A. Folch, *A new method for studying gradient-induced neutrophil desensitization based on an open microfluidic chamber.* Lab on a Chip, 2010. **10**(1): p. 116-122.

110. A. Shamloo, N. Ma, M.-m. Poo, L.L. Sohn, and S.C. Heilshorn, *Endothelial cell polarization and chemotaxis in a microfluidic device.* Lab on a Chip, 2008. **8**(8): p. 1292-1299.

111. S.S. Lee, P. Horvath, S. Pelet, B. Hegemann, L.P. Lee, and M. Peter, *Quantitative and dynamic assay of single cell chemotaxis.* Integrative Biology, 2012. **4**(4): p. 381-390.

112. D. Kim, A. Liu, E. Diller, and M. Sitti, *Chemotactic steering of bacteria propelled microbeads.* Biomed Microdevices, 2012. **14**(6): p. 1009-17.

113. Y.V. Kalinin, L. Jiang, Y. Tu, and M. Wu, *Logarithmic Sensing in Escherichia coli Bacterial Chemotaxis.* Biophysical journal, 2009. **96**(6): p. 2439-2448.

114. Y. Kalinin, S. Neumann, V. Sourjik, and M. Wu, *Responses of Escherichia coli bacteria to two opposing chemoattractant gradients depend on the chemoreceptor ratio.* Journal of bacteriology, 2010. **192**(7): p. 1796-1800.

115. S.-Y. Cheng, S. Heilman, M. Wasserman, S. Archer, M.L. Shuler, and M. Wu, *A hydrogel-based microfluidic device for the studies of directed cell migration.* Lab on a Chip, 2007. **7**(6): p. 763-769.

116. E. Choi, I. Jun, H.-k. Chang, K.M. Park, H. Shin, K.D. Park, and J. Park, *Quantitatively controlled in situ formation of hydrogel membranes in microchannels for generation of stable chemical gradients.* Lab on a Chip, 2012. **12**(2): p. 302-308.

117. T. Ahmed, T.S. Shimizu, and R. Stocker, *Bacterial chemotaxis in linear and nonlinear steady microfluidic gradients.* Nano Lett, 2010. **10**(9): p. 3379-85.

118. J.Y. Cheng, M.H. Yen, C.T. Kuo, and T.H. Young, *A transparent cell-culture microchamber with a variably controlled concentration gradient generator and flow field rectifier.* Biomicrofluidics, 2008. **2**(2): p. 24105.

119. J. Atencia, J. Morrow, and L.E. Locascio, *The microfluidic palette: A diffusive gradient generator with spatio-temporal control.* Lab on a Chip, 2009. **9**(18): p. 2707-2714.

120. E. Choi, H.-k. Chang, C.Y. Lim, T. Kim, and J. Park, *Concentration gradient generation of multiple chemicals using spatially controlled self-assembly of particles in microchannels.* Lab on a Chip, 2012. **12**(20): p. 3968-75.

121. M.A. Qasaimeh, T. Gervais, and D. Juncker, *Microfluidic quadrupole and floating concentration gradient.* Nat Commun, 2011. **2**: p. 464.

122. G.A. Wright, L. Costa, A. Terekhov, D. Jowhar, W. Hofmeister, and C. Janetopoulos, *On-chip open microfluidic devices for chemotaxis studies.* Microsc Microanal, 2012. **18**(4): p. 816-28.

123. H. Kress, J.G. Park, C.O. Mejean, J.D. Forster, J. Park, S.S. Walse, Y. Zhang, D. Wu, O.D. Weiner, T.M. Fahmy, and E.R. Dufresne, *Cell stimulation with optically manipulated microsources.* Nat Methods, 2009. **6**(12): p. 905-9.

124. K. Wolf and P. Friedl, *Mapping proteolytic cancer cell-extracellular matrix interfaces.* Clinical and Experimental Metastasis, 2009. **26**(4): p. 289-298.

125. U. Haessler, Y. Kalinin, M.A. Swartz, and M. Wu, *An agarose-based microfluidic platform with a gradient buffer for 3D chemotaxis studies.* Biomed Microdevices, 2009. **11**(4): p. 827-35.

126. R. Sudo, S. Chung, I.K. Zervantonakis, V. Vickerman, Y. Toshimitsu, L.G. Griffith, and R.D. Kamm, *Transport-mediated angiogenesis in 3D epithelial coculture.* The FASEB Journal, 2009. **23**(7): p. 2155-2164.

127. I. Zervantonakis, S. Chung, R. Sudo, M. Zhang, J. Charest, and R. Kamm, *Concentration gradients in microfluidic 3D matrix cell culture systems.* International Journal of Micro-Nano Scale Transport, 2010. **1**(1): p. 27-36.

128. O. Amadi, M. Steinhauser, Y. Nishi, S. Chung, R. Kamm, A. McMahon, and R. Lee, *A low resistance microfluidic system for the creation of stable concentration gradients in a defined 3D microenvironment.* Biomedical microdevices, 2010. **12**(6): p. 1027-1041.

129. E. Kim, O. Schueller, and P.M. Sweetnam, *Targeting the leukocyte activation cascade: Getting to the site of inflammation using microfabricated assays.* Lab on a Chip, 2012. **12**(12): p. 2255-2264.

130. T. Ahmed and R. Stocker, *Experimental Verification of the Behavioral Foundation of Bacterial Transport Parameters Using Microfluidics.* Biophysical journal, 2008. **95**(9): p. 4481-4493.

131. T. Long and R.M. Ford, *Enhanced transverse migration of bacteria by chemotaxis in a porous T-sensor.* Environmental science & technology, 2009. **43**(5): p. 1546-1552.

132. J.B. Masson, G. Voisinne, J. Wong-Ng, A. Celani, and M. Vergassola, *Noninvasive inference of the molecular chemotactic response using bacterial trajectories.* Proceedings of the National Academy of Sciences, 2012. **109**(5): p. 1802-1807.

133. X. Wang, T. Long, and R.M. Ford, *Bacterial chemotaxis toward a NAPL source within a pore-scale microfluidic chamber.* Biotechnology and bioengineering, 2012. **109**(7): p. 1622-1628.

134. M.J. Kim and K.S. Breuer, *Controlled Mixing in Microfluidic Systems Using Bacterial Chemotaxis.* Analytical Chemistry, 2007. **79**(3): p. 955-959.

135. D.L. Englert, M.D. Manson, and A. Jayaraman, *Flow-based microfluidic device for quantifying bacterial chemotaxis in stable, competing gradients.* Applied and environmental microbiology, 2009. **75**(13): p. 4557-64.

136. J. Chen and Y. Jin, *Motility of Pseudomonas aeruginosa in saturated granular media as affected by chemoattractant.* Journal of Contaminant Hydrology, 2011. **126**(1–2): p. 113-120.

137. H.-H. Jeong, S.-H. Lee, J.-M. Kim, H.-E. Kim, Y.-G. Kim, J.Y. Yoo, W.-S. Chang, and C.-S. Lee, *Microfluidic monitoring of Pseudomonas aeruginosa chemotaxis under the continuous chemical gradient.* Biosensors and Bioelectronics, 2010. **26**(2): p. 351-356.

138. R. Stocker, J.R. Seymour, A. Samadani, D.E. Hunt, and M.F. Polz, *Rapid chemotactic response enables marine bacteria to exploit ephemeral microscale nutrient patches.* Proceedings of the National Academy of Sciences of the United States of America, 2008. **105**(11): p. 4209-14.

139. J.R. Seymour, Marcos, and R. Stocker, *Resource patch formation and exploitation throughout the marine microbial food web.* The American naturalist, 2009. **173**(1): p. E15-29.

140. P.N. Devreotes and S.H. Zigmond, *Chemotaxis in eukaryotic cells: a focus on leukocytes and Dictyostelium.* Annual review of cell biology, 1988. **4**: p. 649-86.

141. D. Fuller, W. Chen, M. Adler, A. Groisman, H. Levine, W.J. Rappel, and W.F. Loomis, *External and internal constraints on eukaryotic chemotaxis.* Proceedings of the National Academy of Sciences, 2010. **107**(21): p. 9656-9659.

142. M. Skoge, M. Adler, A. Groisman, H. Levine, W.F. Loomis, and W.-J. Rappel, *Gradient sensing in defined chemotactic fields.* Integrative Biology, 2010. **2**(11-12): p. 659-668.

143. B. Meier, A. Zielinski, C. Weber, D. Arcizet, S. Youssef, T. Franosch, J.O. Rädler, and D. Heinrich, *Chemotactic cell trapping in controlled alternating gradient fields.* Proceedings of the National Academy of Sciences, 2011. **108**(28): p. 11417-11422.

144. G. Amselem, M. Theves, A. Bae, E. Bodenschatz, and C. Beta, *A stochastic description of Dictyostelium chemotaxis.* PloS one, 2012. **7**(5): p. e37213.

145. G. Amselem, M. Theves, A. Bae, C. Beta, and E. Bodenschatz, *Control Parameter Description of Eukaryotic Chemotaxis.* Physical Review Letters, 2012. **109**(10): p. 108103.

146. D. Irimia, G. Balazsi, N. Agrawal, and M. Toner, *Adaptive-control model for neutrophil orientation in the direction of chemical gradients.* Biophysical journal, 2009. **96**(10): p. 3897-916.

147. E.K. Sackmann, E. Berthier, E.W. Young, M.A. Shelef, S.A. Wernimont, A. Huttenlocher, and D.J. Beebe, *Microfluidic kit-on-a-lid: a versatile platform for neutrophil chemotaxis assays.* Blood, 2012. **120**(14): p. e45-53.

148. B.G. Ricart, B. John, D. Lee, C.A. Hunter, and D.A. Hammer, *Dendritic cells distinguish individual chemokine signals through CCR7 and CXCR4.* Journal of immunology, 2011. **186**(1): p. 53-61.

149. U. Haessler, M. Pisano, M. Wu, and M.A. Swartz, *Dendritic cell chemotaxis in 3D under defined chemokine gradients reveals differential response to ligands CCL21 and CCL19.* Proceedings of the National Academy of Sciences of the United States of America, 2011. **108**(14): p. 5614-9.

150. K. Wong, A. Ayuso-Sacido, P. Ahyow, A. Darling, J.A. Boockvar, and M. Wu, *Assessing neural stem cell motility using an agarose gel-based microfluidic device.* Journal of visualized experiments : JoVE, 2008. **11**(12): p. 674.

151. N. Wadhawan, H. Kalkat, K. Natarajan, X. Ma, S. Gajjeraman, S. Nandagopal, N. Hao, J. Li, M. Zhang, J. Deng, B. Xiang, S. Mzengeza, D.H. Freed, R.C. Arora, G. Tian, and F. Lin, *Growth and positioning of adipose-derived stem cells in microfluidic devices.* Lab on a Chip, 2012. **12**(22): p. 4829-34.

152. Q. Zhang, T. Liu, and J. Qin, *A microfluidic-based device for study of transendothelial invasion of tumor aggregates in realtime.* Lab on a Chip, 2012. **12**(16): p. 2837-2842.

153. B. Mosadegh, W. Saadi, S.J. Wang, and N.L. Jeon, *Epidermal growth factor promotes breast cancer cell chemotaxis in CXCL12 gradients.* Biotechnology and bioengineering, 2008. **100**(6): p. 1205-1213.

154. I. Barkefors, S. Le Jan, L. Jakobsson, E. Hejll, G. Carlson, H. Johansson, J. Jarvius, J.W. Park, N. Li Jeon, and J. Kreuger, *Endothelial Cell Migration in Stable Gradients of Vascular Endothelial Growth Factor A and Fibroblast Growth Factor 2.* Journal of Biological Chemistry, 2008. **283**(20): p. 13905-13912.

155. C. Wu, Sreeja B. Asokan, Matthew E. Berginski, Elizabeth M. Haynes, Norman E. Sharpless, Jack D. Griffith, Shawn M. Gomez, and James E. Bear, *Arp2/3 Is Critical for Lamellipodia and Response to Extracellular Matrix Cues but Is Dispensable for Chemotaxis.* Cell, 2012. **148**(5): p. 973-987.

156. Y. Fu, L.K. Chin, T. Bourouina, A.Q. Liu, and A.M.J. VanDongen, *Nuclear deformation during breast cancer cell transmigration.* Lab on a Chip, 2012. **12**(19): p. 3774-3778.

157. Z. Tong, E.M. Balzer, M.R. Dallas, W.C. Hung, K.J. Stebe, and K. Konstantopoulos, *Chemotaxis of cell populations through confined spaces at single-cell resolution.* PloS one, 2012. **7**(1): p. e29211.

158. S. Han, J.-J. Yan, Y. Shin, J.J. Jeon, J. Won, H. Eun Jeong, R.D. Kamm, Y.-J. Kim, and S. Chung, *A versatile assay for monitoring in vivo-like transendothelial migration of neutrophils.* Lab on a Chip, 2012. **12**(20): p. 3861-3865.

159. N. Godessart and S.L. Kunkel, *Chemokines in autoimmune disease.* Current Opinion in Immunology, 2001. **13**(6): p. 670-675.

160. K.M. Beeh, O. Kornmann, R. Buhl, S.V. Culpitt, M.A. Giembycz, and P.J. Barnes, *Neutrophil chemotactic activity of sputum from patients with COPD: role of interleukin 8 and leukotriene B4.* Chest, 2003. **123**(4): p. 1240-7.

161. N. Agrawal, M. Toner, and D. Irimia, *Neutrophil migration assay from a drop of blood.* Lab on a Chip, 2008. **8**(12): p. 2054-61.

162. R. Zantl and E. Horn, *Chemotaxis of slow migrating mammalian cells analysed by video microscopy.* Methods Mol Biol, 2011. **769**: p. 191-203.

163. S. Kanegasaki, Y. Nomura, N. Nitta, S. Akiyama, T. Tamatani, Y. Goshoh, T. Yoshida, T. Sato, and Y. Kikuchi, *A novel optical assay system for the quantitative measurement of chemotaxis.* J Immunol Methods, 2003. **282**(1-2): p. 1-11.

164. M.A. Vinolo, G.J. Ferguson, S. Kulkarni, G. Damoulakis, K. Anderson, Y.M. Bohlooly, L. Stephens, P.T. Hawkins, and R. Curi, *SCFAs induce mouse neutrophil chemotaxis through the GPR43 receptor.* PloS one, 2011. **6**(6): p. e21205.

165. H. Kato, S. Ueki, W. Ito, M. Takeda, T. Chiba, K. Yamaguchi, H. Kayaba, and J. Chihara, *Eosinophil chemotaxis assay using novel device EZ-TAXIScan.* Arerugi, 2008. **57**(12): p. 1317-1324.

166. K. Nakano, Y. Okada, K. Saito, R. Tanikawa, N. Sawamukai, Y. Sasaguri, T. Kohro, Y. Wada, T. Kodama, and Y. Tanaka, *Rheumatoid synovial endothelial cells produce macrophage colony-stimulating factor leading to osteoclastogenesis in rheumatoid arthritis.* Rheumatology, 2007. **46**(4): p. 597-603.

167. M. Zhao, H. Bai, E. Wang, J.V. Forrester, and C.D. McCaig, *Electrical stimulation directly induces pre-angiogenic responses in vascular endothelial cells by signaling through VEGF receptors.* Journal of cell science, 2004. **117**(3): p. 397-405.

168. M.B.A. Djamgoz, M. Mycielska, Z. Madeja, S.P. Fraser, and W. Korohoda, *Directional movement of rat prostate cancer cells in direct-current electric field involvement of voltagegated Na+ channel activity.* Journal of cell science, 2001. **114**(14): p. 2697-2705.

169. F. Lin, F. Baldessari, C.C. Gyenge, T. Sato, R.D. Chambers, J.G. Santiago, and E.C. Butcher, *Lymphocyte electrotaxis in vitro and in vivo.* J Immunol, 2008. **181**(4): p. 2465-71.

170. M.J. Sato, M. Ueda, H. Takagi, T.M. Watanabe, and T. Yanagida, *Input-output relationship in galvanotactic response of Dictyostelium cells.* Biosystems, 2007. **88**(3): p. 261-72.

171. M. Zhao, B. Song, J. Pu, T. Wada, B. Reid, G. Tai, F. Wang, A. Guo, P. Walczysko, and Y. Gu, *Electrical signals control wound healing through phosphatidylinositol-3-OH kinase-γ and PTEN.* Nature, 2006. **442**(7101): p. 457-460.

172. J. Li and F. Lin, *Microfluidic devices for studying chemotaxis and electrotaxis.* Trends in Cell Biology, 2011. **21**(8): p. 489-497.

173. C. Huang, J. Cheng, M. Yen, and T. Young, *Electrotaxis of lung cancer cells in a multiple-electric-field chip.* Biosens Bioelectron, 2009. **24**(12): p. 3510-6.

174. H.F. Tsai, S.W. Peng, C.Y. Wu, H.F. Chang, and J.Y. Cheng, *Electrotaxis of oral squamous cell carcinoma cells in a multiple-electric-field chip with uniform flow field.* Biomicrofluidics, 2012. **6**(3): p. 034116-034116-12.

175. J. Zhang, M. Calafiore, Q. Zeng, X. Zhang, Y. Huang, R.A. Li, W. Deng, and M. Zhao, *Electrically guiding migration of human induced pluripotent stem cells.* Stem Cell Reviews and Reports, 2011. **7**(4): p. 987-996.

176. Y.S. Sun, S.W. Peng, K.H. Lin, and J.Y. Cheng, *Electrotaxis of lung cancer cells in ordered three-dimensional scaffolds.* Biomicrofluidics, 2012. **6**(1): p. 14102-1410214.

177. E.F. Foxman, J.J. Campbell, and E.C. Butcher, *Multistep navigation and the combinatorial control of leukocyte chemotaxis.* The Journal of cell biology, 1997. **139**(5): p. 1349-1360.

178. K. Schumann, T. Lammermann, M. Bruckner, D.F. Legler, J. Polleux, J.P. Spatz, G. Schuler, R. Forster, M.B. Lutz, L. Sorokin, and M. Sixt, *Immobilized chemokine fields and soluble chemokine gradients cooperatively shape migration patterns of dendritic cells.* Immunity, 2010. **32**(5): p. 703-13.

179. J. Li, L. Zhu, M. Zhang, and F. Lin, *Microfluidic device for studying cell migration in single or co-existing chemical gradients and electric fields.* Biomicrofluidics, 2012. **6**(2): p. 024121.

180. S. Song, H. Han, U.H. Ko, J. Kim, and J.H. Shin, *Collaborative effects of electric field and fluid shear stress on fibroblast migration.* Lab on a Chip, 2013. **13**: p. 1602-1611.

181. P. Rezai, A. Siddiqui, P. Selvaganapathy, and B. Gupta, *Electrotaxis of Caenorhabditis elegans in a microfluidic environment.* Lab Chip, 2010. **10**(2): p. 220-6.

182. P. Rezai, A. Siddiqui, P.R. Selvaganapathy, and B.P. Gupta, *Behavior of Caenorhabditis elegans in alternating electric field and its application to their localization and control.* Applied physics letters, 2010. **96**(15): p. 153702-153702-3.

183. P. Rezai, S. Salam, P.R. Selvaganapathy, and B.P. Gupta, *Effect of pulse direct current signals on electrotactic movement of nematodes Caenorhabditis elegans and Caenorhabditis briggsae.* Biomicrofluidics, 2011. **5**(4): p. 44116-441169.

184. X. Manière, F. Lebois, I. Matic, B. Ladoux, J.-M. Di Meglio, and P. Hersen, *Running Worms: C. elegans Self-Sorting by Electrotaxis.* PloS one, 2011. **6**(2): p. e16637.

185. P. Rezai, S. Salam, P.R. Selvaganapathy, and B.P. Gupta, *Electrical sorting of Caenorhabditis elegans.* Lab on a Chip, 2012. **12**(10): p. 1831-1840.

186. B. Han, D. Kim, U. Hyun Ko, and J.H. Shin, *A sorting strategy for C. elegans based on size-dependent motility and electrotaxis in a micro-structured channel.* Lab on a Chip, 2012. **12**(20): p. 4128-4134.

187. L. Li, R. Hartley, B. Reiss, Y. Sun, J. Pu, D. Wu, F. Lin, T. Hoang, S. Yamada, J. Jiang, and M. Zhao, *E-cadherin plays an essential role in collective directional migration of large epithelial sheets.* Cellular and Molecular Life Sciences, 2012. **69**(16): p. 2779-2789.

188. G. Turato, R. Zuin, and M. Saetta, *Pathogenesis and pathology of COPD.* Respiration, 2001. **68**(2): p. 117-128.

189. Global Initiative for Chronic Obstructive Lung Disease(GOLD), *Global strategy for diagnosis, management, and prevention of chronic obstructive pulmonary disease.* 2014.

190. A. Jatakanon, U.G. Lalloo, S. Lim, K.F. Chung, and P.J. Barnes, *Increased neutrophils and cytokines, TNF-α and IL-8, in induced sputum of non-asthmatic patients with chronic dry cough.* Thorax, 1999. **54**(3): p. 234.

191. W. Thurlbeck, *Pathophysiology of chronic obstructive pulmonary disease.* Clinics in chest medicine, 1990. **11**(3): p. 389.

192. S.I. Rennard, *Inflammation and repair processes in chronic obstructive pulmonary disease.* American journal of respiratory and critical care medicine, 1999. **160**(5): p. S12.

193. C.A. McNulty, F.A. Symon, and A.J. Wardlaw, *Characterization of the integrin and activation steps mediating human eosinophil and neutrophil adhesion to chronically inflamed airway endothelium.* American journal of respiratory cell and molecular biology, 1999. **20**(6): p. 1251.

194. H. Nakamura, K. Yoshimura, H.A. Jaffe, and R. Crystal, *Interleukin-8 gene expression in human bronchial epithelial cells.* Journal of Biological Chemistry, 1991. **266**(29): p. 19611-19617.

195. J. Richman-Eisenstat, P.G. Jorens, C. Hebert, I. Ueki, and J. Nadel, *Interleukin-8: an important chemoattractant in sputum of patients with chronic inflammatory airway diseases.* American Journal of Physiology-Lung Cellular and Molecular Physiology, 1993. **264**(4): p. L413-L418.

196. C. Yamamoto, T. Yoneda, M. Yoshikawa, A. Fu, T. Tokuyama, K. Tsukaguchi, and N. Narita, *Airway inflammation in COPD assessed by sputum levels of interleukin-8.* Chest, 1997. **112**(2): p. 505.

197. R.A. Stockley, *Neutrophils and the Pathogenesis of COPD**. Chest, 2002. **121**(5 suppl): p. 151S-155S.

198. I. Woolhouse, D. Bayley, and R. Stockley, *Sputum chemotactic activity in chronic obstructive pulmonary disease: effect of α1–antitrypsin deficiency and the role of leukotriene B4 and interleukin 8.* Thorax, 2002. **57**(8): p. 709-714.

199. T. Yoshikawa, G. Dent, J. Ward, G. Angco, G. Nong, N. Nomura, K. Hirata, and R. Djukanovic, *Impaired neutrophil chemotaxis in chronic obstructive pulmonary disease.* American journal of respiratory and critical care medicine, 2007. **175**(5): p. 473-479.

200. R. Keller, *Cell migration during gastrulation.* Curr Opin Cell Biol, 2005. **17**(5): p. 533-41.

201. H. Yamaguchi, J. Wyckoff, and J. Condeelis, *Cell migration in tumors.* Curr Opin Cell Biol, 2005. **17**(5): p. 559-64.

202. M. Eisenbach, *Chemotaxis*. 2004: Wiley Online Library.

203. C. Beta and E. Bodenschatz, *Microfluidic tools for quantitative studies of eukaryotic chemotaxis.* Eur J Cell Biol, 2011. **90**(10): p. 811-6.

204. S.B. Kim, H. Bae, J.M. Cha, S.J. Moon, M.R. Dokmeci, D.M. Cropek, and A. Khademhosseini, *A cell-based biosensor for real-time detection of cardiotoxicity using lensfree imaging.* Lab on a Chip, 2011. **11**(10): p. 1801-1807.

205. S.B. Kim, K.-i. Koo, H. Bae, M.R. Dokmeci, G.A. Hamilton, A. Bahinski, S.M. Kim, D.E. Ingber, and A. Khademhosseini, *A mini-microscope for in situ monitoring of cells.* Lab on a Chip, 2012. **12**(20): p. 3976-3982.

206. H. Zhu, S.O. Isikman, O. Mudanyali, A. Greenbaum, and A. Ozcan, *Optical imaging techniques for point-of-care diagnostics.* Lab on a Chip, 2013. **13**(1): p. 51-67.

207. A. Sacan, H. Ferhatosmanoglu, and H. Coskun, *CellTrack: an open-source software for cell tracking and motility analysis.* Bioinformatics, 2008. **24**(14): p. 1647-1649.

208. G.M. Walker, J. Sai, A. Richmond, M. Stremler, C.Y. Chung, and J.P. Wikswo, *Effects of flow and diffusion on chemotaxis studies in a microfabricated gradient generator*. Lab on a Chip, 2005. **5**(6): p. 611-618.

209. P.K. Yuen and V.N. Goral, *Low-cost rapid prototyping of flexible microfluidic devices using a desktop digital craft cutter.* Lab on a Chip, 2010. **10**(3): p. 384-387.

210. V. Kumar and A. Sharma, *Neutrophils: Cinderella of innate immune system.* International immunopharmacology, 2010. **10**(11): p. 1325-1334.

211. D.H. Adams and A. Rlloyd, *Chemokines: leucocyte recruitment and activation cytokines.* The Lancet, 1997. **349**(9050): p. 490-495.

212. B. Heit, S. Tavener, E. Raharjo, and P. Kubes, *An intracellular signaling hierarchy determines direction of migration in opposing chemotactic gradients.* The Journal of cell biology, 2002. **159**(1): p. 91-102.

213. B. Amulic, C. Cazalet, G.L. Hayes, K.D. Metzler, and A. Zychlinsky, *Neutrophil function: from mechanisms to disease.* Annual review of immunology, 2012. **30**: p. 459-489.

214. M. Heinzelmann, M.A. Mercer-Jones, and J.C. Passmore, *Neutrophils and renal failure.* American journal of kidney diseases, 1999. **34**(2): p. 384-399.

215. R.C. Reddy and T.J. Standiford, *Effects of sepsis on neutrophil chemotaxis.* Current opinion in hematology, 2010. **17**(1): p. 18-24.

216. D. Burnett, S. Hill, A. Chamba, and R. Stockley, *Neutrophils from subjects with chronic obstructive lung disease show enhanced chemotaxis and extracellular proteolysis.* The Lancet, 1987. **330**(8567): p. 1043-1046.

217. W. Saadi, S. Wang, F. Lin, and N. Jeon, *A parallel-gradient microfluidic chamber for quantitative analysis of breast cancer cell chemotaxis.* Biomed Microdevices, 2006. **8**(2): p. 109-18.

218. F. Lin, *Chapter 15. A microfluidics-based method for chemoattractant gradients.* Methods Enzymol, 2009. **461**: p. 333-47.

219. E.K.-H. Sackmann, E. Berthier, E.A. Schwantes, P.S. Fichtinger, M.D. Evans, L.L. Dziadzio, A. Huttenlocher, S.K. Mathur, and D.J. Beebe, *Characterizing asthma from a drop of blood using neutrophil chemotaxis.* Proceedings of the National Academy of Sciences, 2014. **111**(16): p. 5813-5818.

220. A. Yamauchi, M. Degawa-Yamauchi, F. Kuribayashi, S. Kanegasaki, and T. Tsuchiya, *Systematic single cell analysis of migration and morphological changes of human neutrophils over stimulus concentration gradients.* Journal of immunological methods, 2014. **404**: p. 59-70.

221. J.K. Quint and J.A. Wedzicha, *The neutrophil in chronic obstructive pulmonary disease.* Journal of Allergy and Clinical Immunology, 2007. **119**(5): p. 1065-1071.

222. E.A. Warner, K.T. Kotz, R.F. Ungaro, A.S. Abouhamze, M.C. Lopez, A.G. Cuenca, K.M. Kelly-Scumpia, C. Moreno, K.A. O'Malley, and J.D. Lanz, *Microfluidics-based capture of human neutrophils for expression analysis in blood and bronchoalveolar lavage.* Laboratory Investigation, 2011. **91**(12): p. 1787-1795.

223. J. Wu, L. Ouyang, N. Wadhawan, J. Li, M. Zhang, S. Liao, D. Levin, and F. Lin, *A compact microfluidic system for cell migration studies.* Biomedical microdevices, 2014: p. 1-8.

224. W. James Metzger, H.B. Richerson, and S.I. Wasserman, *Generation and partial characterization of eosinophil chemotactic activity and neutrophil chemotactic activity during early and late-phase asthmatic response.* Journal of Allergy and Clinical Immunology, 1986. **78**(2): p. 282-290.

225. E. Kolaczkowska and P. Kubes, *Neutrophil recruitment and function in health and inflammation.* Nat Rev Immunol, 2013. **13**(3): p. 159-75.

226. J. Wu, C. Hillier, P. Komenda, R. Lobato de Faria, D. Levin, M. Zhang, and F. Lin, *A Microfluidic Platform for Evaluating Neutrophil Chemotaxis Induced by Sputum from COPD Patients.* PloS one, 2015. **10**(5): p. e0126523.

227. W.M. Nauseef, *Isolation of human neutrophils from venous blood*, in *Neutrophil Methods and Protocols*. 2007, Springer. p. 15-20.

228. S. Zahler, C. Kowalski, A. Brosig, C. Kupatt, B.F. Becker, and E. Gerlach, *The function of neutrophils isolated by a magnetic antibody cell separation technique is not altered in comparison to a density gradient centrifugation method.* Journal of immunological methods, 1997. **200**(1): p. 173-179.

229. B. Hamza and D. Irimia, *Whole blood human neutrophil trafficking in a microfluidic model of infection and inflammation.* Lab on a Chip, 2015. **15**(12): p. 2625-2633.

230. STEMCELL. *EasySep™ Direct Human Neutrophil Isolation Kit*. [cited 2015 July]; Available from: http://www.stemcell.com/en/Products/All-Products/EasySep-Direct-Human-Neutrophil-Isolation-Kit.aspx.

231. A.M. Taylor, M. Blurton-Jones, S.W. Rhee, D.H. Cribbs, C.W. Cotman, and N.L. Jeon, *A microfluidic culture platform for CNS axonal injury, regeneration and transport.* Nature methods, 2005. **2**(8): p. 599-605.

232. I. Chanarin, *Hematology: Principles and Procedures.* Journal of clinical pathology, 1984. **37**(12): p. 1419.

233. J. Wu, L. Ouyang, M. Zhang, S. Liao, C. Hillier, P. Komenda, R.L. de Faria, and F. Lin, *Assessing neutrophil chemotaxis in COPD using a compact microfluidic system*, in *EMBC2014*. 2014: Chicago, U.S.A.

234. I. Halilovic, J. Wu, M. Alexander, and F. Lin, *Neutrophil migration under spatially-varying chemoattractant gradient profiles.* Biomedical microdevices, 2015. **17**(3): p. 1-7.

235. G. Malet-Engra, W. Yu, A. Oldani, J. Rey-Barroso, N.S. Gov, G. Scita, and L. Dupré, *Collective cell motility promotes chemotactic prowess and resistance to chemorepulsion.* Current Biology, 2015. **25**(2): p. 242-250.

Appendix

A.1. A standalone microfluidic device for gradient generation and chemotaxis studies

The microfluidic device design parameters were directly adapted from a previous device we developed for configuring superimposed chemical gradients and electric fields **(Fig. A.1)**. However, the principle of flow-free gradient generation of this device in the present study is different from the flow-based gradient generation as in the previous study [179]. It consists of a 350 μm-wide and 1 cm-long center gradient channel, which is connected to two 8 mm diameter chemical wells by 20 thin channels (40 μm in width and 3 mm in length) on each side. Two 3 mm diameter wells were designed at the two ends of the center gradient channel.

To generate a chemical gradient, all chemical wells were firstly emptied and new solutions were added. Specifically, 25 μL of RPMI media was added to the 3 mm diameter wells at the two ends of the center channel; 150 μL of RPMI media mixed with FITC-Dextran 10 kDa (5 μM) and 145 μL of RPMI media were added to the two 8 mm diameter wells simultaneously. In our experience, the small volume difference between the cell tracker solution and the medium added to the two wells helps quickly establish the cell tracker gradient in the channel. FITC-Dextran gradient was monitored by fluorescent time-lapse microscopy. Our results show that a FITC-Dextran gradient was established in the center gradient channel in less than 5 min and maintained stable for at least 45min **(Fig. A.1B & A.1C)**, which is at least sufficient for experiments with fast migratory cells such as neutrophils and T lymphocytes.

To validate UMCAS for visualizing chemical gradient in the microfluidic device, we first added food-coloring dye to the standalone microfluidic device. Gradients of food-coloring dye can be clearly seen in the center gradient channel using the USB microscope (**Fig. A.1D & A.1E**). Furthermore, we added FITC-Dextran to the standalone microfluidic device. Then we used the blue LED in UMCAS to excite FITC-Dextran in the device and imaged the FITC-Dextran gradient in the center gradient channel using the USB microscope. The image showed clear chemical gradient in the device (**Fig. A.1F**) and thus the system is effective to verify chemical gradient before performing chemotaxis experiment.

Figure A.1 Standalone microfluidic gradient generator.

(A) Schematic illustration of the device design with simulated gradient; **(B)** Image of FITC-Dextran gradient using a traditional microscope; **(C)** Plot of gradient profile over time; **(D)** A picture of the device. The two inlet reservoirs are filled with food coloring dye solutions; **(E)** Image of food-coloring dye gradient taken by UMCAS; (**F**) Image of FITC-Dextran gradient using UMCAS.

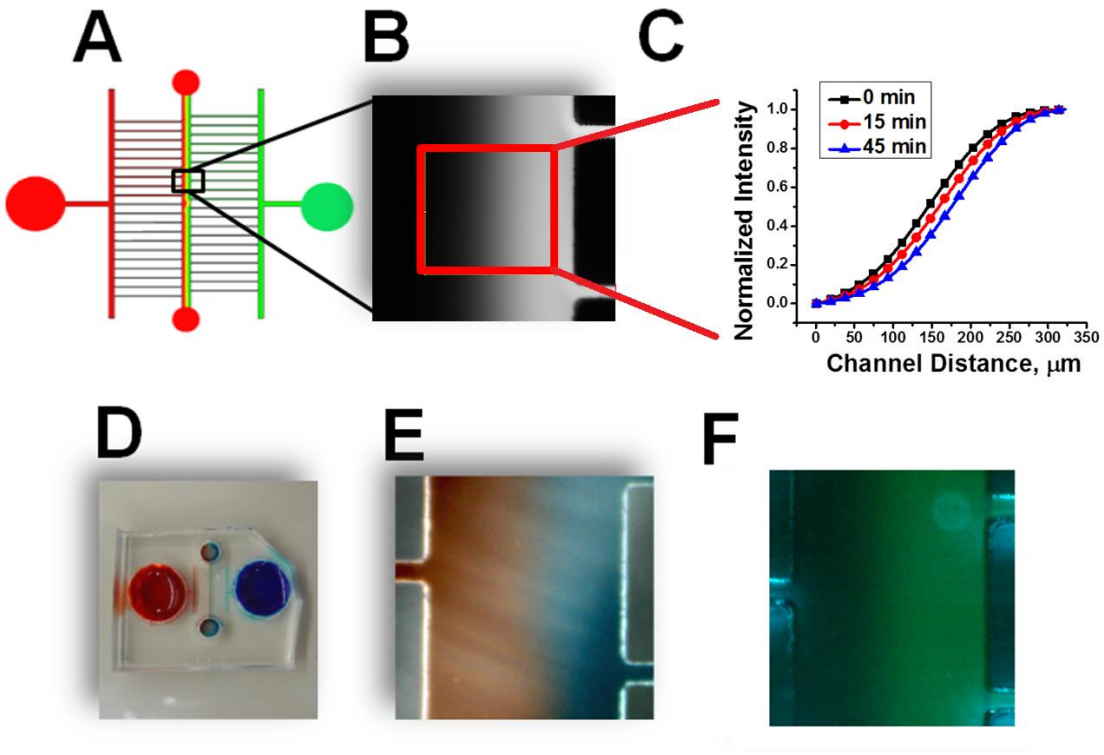

A.2. Craft cut plastic microfluidic device for chemical gradient generation and chemotaxis studies

Following a previously reported craft-cutting method [209], we designed a simple "Y" type microfluidic gradient device using the software Silhouette Studio and cut the design to a double-sided adhesive tape (4Mil Melinex, 100 µm thick, Fralock, CA) using a desktop craft cutter (CAMEO, Silhouette America Inc.). The channel width is ~500 µm. Similarly, holes were cut to a separate transparency film (2Mil Melinex, 50 µm thick, Fralock, CA) that aligns with the inlets and outlet of the channel in the adhesive layer. Next, the protective layers of the tape were removed and the tape was sandwiched between the transparency film and a glass slide to form the microfluidic channel. The inlets were bonded to pre-made PDMS blocks using epoxy glue as the interface for tubing connection (holes that match the tubing size were punched out of the PDMS blocks before bonding). The outlet was bonded to a pipette with the tip removed for waste collection. The whole process from designing to finishing the device assembly can be finished in less than 30 min depending on the complexity of the design (**Fig. A.2A-C**). Chemical gradient was generated in the plastic device by chemical infusion to the device through tubing using syringe pumps (**Fig. A.2D & A.2E**). Furthermore, neutrophil chemotaxis to an IL-8 gradient in the plastic device was successfully demonstrated (**Fig. A.2F & A.2G**). The developed device can be used with UMCAS or a conventional imaging setup for cell migration studies in a rapid and inexpensive manner without the requirement of specialized fabrication facilities and lengthy device preparation procedures.

Figure A.2 The craft-cut plastic microfluidic device for gradient generation and neutrophil chemotaxis studies.

(**A**) A picture of the craft cutter; (**B**) Illustration of device assembly; (**C**) A picture of the completed microfluidic device with PDMS interfaces and the waste outlet; (**D**) Fluorescent picture of FITC-Dextran 10kD gradient in the channel; (**E**) Measured gradient profile; (**F**) Migration tracks of neutrophil to a 12.5 nM IL-8 gradient. in the plastic device. The tracks were normalized to a common origin; (**G**) Chemotaxis Index and Speed of the neutrophil chemotaxis experiment (presented as average ± SEM).

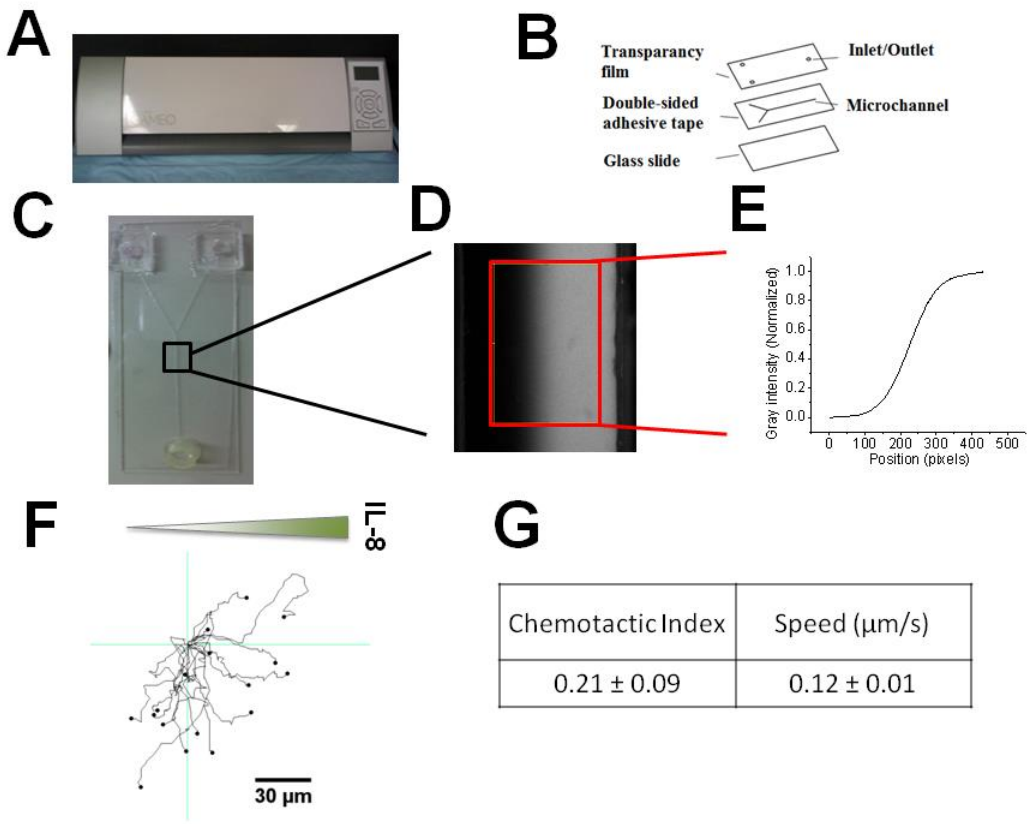

Chemotactic Index	Speed (µm/s)
0.21 ± 0.09	0.12 ± 0.01